AD-A170 802 EROSION STUDY OF AM355 AND AL203 CERAMICS(U) CINCINNATI 1/1
UNIV OH DEPT OF AEROSPACE ENGINEERING AND ENGINEERING
MECHANICS W TABAKOFF ET AL. 15 JAN 87 87-50
UNCLASSIFIED ARO-18560.30-EG DAAG-82-K-0029 F/G 11/6 NL

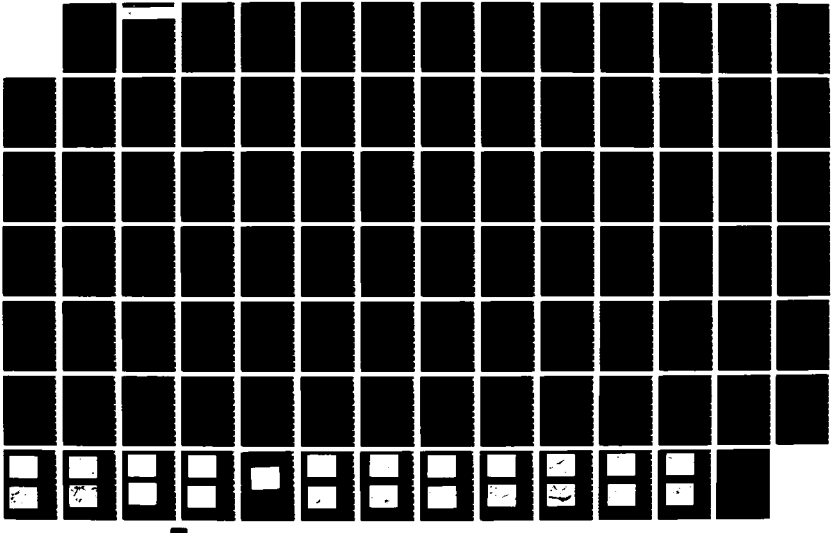

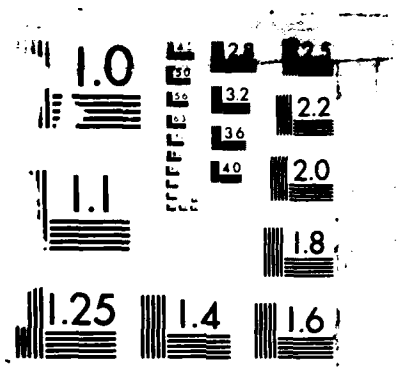

MIC
N-

EROSION STUDY OF AM355 STEEL AND Al_2O_3 CERAMICS

W. TABAKOFF, A. HAMED AND S.Y. KANG

JANUARY 1987

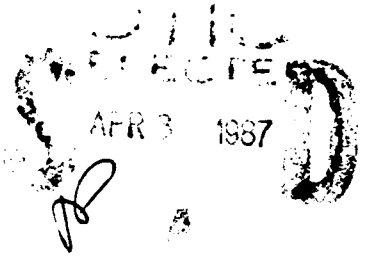

This work was sponsored by the U.S. Army Research Office-Durham, under Contract No. DAAG-29-82-K-0029.

UNCLASSIFIED
SECURITY CLASSIFICATION OF THIS PAGE (When Data Entered)

AD-A178882

REPORT DOCUMENTATION PAGE

READ INSTRUCTIONS BEFORE COMPLETING FORM

1. REPORT NUMBER	2. GOVT ACCESSION NO. N/A; 3. RECIPIENT'S CATALOG NUMBER N/A
4. TITLE (and Subtitle) EROSION STUDY OF AM355 STEEL AND Al_2O_3 CERAMICS	5. TYPE OF REPORT & PERIOD COVERED Technical Report; 6. PERFORMING ORG. REPORT NUMBER 87-58
7. AUTHOR(s) W. Tabakoff, A. Hamed and S.Y. Kang	8. CONTRACT OR GRANT NUMBER(s) DAAG-29-82-K-0029
9. PERFORMING ORGANIZATION NAME AND ADDRESS Dept. of Aerospace Engineering & Engg. Mech. University of Cincinnati Cincinnati, OH 45221-0070	10. PROGRAM ELEMENT, PROJECT, TASK AREA & WORK UNIT NUMBERS
11. CONTROLLING OFFICE NAME AND ADDRESS U. S. Army Research Office Post Office Box 12211 Research Triangle Park, NC 27709	12. REPORT DATE January 15, 1987; 13. NUMBER OF PAGES 86
14. MONITORING AGENCY NAME & ADDRESS (if different from Controlling Office)	15. SECURITY CLASS. (of this report) Unclassified; 15a. DECLASSIFICATION/DOWNGRADING SCHEDULE

16. DISTRIBUTION STATEMENT (of this Report)

Approved for public release; distribution unlimited.

17. DISTRIBUTION STATEMENT (of the abstract entered in Block 20, if different from Report)

NA

18. SUPPLEMENTARY NOTES

The view, opinions, and/or findings contained in this report are those of the author(s) and should not be construed as an official Department of the Army position, policy, or decision, unless so designated by other documentation.

19. KEY WORDS (Continue on reverse side if necessary and identify by block number)

Erosion ductile material,
Erosion nonductile material,
steel, alloys, ceramic materials,
helicopter engines,
Aluminum oxide

20. ABSTRACT (Continue on reverse side if necessary and identify by block number)

The need for the knowledge and better understanding of material erosion behavior is necessary for the use of these materials in future helicopter engines with confidence. The present experimental investigation presents a detailed study of the erosion behavior of a typical ductile material (steel AM355 alloy) and a nonductile (brittle) material (Al_2O_3). The experimental results show the influence of the particle size, particle velocity and temperature on the erosion rate. Electron micrographs of the eroded surfaces under various conditions are presented and compared. Empirical correlations for the erosion results are also presented.

DD FORM 1 JAN 73 1473 EDITION OF 1 NOV 65 IS OBSOLETE

UNCLASSIFIED
SECURITY CLASSIFICATION OF THIS PAGE (When Data Entered)

REPORT NO. 87-58

EROSION STUDY OF AM355 STEEL AND Al_2O_3 CERAMICS

W. TABAKOFF, A. HAMED AND S.Y. KANG

Department of Aerospace Engineering and Engineering Mechanics
University of Cincinnati
Cincinnati, Ohio 45221

JANUARY 1987

This work was sponsored by the U.S. Army Research Office-Durham, under Contract No. DAAG-29-82-K-0029.

TABLE OF CONTENTS

LIST OF TABLES

LIST OF FIGURES

ABSTRACT

The performance of aircraft engines is known to deteriorate rapidly when they operate in areas where the atmosphere is laden with solid particles. The particles may be sand, dust, ash, chemical products or others. Continued operation under such conditions can erode the engine components surfaces and reduce the reliability and life of the engine. In recent years, interest was renewed in the use of ceramics for gas turbines components. The need for the knowledge and better understanding of material erosion behavior is necessary for the use of these materials in future engines with confidence. The present experimental investigation presents a detailed study of the erosion behavior of a typical ductile material (steel AM355 alloy) and a non-ductile (brittle) material (Al_2O_3). The experimental results show the influence of the particle size, particle velocity and temperature on the erosion rate. Electron micrographs of the eroded surfaces under the various conditions are presented and compared. Empirical correlations for the erosion results are also presented.

INTRODUCTION

Many of the models for ductile materials erosion stem from the study of single particle impact. The best known erosion mechanisms are plowing deformation [1, 2, 3], usually caused by angular particles, cutting deformation type I [4], cutting deformation type II [2], and local melting [5, 6]. The above classification of the first three modes of deformation is best illustrated in reference [1] by a series of high speed photographs and by the outlines of the crater sections. Finnie [7] concluded that the erosion mechanism is one of cutting or micro-machining. The sharp corners of individual particles act as miniature single point tools. He developed an expression for the erosion rate (Q) which is proportional to the total available kinetic energy of the particle and inversely proportional to the minimum flow shear stress:

$$Q = C\, f(\alpha)\, MV^2/\sigma$$

where: C = constant for specific erosion system,

$f(\alpha)$ = function of angle of attack,

M = mass of particle,

V = particle approach velocity,

σ = minimum flow stress related to that measured, in a tension or compression test.

Finnie's equation is not suitable for predicting the erosion rate at normal angle of attack. Also, the velocity exponent has subsequently been found to be generally different from 2.0. Bitter [8] obtained better fitting equations to the test results by modifying Finnie's original relationship using two separate relations to express the wear due to the repeated deformation, and that due to the cutting action. Nielson and Gilchrist [9] also utilized the idea of both cutting and repeated deformation to develop a

simpler set of equations. Head and Harr [10] concluded that while the rigorous models such as Bitter's model are useful in identifying important parameters, they do not adequately describe erosion by naturally occurring contaminants due to their non-homogeneous nature. They described the data in a statistical manner and developed a model that fits their experimental data reasonably well. The parametric relationship used in their analysis was determined using the Buckingham Pi theorem. More recently, Levy [11] demonstrated that the erosion of ductile metal alloys by small impacting solid particles is not by micromachining but is a result of the extrusion and forging of thin platelets which are subsequently knocked off the surface.

The mechanism of brittle materials erosion is one of constant battering and fatigue leading to surface cracking and spalling of the target surface. Microstructural examination of target surface have validated this theory. Brittle materials, exposed to single impacts have been treated as static and dynamic plastic indentation. The plastic indentation is characterized by plastic deformation of the contact area between the particle and the target, with radial cracks propagating outward from the contact zone, and with surface lateral cracks propagating outward on planes nearly parallel to the surface. The former are considered a source of strength degradation and the latter a potential source of material removal. Evans [12] analyzed the erosion mechanism of brittle materials at high angles of attack and treated the phenomenon as plastic indentation. This plastic deformation of the contact zone between the particle and target promotes radial cracks which propagate away from the zone. Subsurface lateral cracks run on the planes nearly parallel to the surface. This type of damage, which is referred to as elastic-plastic, has been observed to be caused by the impact of the

angular particles of generally greater hardness than the target material [12]. At low angles of impingement, it has been reported that the primary mechanism of erosion for brittle materials is plowing [13] in a manner similar to the one described for the erosion of metals. Based on the elastic-plastic analysis, two models by Evans [14] and Ruf and Widerhorn [15] have been proposed which relate the erosion volume to both target and particle mechanical properties. Diamond [16] tested sintered alumina, basalt, and glass at ambient temperature. The impingement angles ranging between 15° and 90° at a mean particle velocities of 46 m/sec and 40 m/sec for SiC and SiO particles. Dimond's plot of the experimental results according to the Evan's model fits equally as well as to that of Ruff and Wiederhorn.

Effect of Target Material Properties

Finnie [17] proposed that high hardness results in greater erosion resistance, but this basic premise has been disproved for metallic alloys by Christman and Shewman [18], Stalik and Buckley [19]. Levy arrived at the following conclusions in his recent study [11]:

1. The strength and hardness of ductile metals, except for solid solution strengthened alloys, do not directly correlate with the erosion resistance of alloys.
2. A sub-surface, cold worked zone which acts as an anvil to increase the erosion efficiency of the impacting particles is developed by the plastic deformation which results from the force applied by the impacting particles.
3. The strain hardening coefficient of alloys relates to how soon the alloys reach a steady state erosion condition, i.e., to the development

of their sub-surface cold worked zone, but not the magnitude of the steady state erosion rate.

Tilly [20] has shown that some brittle materials tend to become less resistant at higher hardness.

Effect of Particle Velocity

The effect of particle velocity on erosion rate was first observed by Stoker [21], in 1949, and has since been an important parameter in most erosion investigations. Finnie [22] assumed that erosion loss is proportional to the kinetic energy of the erosive particle and, therefore, erosion loss would be proportional to the square of the velocity. Velocity exponents greater than 2 were determined in subsequent investigations. Sheldon [23] measured velocity exponents for ductile materials in the range of 2.4 to 2.7, while Finnie [17], Sheldon and Kanhere [24], and Goodwin [25] found velocity exponents as high as 3.0. Grant [26] measured a velocity exponent of 4.0 for normal impacts of alumina particles on a 2024 aluminum target. Wakeman [27] and Tabakoff [28] demonstrated that for ductile materials the velocity exponents are strongly dependent of the temperature and the impingement angle.

For brittle materials, existing erosion models are based on the analysis of the volume of materials removed by the lateral cracks in single particle impact. Interaction effects are assumed to be negligible so that the cumulative effect of multiple impacts is obtained by summing the volumes removed by individual impacts. Two quantitative models were developed for predicting the erosion of brittle materials. One is based on the analysis of the quasi-static indentation and the upper bound quasi-static impulse load [29, 30]. The second model is based on a dynamic analysis of the

elastic, plastic stress field [31, 32]. Marshall [33] confined his interest to particle size and velocity effects in a given projectile target system and derived a new relation. He found that the erosion volume loss is proportional to particle velocity to the power 3 for SiC particles impacting single crystal silicon target material perpendicular to the surface. Gulden [34] obtained a relationship between the particle radius and its velocity and the resulting erosion. He tested natural quartz particles using six particle sizes ranging between 10 and 385 microns at five different velocities ranging between 24 m/sec and 285 m/sec (79 ft/sec and 935 ft/sec) to arrive at his relations.

Effect of Particle Size

For brittle materials, Sheldon and Finnie [35] reported an exponential relationship between the erosion volume loss and the particle radius. The values of the exponent ranged between 3.14 to 5.12 for spherical particles and 3.58 to 4.25 for angular particles. It was observed that the material may exhibit a transition from the brittle to the ductile behavior when eroded by progressively smaller particles [36]. Marshall [33] also expressed the erosion rate in terms of the particle diameter.

For ductile materials, Sage and Tilly [37], Grant and Tabakoff [26] and Kotwal and Tabakoff [38] found that at a given particle velocity, erosion increases with increased particle size until the onset of a "saturation plateau". However, Sage and Tilly [37] reported that for the brittle material, there is no plateau value, and the erosion rate is proportional to the square of the particle diameter. One can therefore conclude that generally the value of the exponent strongly depends on the target and particle material.

Effect of Temperature

Very few studies investigated the effect of target material temperature on erosion rate mostly through heating the target using electrical resistance. In most cases, the maximum temperature was less than 816°C (1500°F), and the target temperatures were not in excess of 0.5 times of the material melting temperature.

Theoretically, Bitter [8] has indicated that the energy required to remove a unit volume of material is strongly dependent on temperature. As temperature rises, the erosion goes up. Bitter [8] explains that this phenomenon depends on the recovery of lattice dislocations which takes place at higher rate as the temperature rises. When recrystallization temperature is exceeded, erosion is infinitely large. For brittle material, heterogeneous materials such as cement, Bitter predicted that erosion is dependent on the strength of the bonds between the cement conglomerates, thus scarcely depending on temperature. Tabakoff and Vittal [39] tested INCO 600 materials at the temperatures of 700, 920 and 1070°F, and found that the erosion rate at these temperatures is much higher than at the ambient temperature. Gat [40] concluded that erosion rate may decrease or increase with increased temperatures depending on the material properties and impact condition. Tabakoff and Wakeman [41] investigated the erosion of different alloys at high temperatures. Additional experimental data are presented in references [27] and [28].

Presently available data on the erosion experiments at high temperatures are summarized in Table 1 which lists the target materials, target temperatures, particle materials, sizes, velocities and angles of attack.

Effect of Particle Hardness and Shape

Goodwin [25] suggested that since hardness and shape are interrelated, the erosiveness of a particle is given by a power law:

$$E \alpha H^{2.3}$$

where:

E = erosion rate

H = diamond pyramid hardness

Grant [26] observed that erosion rates are 48% to 68% smaller for SiO_2 (quartz) than for Al_2O_3 (alumina) particles. Head [42] found that fluorite (CaF_2) particles are more erosive than alumina (Al_2O_3) particle. He concluded that some properties, other than hardness must be considered in determining relative erosiveness, since the hardness of CaF_2 is 4 and Al_2O_3 is 9 on Moh's scale. Also, Wood [43] suggested that erosion decreased with increasing hardness.

Effect of Impingement Angle

During the early studies it was found that the erosion rate increases from zero angle of impingement to a maximum at approximately 25 to 30 degrees for a ductile target material. The erosion rate then decreases as the angle is further increased until a minimum and a non-zero value is reached at a normal (90°) impingement angle. For brittle materials the erosion rate was found to continually increase from a zero value at a zero impingement angle to a maximum value at normal impingement angle (90°). Typical curves for these two modes of erosion are shown in Fig. 1. It was concluded in the early studies that the mechanical properties of the eroded material determined the type of erosion that prevailed.

From the preceding literature review, it is clear that the effect of the target temperature on the resulting erosion is not completely understood and the experimental results are lacking for both brittle and ductile material erosion at high temperatures. In addition, there is not enough experimental data to study the effect of particle size on material erosion. There are several inconsistencies among the existing experimental results and there is very little data available for particles larger than 200 micron in diameter. The experimental work in the present study was conducted to investigate the effect of temperature and particle size on the erosion of ductile and brittle materials.

EXPERIMENTAL SET-UP

In the present study, the existing high temperature erosion test facility at the University of Cincinnati was used to investigate the effect of particle size and sample temperature on ductile and brittle material erosion. The erosion of stainless steel (AM 355) alloy, a material used in turbomachinery blading, by silica sand up to 1981 microns in diameter was investigated. The tests were conducted at different temperatures ranging between standard sea level and 550°C. In addition the particle concentrations were varied between 0.014 mg/cm^3 and 0.5 mg/cm^3 since there was no prior data available in this range. The effect of temperature on erosion was also studied for pure Al_2O_3 (brittle material) using silica sand impacting particles. The tests were conducted at five different impingement angles (20°, 30°, 45°, 60° and 90°). The properties of Al_2O_3 material are presented in Table 2, and the analysis for fly ash particles for different

types of silica sand are shown in Tables 3, 4, 5 and 6. The test conditions are summarized in Table 7.

The high temperature erosion test facility was designed to provide erosion and rebound data in the range of operating temperatures experienced in compressors and turbines. For that purpose, this facility has been designated to operate at a test section temperature in the range of ambient to 1093°C (2000°F). In addition to the high temperatures, the facility properly simulates all erosion parameters which were found to be important from aerodynamics point of view as it was previously established at ambient temperatures erosion wind tunnel. These parameters include particle velocity, angle of impact, particle size, particle concentration, and sample size. Close attention was given to aerodynamic effects to insure that important parameters, such as angle of attack, are not masked or altered.

A schematic of the test apparatus is shown in Fig. 2; it consists of the following components: particle feeder (A), main air supply pipe (B), combustor (C), particle preheater (D), particle injector (E), acceleration tunnel (F), test section (G), and exhaust tank (H).

The equipment functions as follows. A measured amount of abrasive grit of a given constituency is placed into the particle feeder (A). The particles are fed into a secondary air source and blown up to the particle preheater (D), and then to the injector (E), where they mix with the main air supply (B), which is heated by the combustor (C). The particles are then accelerated by the high-velocity air in a constant-area steam-cooled duct (F) and impact the specimen in the test section (G). The particulate flow is then mixed with the coolant and dumped in the exhaust tank. This facility is capable of supplying erosion data at temperatures in the range

of ambient to 1093°C (2000°F). The expected range of testing parameters is given in Table A, but is not necessarily restricted to the tabulated values.

TABLE A - EROSION PARAMETERS

Parameters	
Temperature	10 to 1093°C (50 to 2000°F)
Particle Angle of Attack	0 to 90 degree
Particle Velocity	60 to 450 m/s (200 to 1500 ft/sec)
Particle Concentration	0 to 5 percent
Particle Size	1 to 2000 microns
Particle Type and Material	Silica sand, alumina, ash
Specimen Size	6.35 to 25.4 mm (1/4 to 1 in.)
Specimen Material	Various Jet Engine Materials

In the high temperature erosion facility, the particle velocity is controlled by adjusting the tunnel air flow, while the impingement angle is set by rotating the sample relative to the flow stream. The sample temperature is controlled through the combustor heating the flow stream which in turn affects the material sample temperature. Further description of the facility may be found in reference [53].

RESULTS AND DISCUSSION

The erosion results are presented for the erosion volume parameter which is defined as the volume of material removed per unit weight of the impacting particle. This was preferred over the erosion mass parameter as it provides a better estimate of blade damage with respect to the change of blade profile.

a) Effect of Amount of Impacting Particles

The results of erosion testing for steel alloy (AM355) and ceramic (Al_2O_3) are presented in Fig. 3 at the corresponding maximum erosive impingement angles of attack, (30° for AM355 and 90° for Al_2O_3). At ambient temperature, the velocity of impacting silica sand particles was 70 m/s (250 ft/sec) and the particle diameters ranged between 125-177 microns. The amount of impacting particles was gradually increased, and the resulting erosion was measured. The results which are presented in Fig. 3 show that the ceramic (Al_2O_3) takes approximately six times the amount of particles to reach steady state erosion rate compared to the steel alloy (AM355).

b) Effect of Particle Velocity

Erosion loss is known to be proportional to some exponent 'n' of the particle velocity at a given temperature and angle of attack.

$$\frac{E_1}{E_2} = \left(\frac{V_1}{V_2}\right)^n$$

where: E_1 = erosion rate at velocity V_1

E_2 = erosion rate at velocity V_2.

The velocity index 'n' can be calculated from the experimental results using the above equation, or it can be determined from the logarithmic plots of the erosion versus velocity.

The experimental results for stainless steel erosion are presented for fly ash and sand particles in Figures 4 through 14. The values of 'n' are computed in Tables 8 through 10. The velocity index 'n' for Al_2O_3 erosion by silica sand (125 - 177 microns) was found to be 0.468 at room temperature, 90° angle of attack, and particle velocities of 76, 99, and 137 m/sec.

c) Effect of Particle Size

Some investigators such as Sage and Tilly [37], Grant [26] and Kotwal [38] have demonstrated that at a given velocity, the erosion rate increased with the particle size until the onset of 'saturation plateau'. In the present investigation it was observed that the erosion rates continuously increased up to the maximum particle size of 1981 microns which was used in this study. Therefore, no 'saturation plateau' in regard to particle sizes was observed in this study, which extends over a larger range of particle sizes compared to the previous investigation. Figures 15 through 19 present the pertinent results, from which one can conclude that at room temperature and 30° impingement angle, the erosion rate is proportional to the exponent of the particle sizes. The value of the exponent 'a' were found to be 0.568 for the silica sand particles ranging in size between 125 and 308 microns, and 0.696 for the silica sand particles with sizes in the range between 950 and 1981 microns.

d) Effect of Temperature

Experimental results were obtained for the erosion rate of steel alloy (AM355) at two different temperatures (316°C and 538°C). Figures 20-26 show plots of the erosion volume parameter versus the angle of attack at the two temperatures for different particle velocities. One can observe an increasing trend in the erosion rate with increased temperature in all the figures. The increase in the erosion rate due to temperature rise are much larger at the maximum erosive impingement angle (around 30°) than all other impingement angles. This is particularly true for the fly ash particle and large silica sand (over 950 microns) whereas the difference is very small for sand particles smaller than 600 microns.

Erosion tests were also performed in order to study the effect of the temperature on the erosion of Al_2O_3 (a brittle material) using silica sand particles at particle velocity of 137 m/s (450 ft/sec). The results of erosion volume parameter which are given in Fig. 27 at four different temperatures of 20°C (68°F), 316°C (600°F), 427°C (800°C), and 538°C (1000°F) were obtained. One can see that the erosion rate at 316°C (600°F) is a little higher than that at room temperature, but for temperatures above 316°C and up to 538°C (1000°F), the erosion rate decreases linearly with the temperature. One can therefore conclude the effect of temperature on Al_2O_3 (brittle materials) is totally different from that of steel alloy. Additional measurements are needed to determine the temperature at which this trend will change and the erosion rate will increase again with temperature.

e) Effect of Particle Concentration

It has been observed experimentally by several investigators that a decrease in particle concentration led to an increase in the erosion rate. In order to investigate this effect, petroleum product particles were used to impact a steel alloy at room temperature. Four different sizes (1/8", 3/16", 5/16" and 7/16") of particle feeder nozzle were used to obtain different particle concentrations. the results are presented in Fig. 28 which shows that the erosion rate decreases with increased particle concentration above 0.25 mgm/cm^3 (Figs. 28 and 29), i.e., when the particle mass flow ratio is greater than 16% of the total mass flow. This result suggests that using the smallest size of particle feeder nozzle is desirable to minimize the p ssible particle interaction during the testing in the erosion wind tunnel.

f) Effect of Angle of Attack

This effect was studied for two different materials, namely steel alloy (AM355) and Al_2O_3, by testing the steel alloy at nine different angles of attack and the Al_2O_3 at five different angles of attack. An examination of Figs. 30 and 31 for the steel alloy reveals that the erosion rate shows a typical trend of ductile behavior with the impingement angle. The erosion rate increases to a maximum at about 25° and then decreases to a residual value at the normal impact. This behavior was always observed in the case of the steel alloy, independent of the particle velocity, the temperature, or the type of impinging particles (Figs. 4, 5, 7, 9, 12, 14, 16, 17, 18 and 20-26. A typical trend of brittle behavior, i.e the erosion rate increases with increased angle of attack, can be seen in Fig. 32 for Al_2O_3.

Erosion Prediction Model for Steel Alloy (AM355)

Assuming that the erosion process is dependent on two mechanisms: one at low angle of attack, one at high angle of attack, and a combination of the two at intermediate approach angles, Grant and Tabakoff [26] developed a semi-empirical equation for predicting ductile erosion at room temperature. The relationship for erosion rate may be expressed as:

$$E = K_1 f(\beta_1) (V_{1T}^2 - V_{2T}^2) + f(V_{1N}) \quad (1)$$

where: E = Erosion weight loss per unit mass of impacting particles,

K_1 = Material constant,

$f(\beta_1)$ = Empirical function of particle impact angle,

V_{1T} = Tangential component of incoming particle velocity,

V_{2T} = Tangential component of rebounding particle velocity,

$f(V_{1N})$ = Component of erosion due to the normal component of velocity.

In the above equation, the first term represents the erosion mechanism at low angles of attack, while the second term represents the erosion mechanism at normal impact.

At normal impact, the erosion can be approximated by:

$$f(V_{1N}) = K_3 (V_1 \sin\beta_1)^n \quad (1)$$

The erosion rate was found experimentally at $\beta_1 = 90°$ and the exponent "n" and the constant K_3 were then determined from equation (1).

By defining the tangential restitution ratio as

$$R_T = V_{2T}/V_{1T}$$

One can write

$$E = K_1 f(\beta_1) V_1^2 \cos^2\beta_1 [1 - R_T^2] + f(V_{1N}) \quad (2)$$

with

$$f(\beta_1) = [1 + CK (K_{12} \sin (\frac{90}{\beta_o} \beta_1)]^2 \quad (3)$$

where

β_o = angle of attack where maximum erosion occurs

$CK = 1 \quad \beta_1 \leq 2 \beta_o$

$CK = 0 \quad \beta_1 > 2 \beta_o$

K_{12} = Material constant.

To find the other constants K_1 and K_{12}, the following two restitution ratios were used:

For silica sand (125-177) impacting steel alloy:

$$R_T = 1.0 - 0.0017 V_1 \sin\beta_1$$

For fly ash impacting steel alloy (Tabakoff and Malak [51]):

$$R_T = 1 + 0.15987 \beta_1 - 2.14461 \beta_1^2 + 1.74705 \beta_1^3$$

where the angle of attack β_1 in the above equations is measured in radians.

The constants K_1, K_{12}, K_3 and exponent "n" as determined from the stainless steel experimental erosion measurements at the different angles of attack are given in Table 11.

Figures 33 through 36 present the computed results using the new models and the corresponding test results. Figures 33 and 34 show that the new prediction models agree with the experiments for fly ash particles at temperatures of 600°F and 1000°F when the particle velocity is below

700 ft/sec. The comparison between the prediction model and the experimental results using sand particles (125-177 microns) is presented in Figs. 35 and 36 for gas temperatures of 600°F and 1000° respectively. From the two figures it can be seen that the agreement is less satisfactory at higher particle velocities.

Scanning Electron Microscopy Studies of Abrasive Particles And Eroded Surfaces

One of the objectives of the present study was to observe the abrasive particles and topography of eroded specimens at different angles of attack, particle velocities and fluid temperatures. The observations were made using a scanning electron microscope ;(25 kw Cambridge Stereoscan 600) equipped with an energy dispersive X-ray analyzer (EDAX). Figures 37, 38 and 39 show the scanning electron micrographs of three samples of fly ash, petroleum product and silica sand particles used in the present study. It is seen from Fig. 37 that the fly ash is composed of discrete, spherical particles. The observations under the microscope revealed that the majority of the particles are smaller than 30 microns. The scanning electron micrograph of petroleum product and silica abrasive are shown in Figs. 38 and 39. The petroleum particles are spherical and 50 microns in diameter. The silica particles characteristics were found to be very different depending on the particle sizes. The micrograph of the 150 microns silica particles shows that their corners are not very sharp for this particle size, however, larger particles were found to have sharp corners (Fig. 39).

Figure 40 shows scanning electron micrographs of two untested samples, one of steel alloy (AM355) and the other of ceramic Al_2O_3. Figure 41 shows the micrographs of the Al_2O_3 and AM355 steel eroded surfaces after being

exposed to petroleum particles impacting at 30° angle of attack. Figures 42a through 42e show the eroded surfaces of five steel alloy (AM355) specimens impacted by fly ash particles at 30° angle of attack. The test temperatures were 60°F, 600°F and 1000°F, and the velocities of 325 ft/sec, 400 ft/sec, 700 ft/sec and 1000 ft/sec. The general appearance of the eroded surfaces is that of intensive surface material flow and plastic deformation. Scanning electron micrographs of steel alloy surface impacted at 30° angle of attack by 150 and 275 microns silica sand, at 325 ft/sec and room temperature (70°F) are shown in Fig. 43. From the inspection of these micrographs, it is clear that under these conditions the surface impacted by the larger particles (275 microns) has deteriorated more than the one impacted by the smaller particles (150 microns). Additional documentation of the influence of the particle size on the surface destruction for steel samples are shown in Figs. 44 and 45. Three different silica sand particle sizes (150, 580 and 1981 microns) were used. The test conditions were as follows: particle velocities of 325, 400 and 700 ft/sec, temperature of 70°F and 1000°F and 30° angle of attack. The scanning electron micrographs in Fig. 44 demonstrates the increase in the surface erosion damage with increased particle velocities when the rest of the test conditions are unchanged. Figure 45 shows that the maximum surface damage is produced by the largest particles at the same ambient temperatures, particle velocities and the angles of attack. Figures 46 and 47 show the eroded surfaces of ceramic (Al_2O_3) material due to silica sand particle impacts normal to the surface at two different temperatures. Figure 46 shows two micrographs of the eroded surfaces impacted by 150 microns silica sand particles at 325 and 450 ft/sec at maximum angle of attack of 90 degrees and ambient temperature of 70°F. Inspection of the two eroded surfaces reveals that the relatively

small increase in the particle velocities does not significantly affect the erosion damage of the ceramic material. Micrographs of another two ceramic surfaces eroded at higher temperatures of 600°F and 1000°F by 150 microns solid particles are shown in Fig. 47. Detailed study of the two scanning micrograph surfaces shows that the increase in the temperature from 600°F to 1000°F did not increase the erosion damage.

SUMMARY AND CONCLUSIONS

1. The velocity exponent 'n' in the erosion prediction model is dependent on the temperature, angle of attack, particle property and target material characteristics. The velocity exponent 'n' of the Al_2O_3 was considerably low compared to the steel alloy.
2. The experimental results of the effect of particle size on the erosion rate did not confirm the theory of the so-called by many authors 'saturation plateau'. The results which were obtained for the particle sizes ranging between 2 and 1981 microns at a given particle velocity shows that the erosion rate is proportional to the size of particles.
3. The effect of temperature on the erosion rate was found to be dependent on the target material. The steel alloy exhibited an increasing erosion rate with increasing temperature, while the ceramic showed a decreasing erosion rate with the temperatures in the range between 316°C (600°F) and 538°C (1000°F).
4. The present measurements confirmed the earlier observations by Grant [26] regarding the negligible influence of the particle concentration on the erosion rate. While this was true up to 0.014 mgm/cm^3 particle

concentrations, it was found that there is a decreasing trend of erosion by increasing the concentrations above 0.25 mgm/cm^3.

5. Grant's [26] erosion prediction models give results that are in agreement with the experimental results at particle velocities below 700 ft/sec.

6. Scanning Electron Micrographs proved that the volume loss of steel alloy (AM355) is larger than that of ceramic (Al_2O_3) and the conclusions 1 and 2.

REFERENCES

1. Hutchings, I.M., "Mechanisms of the Erosion of Metals by Solid Particles," ASTM STP 664 (1977), pp. 59-75.

2. Hutchings, I.M. and Winter, R.E., "Particle Erosion of Ductile Metals: A Mechanism of Material Removal," Wear, 27 (1974), pp. 121-128.

3. Tilly, G.P., "Erosion Caused by Airborne Particles," Wear, 14 (1969), pp. 63-79.

4. Winter, R.E. and Hutchings, I.M., "Solid Particle Erosion Studies Using Single Angular Particles," Wear, 29 (1974), pp. 181-194.

5. Smeltzer, G.E., Gulden, M.E. and Compton, W.A., "Mechanism of Metal Removal by Impacting Dust Particles," Journal of Basic Engineering, September 1970, pp. 639-646.

6. Hutchings, I.M., "Deformation of Metal Surfaces by the Oblique Impact of Square Plates," International Journal of Mechanical Science, 19 (1977), pp. 45-52.

7. Finnie, I., "Erosion of Surfaces by Solid Particles," Wear, 3 (1960), pp. 87-103.

8. Bitter, J.G.A., "A Study of Erosion Phenomena, Part I and II," Wear, 6 (1963), pp. 5-21, 169-190.

9. Neilson, J.M. and Gilchrist, A., "Erosion by a Stream of Solid Particles," Wear, 2 (1968), pp. 111-122.

10. Head, W.J. and Harr, M.E., "The Development of a Model to Predict the Erosion of Materials by Natural Contaminants," Wear, 15 (1970), pp. 1-46.

11. Levy, A.V., "The Platelet Mechanism of Erosion of Ductile Metals," Lawrence Berkeley Laboratory 15240 Rev. Preprint, May 1984.

12. Evans, A.G. and Gulden, M.E., Rosenblatt, M., Proc. R. Soc. London, A 361 (1706), pp. 343-365 (1978).

13. Tilly, G.P., "A Two Stage Mechanism of Ductile Erosion," Wear, 23 (1973), pp. 87-96.

14. Evans, A.G., Treatise on Materials Science and Technology, 16, edited by C.M. Preece, Academic Press, New York (1972), pp. 1-68.

15. Ruff, A.W. and Wiederhorn, S.M., same as reference 14, pp. 69-126.

16. Dimond, C.R., Kirk, J.N. and Briggs, "The Evaluation of Existing Models for Impact Erosion and Abrasive Wear of Ceramic Materials," Morgan Thermic Limited Starport-on-Severn, Worchestershire, United Kingdom.

17. Finnie, I., Wolak, J., and Kabil, Y., "Erosion of Metals by Solid Particles," Journal of Materials, 2 (1967), ASME, pp. 682-700.

18. Christman, T. and Shewmon, P., "Erosion of a Strong Aluminum Alloy," Wear, 52, No. 1, January 1979, pp. 57-70.

19. Salik, J. and Buckley, D., "Effect of Mechanical Surface and Heat Treatments on Erosion Resistance," Proceedings of the International Conference on Wear of Materials: ASME, San Francisco, CA, March-April 1981.

20. Tilly, G.P., "Sand Erosion of Metals and Plastics, A Brief Review," Wear, 14 (1969), pp. 241-243.

21. Stoker, R.L., "Erosion Due to Dust Particles in a Gas Stream," Ind. Eng. Chem., 41 (1949), pp. 1196-1199.

22. Finnie, I., "The Mechanism of Erosion of Ductile Metals," Proceedings of 3rd National Congress of Applied Mechanics, ASME Trans., (1958), pp. 527-532.

23. Sheldon, G.L., "Similarities and Differences in the Erosion Behavior of Materials," Trans. ASME, Journal of Basic Engineering, 92D (1970), pp. 619-626.

24. Sheldon, G.L. and Kanhere, A., "An Investigation of Impingement Erosion Using Particles," Wear, 21, (1972), pp. 195-209.

25. Goodwin, J.E., Sage, W. and Tilly, G.P., "Study of Erosion by Solid Particles," Pro. Inst. of Mech. Engineers, Vol. 184, Part I, No. 15 (1969-1970), pp. 279-292.

26. Grant, G. and Tabakoff, W., "Erosion Prediction in Turbomachinery Resulting from Environmental Solid Particles," AIAA Journal of Aircraft, Vol. 12, No. 5, May 1975, pp. 471-478.

27. Wakeman, T. and Tabakoff, W., "Erosion Behavior in a Simulated Gas Turbine Engine Compressor Environment," AIAA Journal of Airacraft, Vol. 16, No. 12, December 1979, pp. 828-833.

28. Tabakoff, W, Hamed, A. and Ramachandran, J., "Study of Metals Erosion in High Temperature Coal Gas Stream," Journal of Engineering for Power, Vol. 102, January 1980, pp. 148-152.

29. Hackey, B.J., Wiederhorn, S.M., Proc. 5th Int. Conf. "On Erosion by Solid and Liquid Impact," 1979, ch. 26.

30. Ruff, A.W. and Wiederhorn, S.M., Treatise on Materials Science and Technology, Vol. 16, Edited by C.M. Preece, Academic Press, 1979, p. 69.

31. Evans, A.G., Treatise on Materials Science and Technology, Vol. 16, Edited by C.M. Preece, Academic Press, 1979, p. 1.

32. Evans, A.G., Gulden, M.E. and Roseblatt, M., Proc. Royal Soc. Lon., A, 361 (1978), 343.

33. Marshall, D.B., Evans, A.G., Gulden, M.E., Routhort, J.L. and Scattergood, R.O., "Particle-Size Distribution Effects on Solid Particle Erosion of Brittle Materials," Chapter IX of the Final Reports to the Office of Naval Research Contract No.: N00014-79-C-0159, January 1, 1980 - December 31, 1980.

34. Gulden, M.E., "Solid Particle Erosion of High-Technology Ceramics," STP 664 (1977), pp. 101-121.

35. Sheldon, G.L. and Finnie, I., "The Mechanism of Material Removal in the Erosive Cutting of Brittle Materials," Journal of Eng. for Ind., 11 (1966), pp. 393-400.

36. Sheldon, G.L. and Finnie, I., "On the Ductile Behavior of Nominally Brittle Materials During Erosive Cutting," Journal of Eng. for Ind., November 1966, pp. 387-392.

37. Sage, W. and Tilly, G.P., "The Significance of Particle Size in Sand Erosion of Small Gas Turbine," J. Roy. Aeron. Soc., Vol. 73, May 1969.

38. Kotwal, R. and Tabakoff, W., "A New Approach for Erosion Prediction Due to Fly Ash," ASME Paper 80-GT-96, New Orleans, 1980.

39. Tabakoff, W. and Vittal, B., "High Temperature Erosion Study of INCO 600 Metal," Journal of Wear, 1983, pp. 89-99.

40. Gat, N., and Tabakoff, W., "Effects of Temperature on the Behavior of Metals Erosion by Particulate Matter," Journal of Testing and Evaluation, Vol. 8, No. 4, 1980.

41. Tabakoff, W. and Wakeman, T., "High Temperature Erosion Study of Metals Used in Turbomachinery," ASME Paper 84-GT-168.

42. Head, J., Lineback, L. and Manning, C., "Modification and Extension of a Model for Predicting the Erosion of Ductile Materials," Wear, 23 (1973), pp. 291-298.

43. Wood, C.D. and Espenschade, P.W., "Mechanism of Dust Erosion," SAE Trans., Vol. 73 (1965).

44. Gomaa, N., "Metallurgical Evaluation of Erosion Test Samples of Al 2024 and IN 718," MS Thesis, Univ. of Cincinnati (1982).

45. Young, J.P. and Ruff, A.W., "Particle Erosion Measurement on Metals," Journal of Eng. Materials and Technology, ASME Trans., April 1979, pp. 121-125.

46. Raask, E., "Tube Erosion by Ash Impaction," Wear, 13 (1969), pp. 301-315.

47. Neilson, J.H. and Gilchrist, A., "An Experimental Investigation Into Aspects of Erosion in Rocket Motor Tail Nozzles," Wear, 11 (1968), pp. 123-143.

48. Levy, A., Slamovich, E. and Jee, N., "Elevated Temperature Combined Erosion - Corrosion of Steels," Lawrence Berkeley Laboratory - 17243 Preprint, April 1984.

49. Maasberg, J.A. and Levy, A.V., "Erosion of Elevated Temperature Corrosion Scales on Metals," Wear, Vol. 73 (1981), pp. 355-370.

50. Sargent, G.A. and Vadjikar, R.M., "Impact of Aluminum by Single Spherical Particles as a Function of Temperature," Wear, Vol. 96, (1984), pp. 143-152.

51. Tabakoff, W. and Malak, M.F., "Laser Measurements of Fly Ash Rebound Parameters for Use in Trajectory Calculations," March 1985.

52. Tabakoff, W. and Ball, R., "An Experimental Investigation of the Particle Dynamics of Quartz Sand Impacting 6A1-4V Titanium in an Erosive Environment," Technical Report, Univ. of Cincinnati, 1974.

53. Tabakoff, W. and Wakeman, T., "Test Facility for Material Erosion at High Temperature," Erosion-Prevention and Useful Applications, ASTM STP 664, 1979, pp. 123-135.

TABLE 1. SUMMARY OF EROSION EXPERIMENTS AT HIGH TEMPERATURE (1958 - 1985)

TARGET MATERIAL	TARGET TEMP.(°F)	PARTICLE MATERIAL	PARTICLE SIZE (MICRONS)	PARTICLE VEL. (FT/SEC)	ANGLE OF ATTACK (DEGREES)	REFERENCE
Aluminum	Amb. - 932	silica	60 - 125	340	40, 90	3
2024 Al	700	Arizona dust	43 - 74	650, 1000	37.5, 60	5
2024 Al	70 - 300	quartz	164	380	20, 60, 90	40
2024 Al	65,300,700	silica sand alumina ash	1 - 2000	200 - 1500	25, 45	27
2024 Al	65,300,800	silica sand alumina ash	1 - 2000	200 - 1500	90	27
A 286	amb.	fly ash		450, 600	15, 25, 45 60, 75, 90	28
A 286	300	fly ash		600, 800	15, 25, 45 60, 75, 90	28
A 286	600 900 1200	fly ash		600,800,1000	15, 25, 45 60, 75, 90	28
11% Cr steel	amb. -932	silica	60 - 125	340	40, 90	3
410 steel	amb. - 700	Arizona dust	43 - 74	650 - 1100	60	5
410 steel	amb. - 300	silica	138	400	20, 60, 90	40

TABLE 1 (Cont'd.). SUMMARY OF EROSION EXPERIMENTS AT HIGH TEMPERATURE (1958 - 1985).

TARGET MATERIAL	TARGET TEMP.(°F)	PARTICLE MATERIAL	PARTICLE SIZE (MICRONS)	PARTICLE VEL. (FT/SEC)	ANGLE OF ATTACK (DEGREES)	REFERENCE
304 steel	77, 932	Al_2O_3	50	110	10 - 90	45
304 steel	900	alumina	7.7 - 185	600, 800, 1000	30	38
304 steel	900	silica	35 - 137.5	600, 800, 1000	30	38
304 steel	900	CG & E fly ash		600, 800, 1000	30	38
304 steel	900	fly ash composition A. G. L.		600, 1000	30	38
304 steel	amb.	fly ash		450, 600	15, 25, 45, 60, 75, 90	28
304 steel	300	fly ash		600, 800	15, 25, 45, 60, 75, 90	28
304 steel	600, 900, 1200	fly ash		600, 800, 1000	15, 25, 45, 60, 75, 90	28
17 - 7 PH steel	amb., 700	Arizona dust	43 - 74	650, 1100	60	5
Mild steel	amb., 755	silica	100	33 - 130	90	46
Nickel alloy	amb. - 932	silica	60 - 125	340	40, 90	3

TABLE 1 (Cont'd.). SUMMARY OF EROSION EXPERIMENTS AT HIGH TEMPERATURE (1958 - 1985).

TARGET MATERIAL	TARGET TEMP.(°F)	PARTICLE MATERIAL	PARTICLE SIZE (MICRONS)	PARTICLE VEL. (FT/SEC)	ANGLE OF ATTACK (DEGREES)	REFERENCE
Titanium alloy	amb. - 932	silica	60 - 125	340	40, 90	3
6Al-4V-Ti	amb., 700	Arizona dust	43 - 74	65, 1000	60	5
6Al-4V-ti	amb. - 300	silica	164	- 390	20, 60, 90	40
Ti 6-4	65, 800, 1300	silica sand alumina ash	1 - 2000	200 - 1500	25, 45, 90	27
Rene 41	900	alumina	7.7 - 185	500 - 1000	30	38
Rene 41	900	silica	35 - 137.5	500 - 1000	30	38
Rene 41	900	CG & E fly ash		500 - 1000	30	38
Rene 41	900	fly ash composition A. G. L.		600, 1000	30	38
Rene 41	amb.	fly ash		450, 600	15, 25, 45, 60, 75, 90	28
Rene 41	300	fly ash		600, 800	15, 25, 45, 60, 75, 90	28
Rene 41	600, 900, 1200	fly ash		600, 800, 1000	15, 25, 45, 60, 75, 90	28

TABLE 1 (Cont'd.). SUMMARY OF EROSION EXPERIMENTS AT HIGH TEMPERATURE (1958 - 1985).

TARGET MATERIAL	TARGET TEMP.(°F)	PARTICLE MATERIAL	PARTICLE SIZE (MICRONS)	PARTICLE VEL. (FT/SEC)	ANGLE OF ATTACK (DEGREES)	REFERENCE
INCO 718	900	alumina	7.7 - 185	600, 800, 1000	30	38
INCO 718	900	silica	90 - 140	600, 800, 1000	30	38
INCO 718	900	CG & E fly ash		500 - 1000	30	38
INCO 718	900	fly ash composition A, G, L		600, 1000	30	38
INCO 718	amb.- 1500	silica sand	165	20 - 1000	25, 45, 90	27
Tantalum	amb.- 300	silica	1 - 150	400	20, 60, 90	40
Cerrowbend alloy	amb.- 140	alumina	210		90	47
Tungsten	amb.- 400	silica	1 - 120	450	60, 90	40

TABLE 1 (Cont'd.). SUMMARY OF EROSION EXPERIMENTS AT HIGH TEMPERATURE (1958 - 1985).

TARGET MATERIAL	TARGET TEMP.(°F)	PARTICLE MATERIAL	PARTICLE SIZE (MICRONS)	PARTICLE VEL. (FT/SEC)	ANGLE OF ATTACK (DEGREES)	REFERENCE
Al 2024	amb.- 920	quartz	- 165	180 - 680	25, 60, 90	44
INCO	530 - 1410	quartz	- 165	242 - 764	25, 90	44
Steel	1470 - 1740	coal ash	5	49	45	48
Steel	1470 - 1740	Al_2O_3	50, 100	49	45	48
310 Stainless Steel	1652, 1796	SIC	50	197		49
Aluminum	662	Steel ball	1570, 2380	131	90	50

TABLE 2. ANALYSIS OF Al_2O_3 TARGET MATERIAL

PURITY	99.8% Al_2O_3
DENSITY	3.88 GRAMS/CC (97.5% OF THEORETICAL)
POROSITY	IMPERVIOUS TO GASES
HARDNESS	91.5 - 93.5 ROCKWELL A
TRANSVERSE STRENGTH	35,000 - 60,000 PSI
COMPRESSIVE STRENGTH	400,000 - 450,000 PSI
OXIDATION RESISTANCE	OK TO OVER 3000 DEGREES F
CORROSION RESISTANCE	RESISTANT TO MOST ACID AND ALKALINE SOLUTIONS. SLIGHTLY ATTACKED BY MOLTEN ALKALIES
THERMAL CONDUCTIVITY	16.5 - 17.0 BTU/HR/FT^2/°F/FT
COEFFICIENT OF THERMAL EXPANSION	3.9 X 10^{-6} °f (70° - 1000°F)
COEFFICIENT OF FRICTION	AGAINST ITSELF: .06 - WET; 0.02 - DRY
DIELECTRIC STRENGTH (ELECTRICAL RESISTANCE)	230 VOLTS/MIL

TABLE 3. ANALYSIS OF FLY ASH PARTICLE

DENSITY	2.0641 gm/cc
PARTICLE SIZE	1 ≈ 40 microns

COMPOSITION	PERCENT WEIGHT
SiO_2	57.09 (%)
Al_2O_3	28.36
TiO_2	1.78
Fe_2O_3	5.20
CaO	0.42
MgO	0.81
K_2O	2.11
Na_2O	0.37
SO_3	0.45
P_2O_3	0.16
Undetermined	3.25

TABLE 4. ANALYSIS OF SILICA SAND PARTICLE
(CENTRAL CO.)

DENSITY	2.6395 gm/cc
PARTICLE SIZE	125 - 177, 243 - 308 microns

COMPOSITION	PERCENT WEIGHT
SiO_2	99.6 (%)
Fe_2O_2	0.018
TiO_2	0.028
Al_2O_3	0.27
LOI	0.10

TABLE 5. ANALYSIS OF FLINT SILICA SAND PARTICLE
(OTTAWA CO.)

DENSITY	2.64106 gm/cc
PARTICLE SIZE	560 - 600 microns

COMPOSITION	PERCENT WEIGHT
SiO_2	98.0 (%)
Fe_2O_2	0.07
TiO_2	0.04
Al_2O_3	1.50
CaO	0.08
LOI	0.25
MgO	0.06
Color	White

TABLE 6. ANALYSIS OF 4 FLINT ABRASIVE SILICA SAND PARTICLE
(INDEPENDENT CO.)

DENSITY	2.61371 gm/cc
PARTICLE SIZE	950 - 1000, 1651 - 1981 microns

COMPOSITION	PERCENT WEIGHT
SiO_2	97.7 (%)
Fe_2O_2	0.30
Al_2O_3	0.45
LOI	0.50
$CaCo_3$	0.55
CI	0.0004
Hardness (HOH's)	6.5 - 7%
PH Factor	6.55%
Moisture (H_2O)	0.02%
Color	Yellow

TABLE 7. SUMMARY OF THE EXPERIMENTS.

TARGET MATERIAL	PARTICLE MATERIAL		TARGET TEMP. (°F)	PARTICLE VEL. (FT/SEC)	ANGLE OF ATTACK (DEGREES)
AM355	Petroleum Product		70	325	15,20,25,30,35, 45,60,75,90
	Fly Ash		70	325	15,20,25,30,35, 45,60,75,90
			600,1000	400,700,1000	20,30,45,60,90
	Silica Sand	125-177μ	70	325,500	20,30,45,60,90
			600,1000	400,700	20,30,45,60,90
		177-243μ	70	325	30
		243-308μ	70	325	20,30,45,60,90
			600,1000	400	20,30,45,60,90
		560-600μ	70	325	20,30,45,60,70
			600,1000	400	20,30,45,60,90
		950-1000μ	70	325	20,30,45,60,90
			600,1000	400	20,30,45,60,90
		1000-1651μ	70	325	30
		1651-1981μ	70	325	20,30,45,60,90
Al_2O_3	Silica sand	125-177μ	70	250	90
			70	325	20,30,45,60,90
			70,600,800,1000	450	90

TABLE 8. FLY ASH IMPACT ON AM355.

Temperature °C (°F)	Angle of Attack (°)	Erosion Volume Parammeter ($cm^3/gm \times 10^4$)			Velocity Index 'n'
		V_p=122m/ses	V_p=213m/sec	V_p=305m/sec	
316 (600)	20	o.o75	0.285	0.831	2.623
	30	0.091	0.324	0.938	2.546
	45	0.069	0.253	0.741	2.591
	60	0.048	0.195	0.514	2.588
	90	0.029	0.080	0.229	2.255
538 (1000)	20	0.069	0.360	1.188	3.106
	30	0.080	0.421	1.463	3.172
	45	0.059	0.309	1.106	3.199
	60	0.035	0.213	0.813	3.433
	90	0.011	0.081	0.418	3.970

TABLE 9. SILICA SAND (125 - 177 MICRONS) IMPACT ON AM355.

Temperature °C (°F)	Angle of Attack (°)	Erosion Volume Parameter ($cm^3/gm \times 10^4$)				Velocity Index 'n'
		V_p=99m/sec	V_p=122m/sec	V_p=152m/sec	V_p=213m/sec	
20 (68)	20	0.386		1.034		2.298
	30	0.453		1.090		2.048
	45	0.373		1.052		2.418
	60	0.320		0.877		2.351
	90	0.266		0.586		1.842
316 (600)	20		0.589		1.998	2.192
	30		0.645		2.363	2.330
	45		0.506		2.097	2.551
	60		0.450		1.700	2.385
	90		0.322		1.148	2.281
538 (1000)	20		0.650		2.387	2.334
	30		0.677		2.712	2.490
	45		0.564		2.401	2.599
	60		0.480		1.936	2.503
	90		0.338		1.332	2.461

TABLE 10. SILICA SAND (125 - 177 MICRONS) IMPACT ON Al_2O_3.

Temperature °C (°F)	Angle of Attack (°)	Erosion Volume Parameter ($cm^3/gm \times 10^4$)			Velocity index 'n'
		V_p=76m/sec	V_p=99m/sec	V_p=137m/sec	
20 (68)	90	0.268	0.2912	0.3531	0.468

TABLE 11. EROSION MODEL CONSTANTS

PARTICLE	TEMP (f)	Vp(fPS)	K_1	K_{12}	K_3	'n'
Fly Ash	70	325	1.94×10^{-6}	0.2383	0.024	
"	600	400–700	1.37×10^{-6}	0.1945	1.3×10^{-8}	2.37
		1000	2.14×10^{-6}	0.2165	1.3×10^{-8}	2.37
"	1000	400–700	1.54×10^{-6}	0.194	1.45×10^{-13}	4.112
		1000	3.31×10^{-6}	0.1516	1.45×10^{-13}	4.112
Silica Sand (126 - 177)	70	325–500	7.765×10^{-6}	0.0299	5.052×10^{-6}	1.8303
(126 - 177)	600	400–700	6.46×10^{-6}	-0.0037	3.0×10^{-7}	2.27
	1000	400–700	7.065×10^{-6}	0.02625	1.07×10^{-7}	2.449

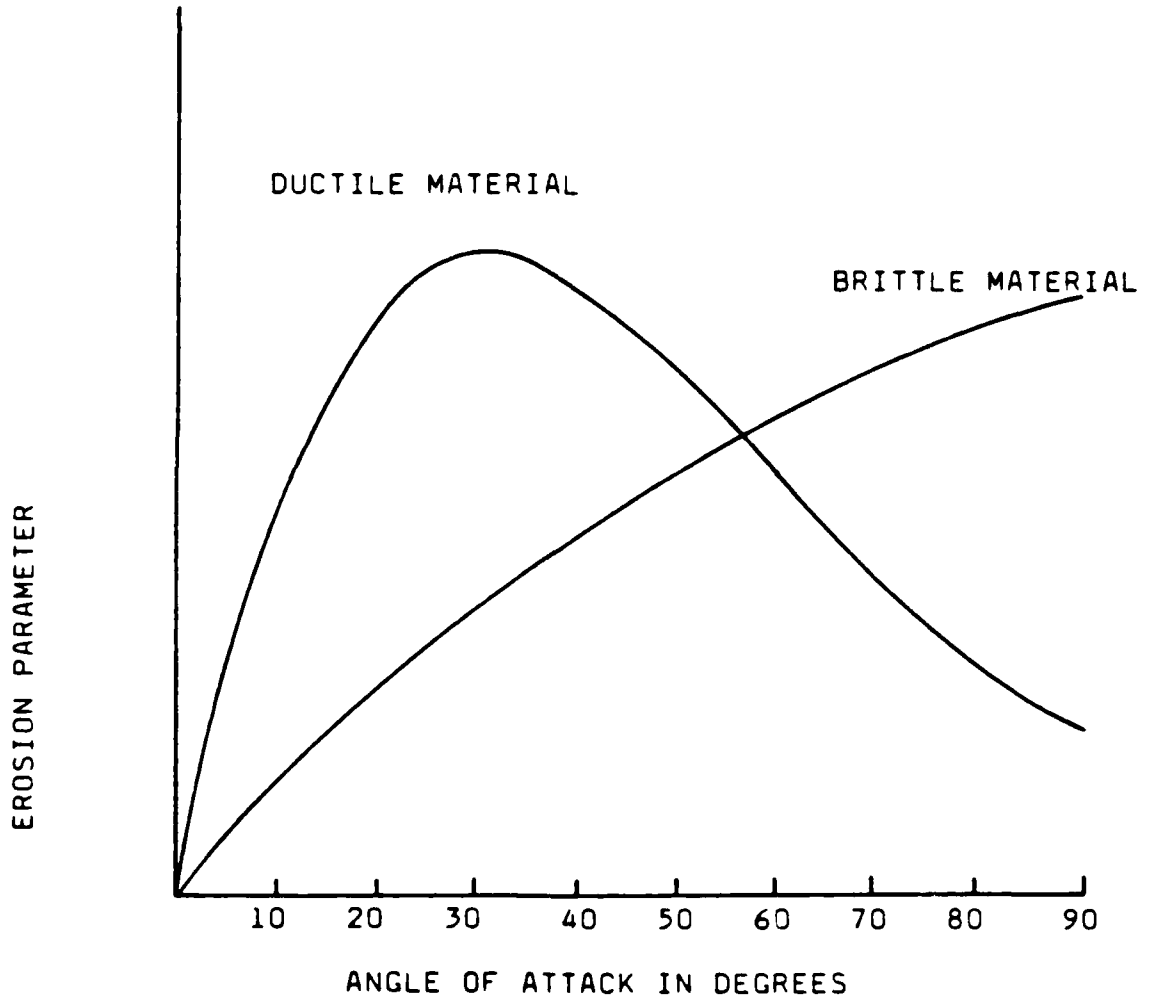

FIG. 1. EFFECT OF ANGLES OF ATTACK

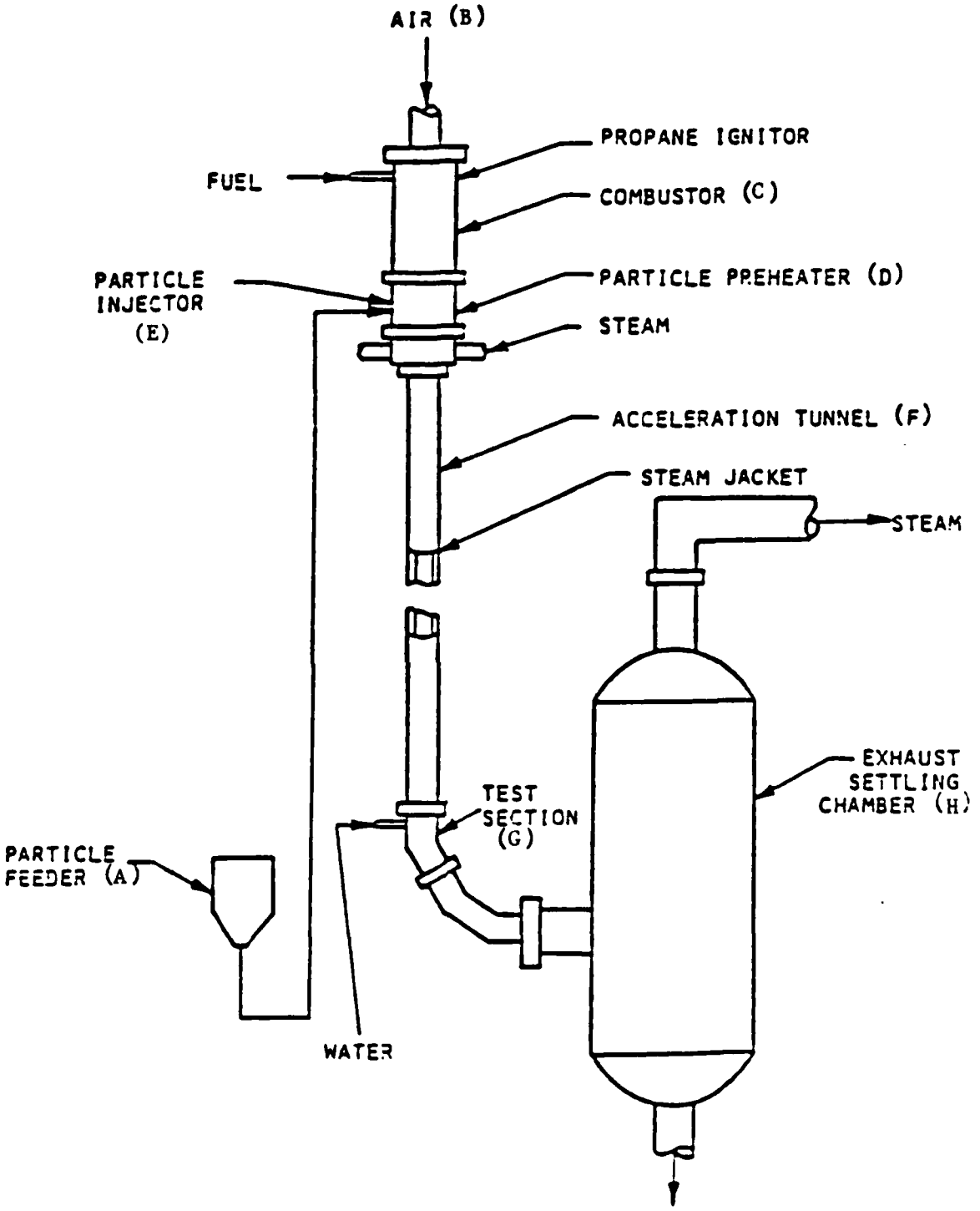

FIG. 2. SCHEMATIC OF TEST APPARATUS.

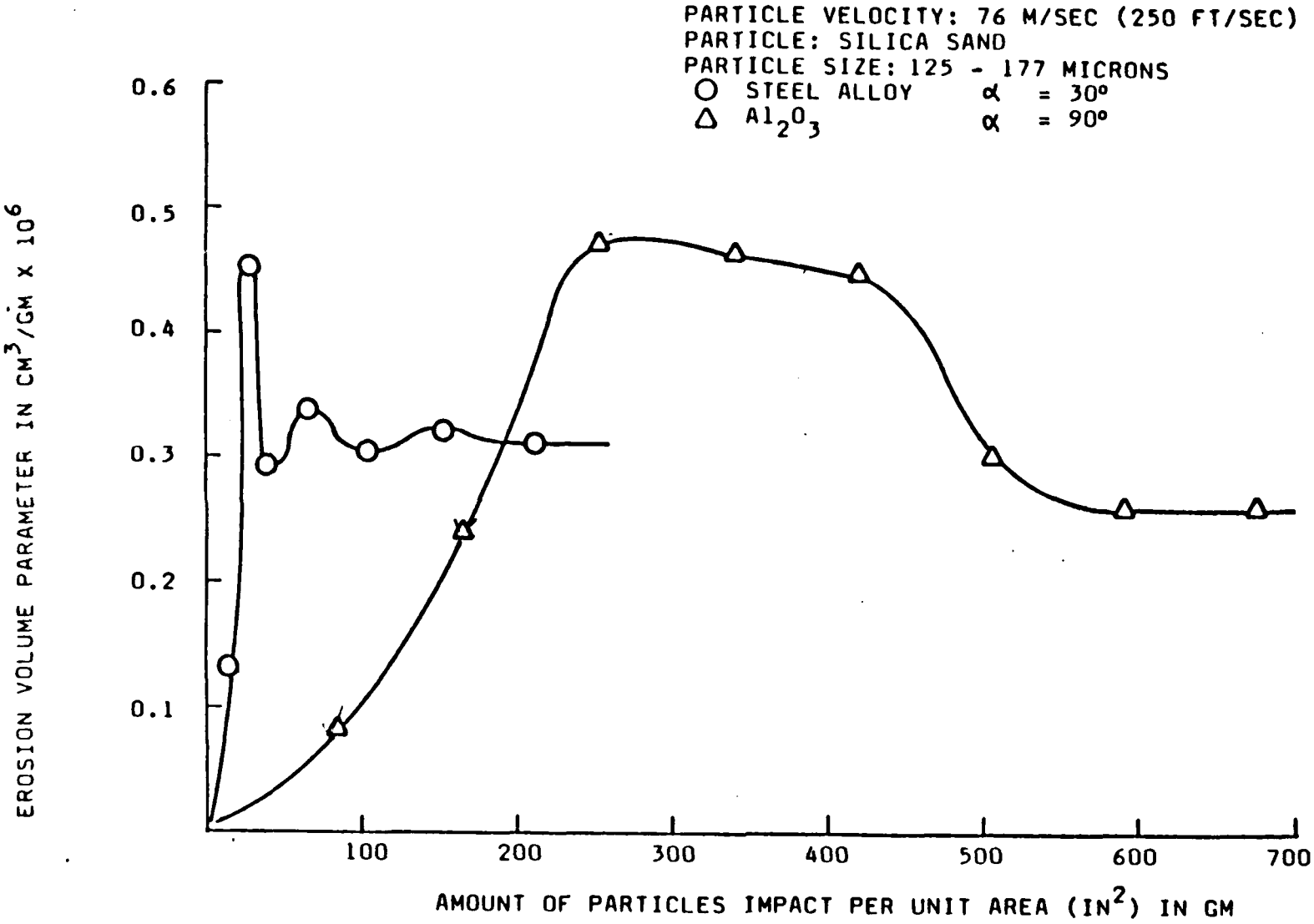

FIG. 3. EFFECT OF PARTICLE QUANTITIES AT MAXIMUM EROSIVE ANGLE OF ATTACK AND AT ROOM TEMPERATURE

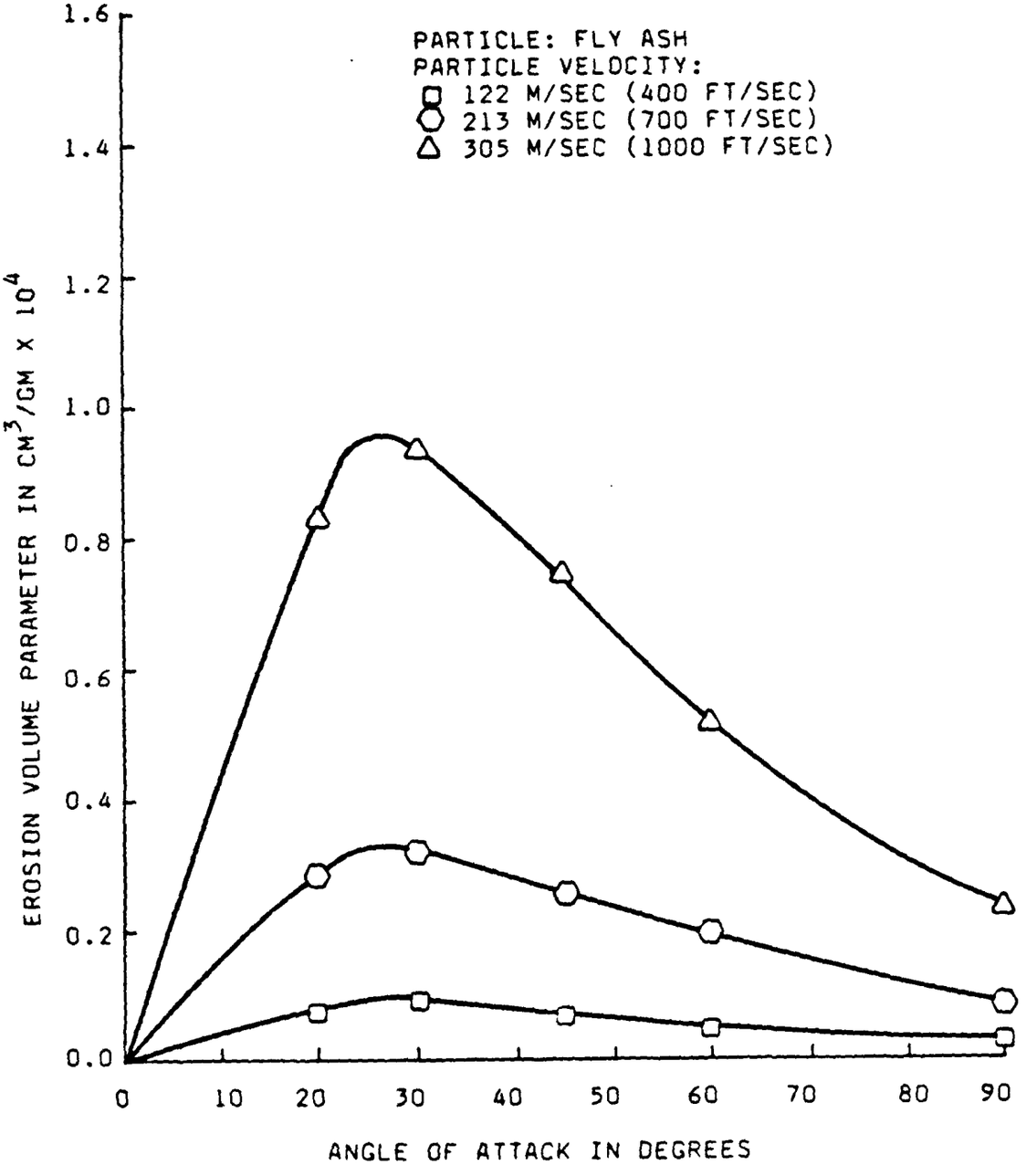

FIG. 4 EFFECT OF PARTICLE VELOCITY AND ANGLE OF ATTACK ON AM355 ALLOY AT 316°C (600°F)

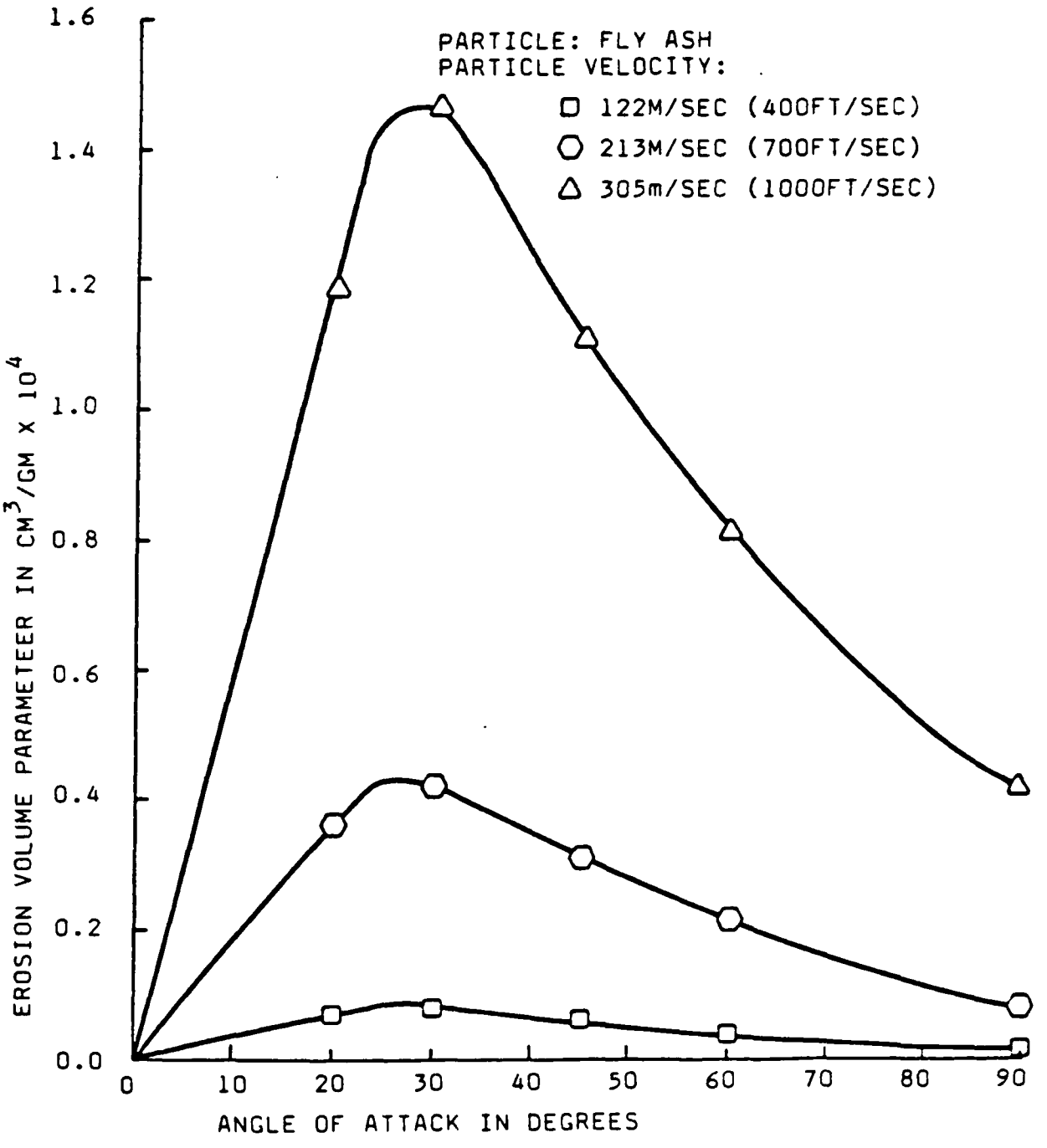

FIG. 5. EFFECT OF PARTICLE VELOCITY AND ANGLE OF ATTACK ON AM355 ALLOY AT 538°C (1000°F)

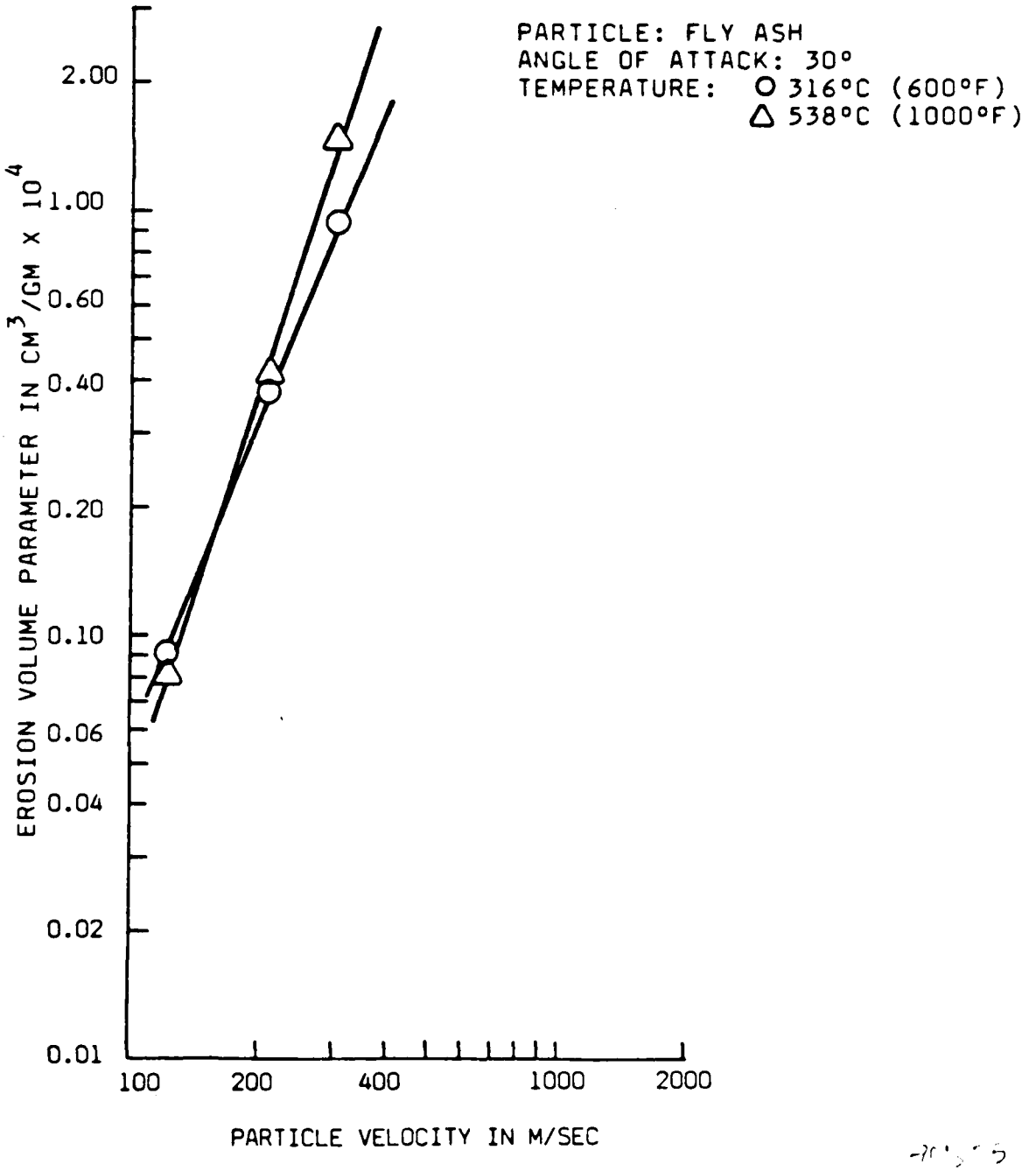

FIG. 6. EFFECT OF PARTICLE VELOCITY ON AM355 ALLOY AT MAXIMUM EROSIVE ANGLE OF ATTACK

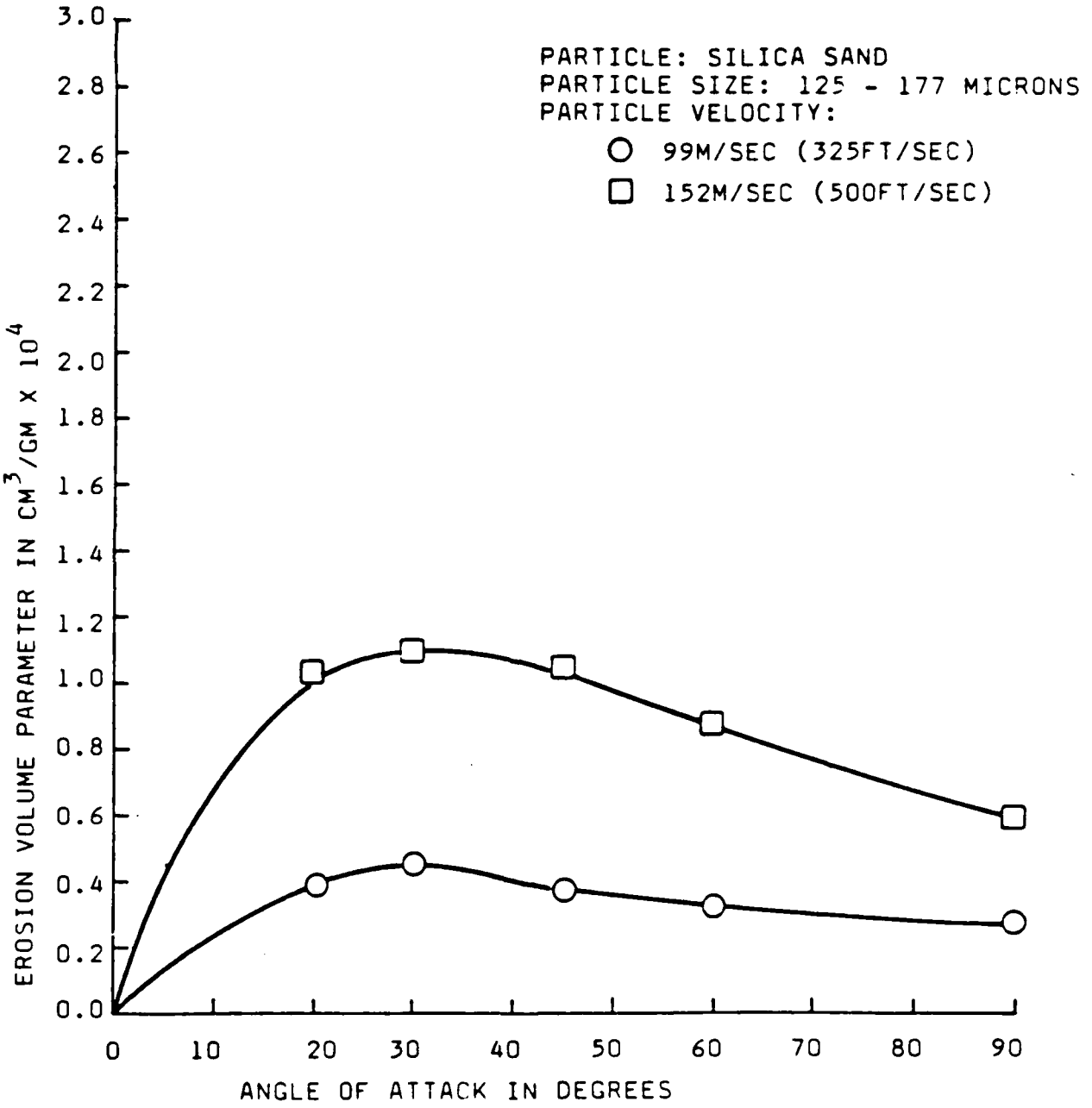

FIG. 7. EFFECT OF PARTICLE VELOCITY AND ANGLE OF ATTACK ON AM355 ALLOY AT ROOM TEMPERATURE

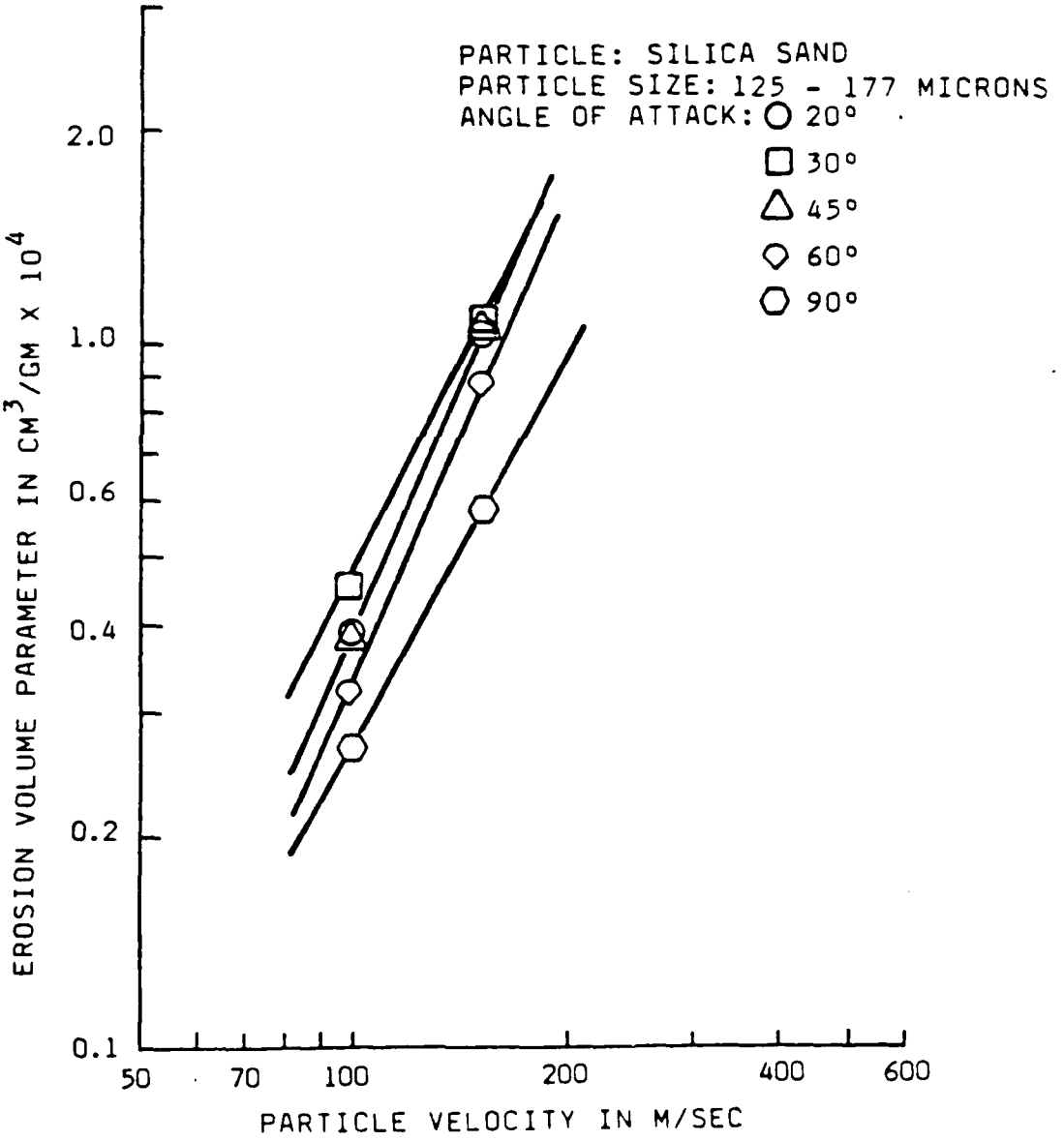

FIG. 8. EFFECT OF PARTICLE VELOCITY AND ANGLE OF ATTACK ON AM355 ALLOY AT ROOM TEMPERATURE

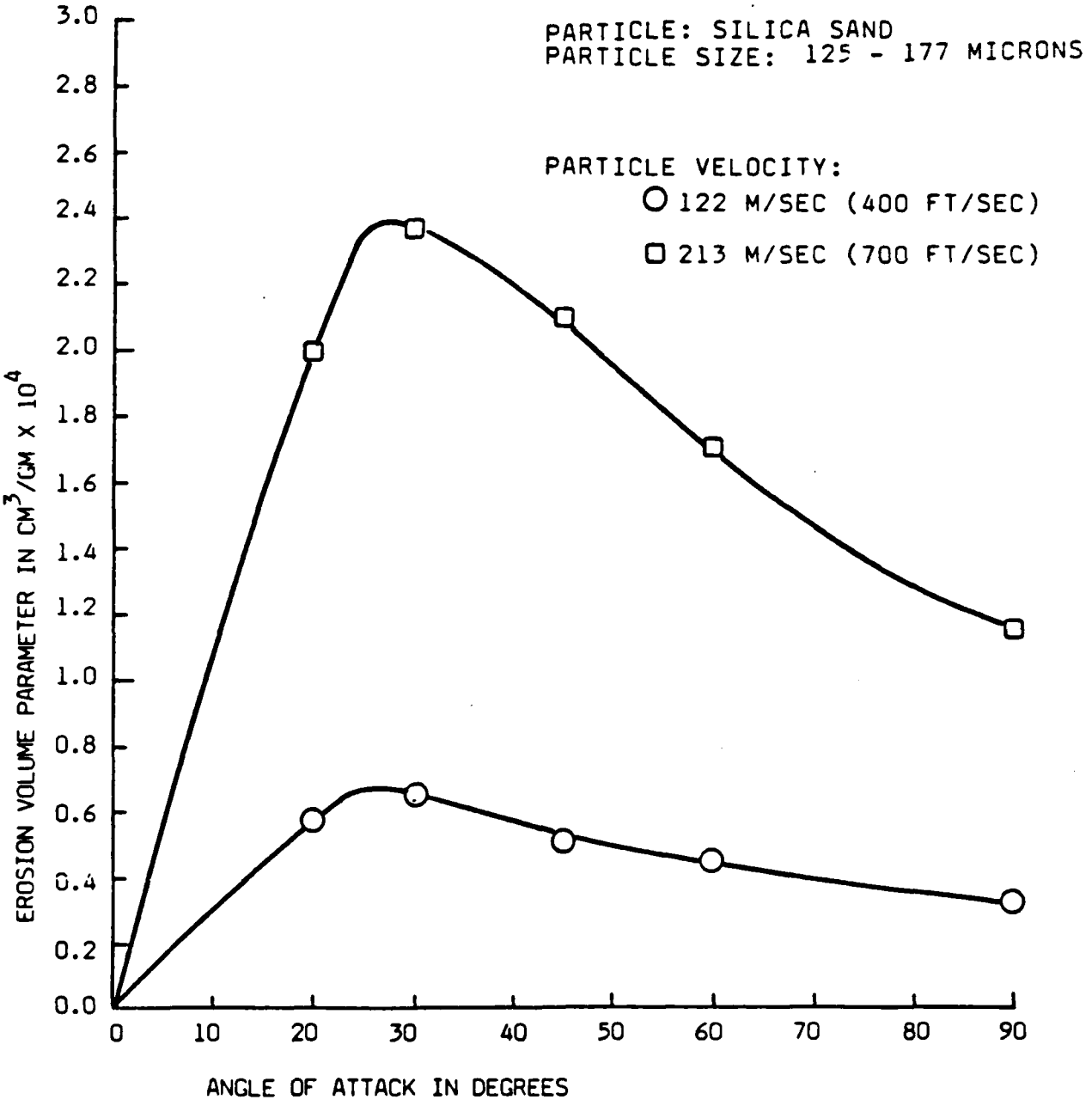

FIG. 9. EFFECT OF PARTICLE VELOCITY AND ANGLE OF ATTAC‹ ON AM355 ALLOY AT 316°C (600°F)

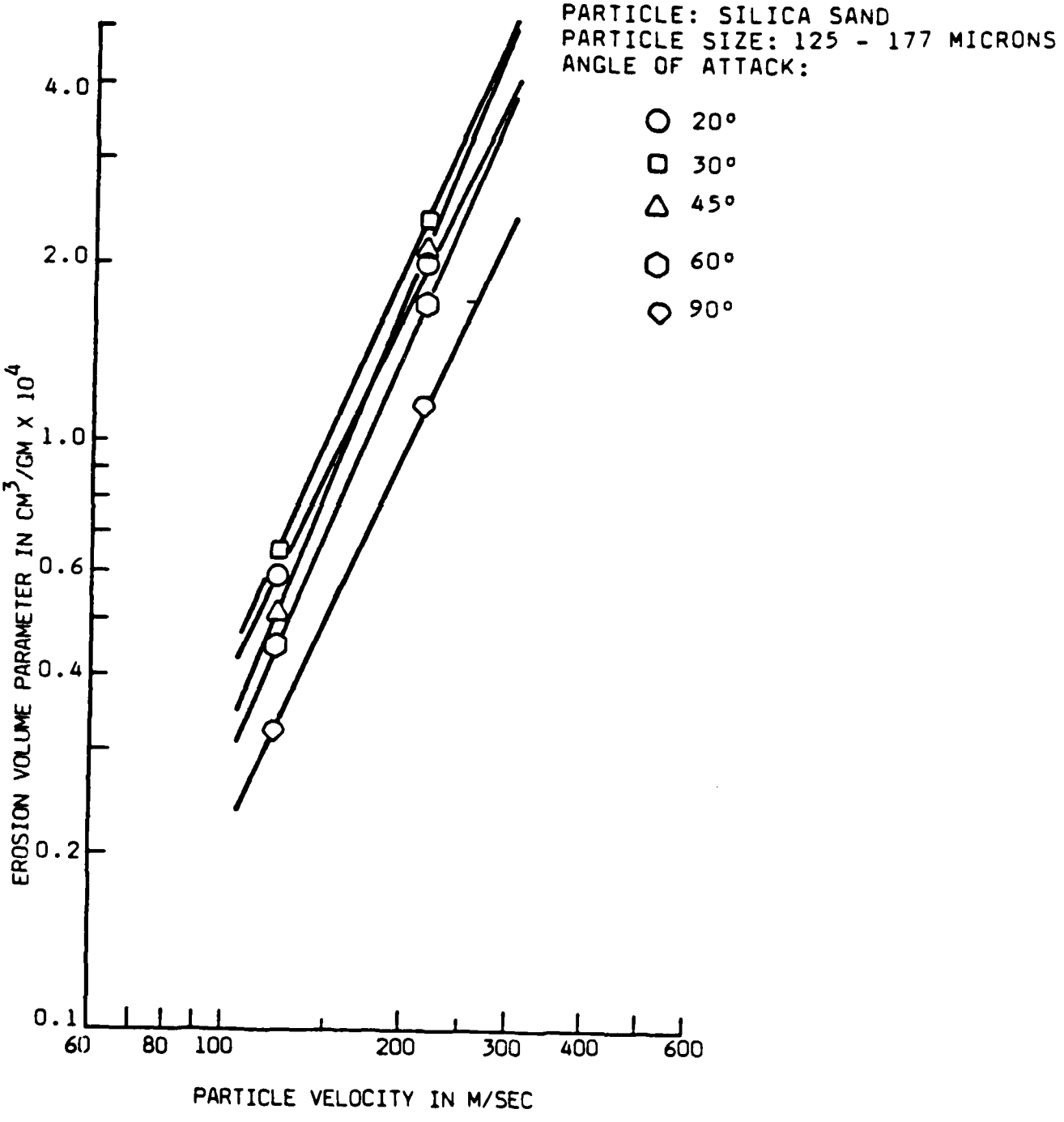

FIG. 10. EFFECT OF PARTICLE VELOCITY AND ANGLE OF ATTACK ON AM355 ALLOY AT 316°C (600°F)

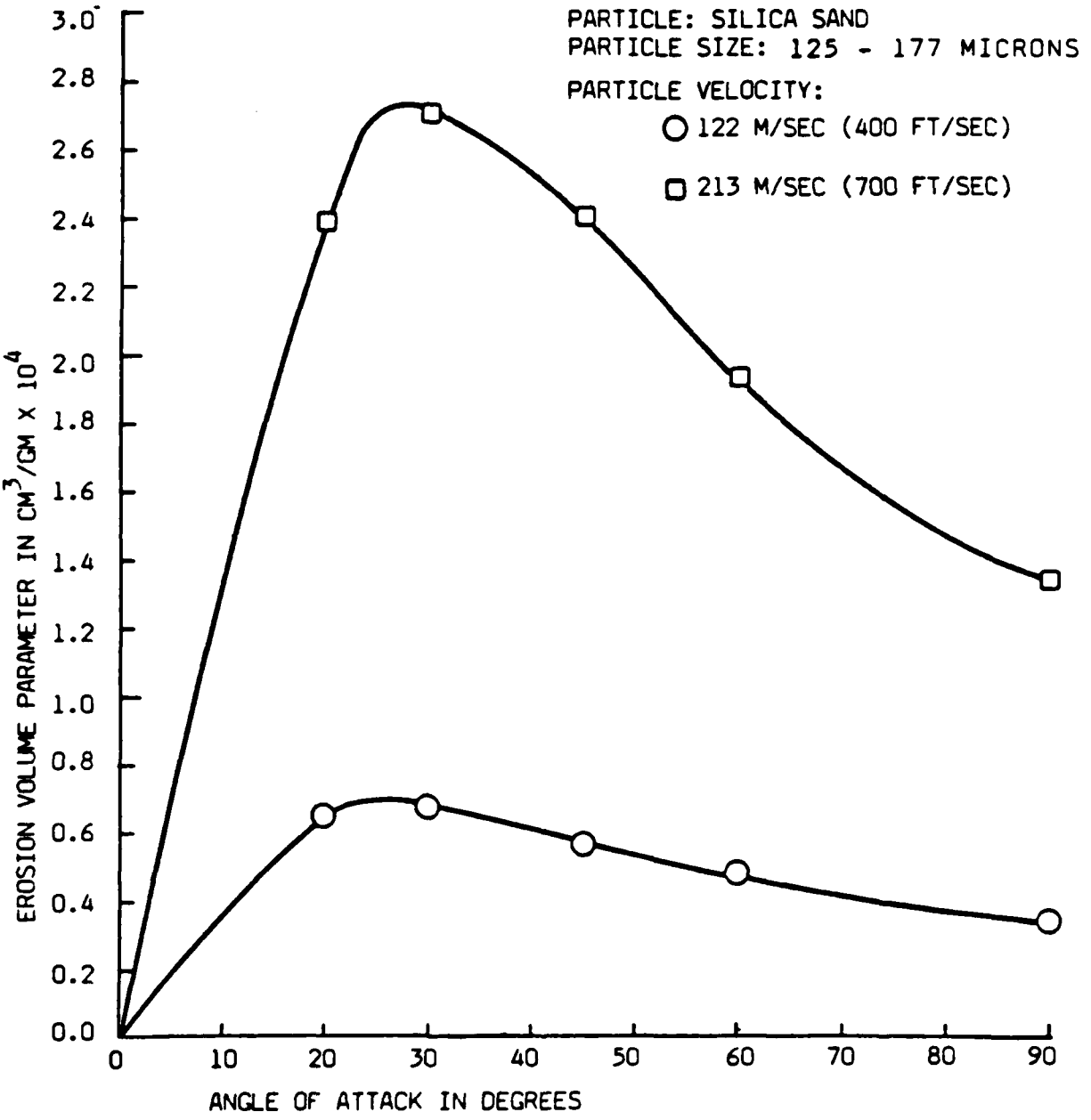

FIG. 11. EFFECT OF PARTICLE VELOCITY AND ANGLE OF ATTACK ON AM355 ALLOY AT 538°C (1000°F)

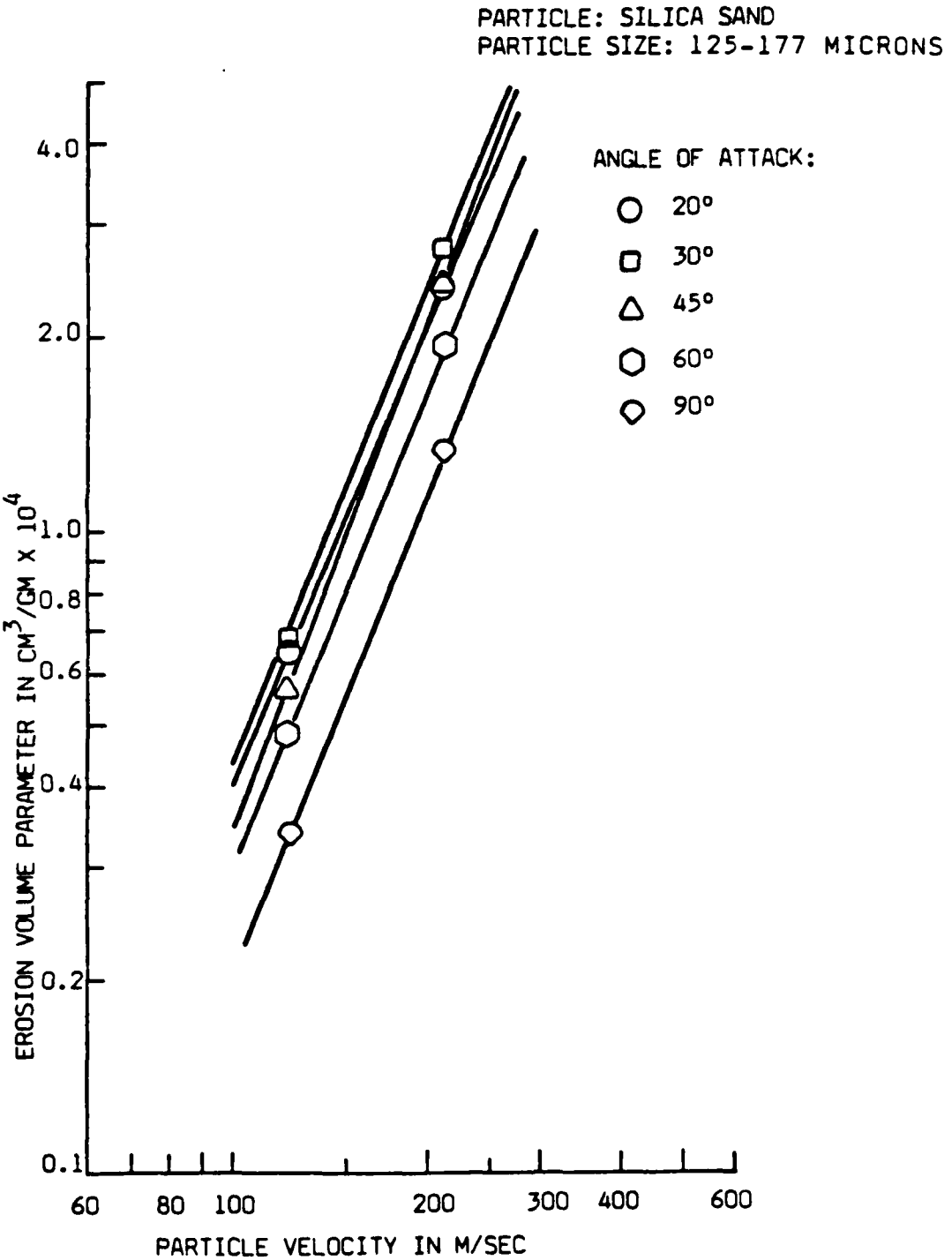

FIG. 12. EFFECT OF PARTICLE VELOCITY AND ANGLE OF ATTACK ON AM355 ALLOY AT 538°C (1000°F)

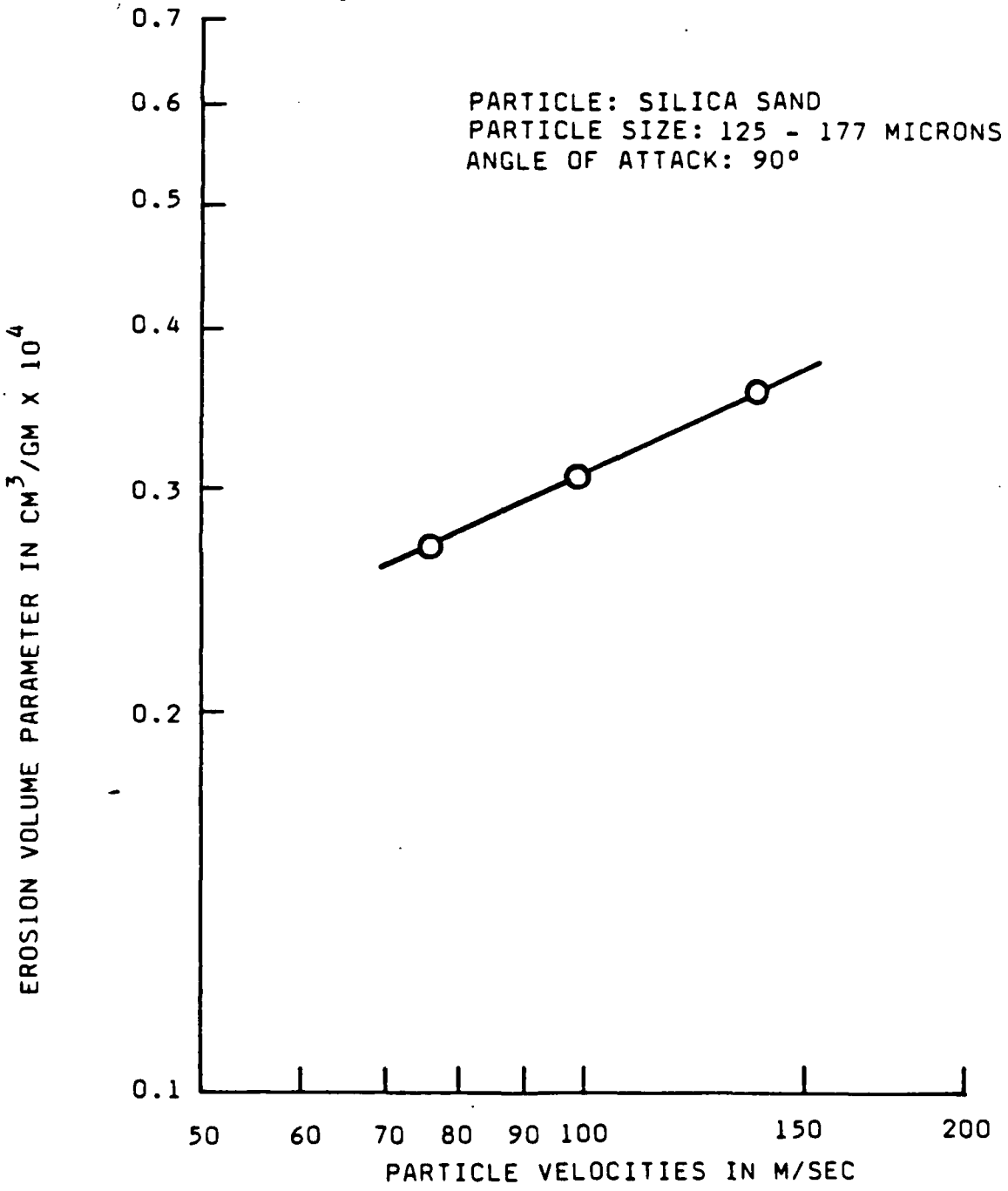

FIG. 13. EFFECT OF PARTICLE VELOCITY ON Al_2O_3 AT ROOM TEMPERATURE

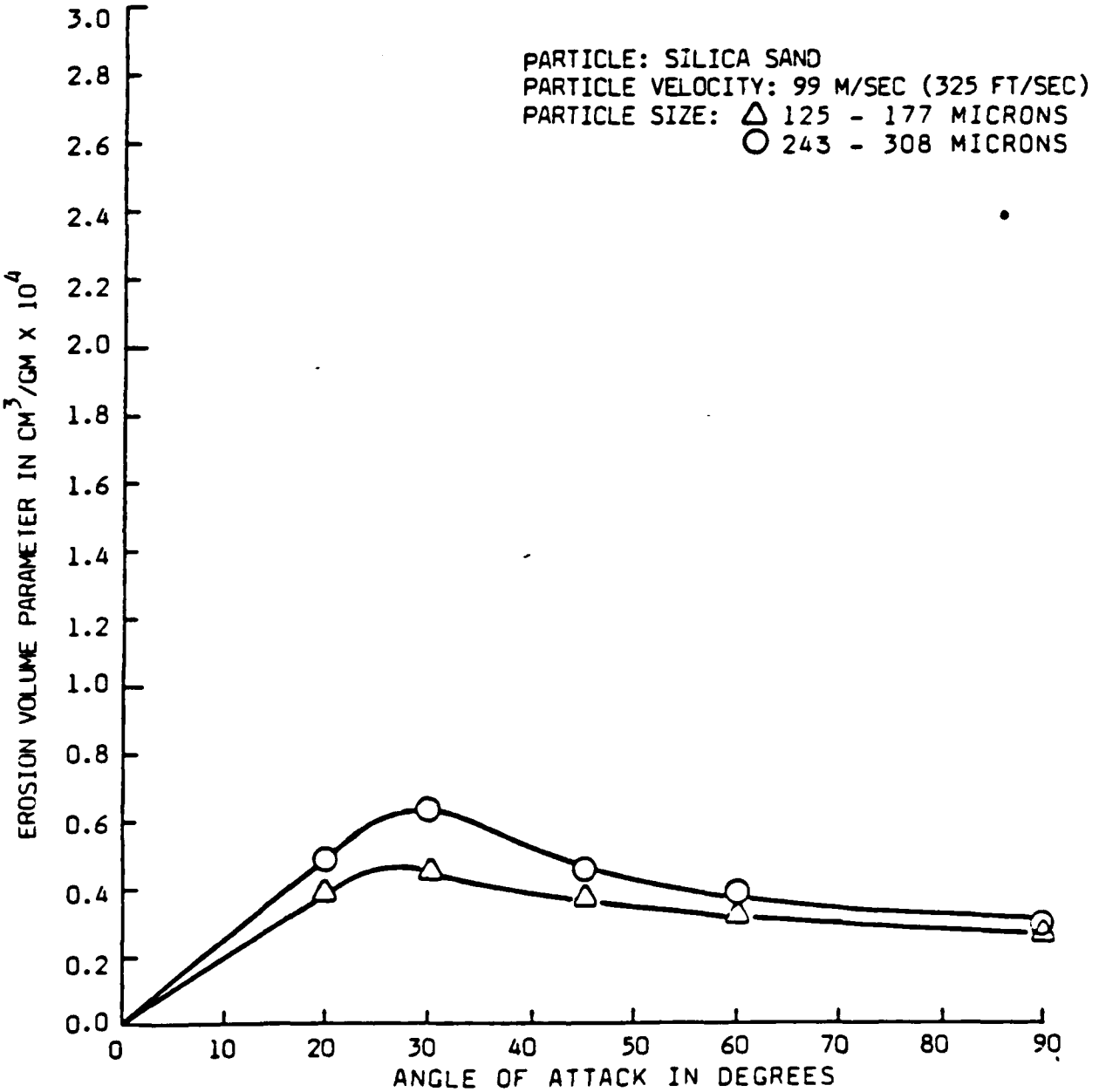

FIG. 14. EFFECT OF PARTICLE SIZE AND ANGLE OF ATTACK ON AM355 ALLOY AT ROOM TEMPERATURE

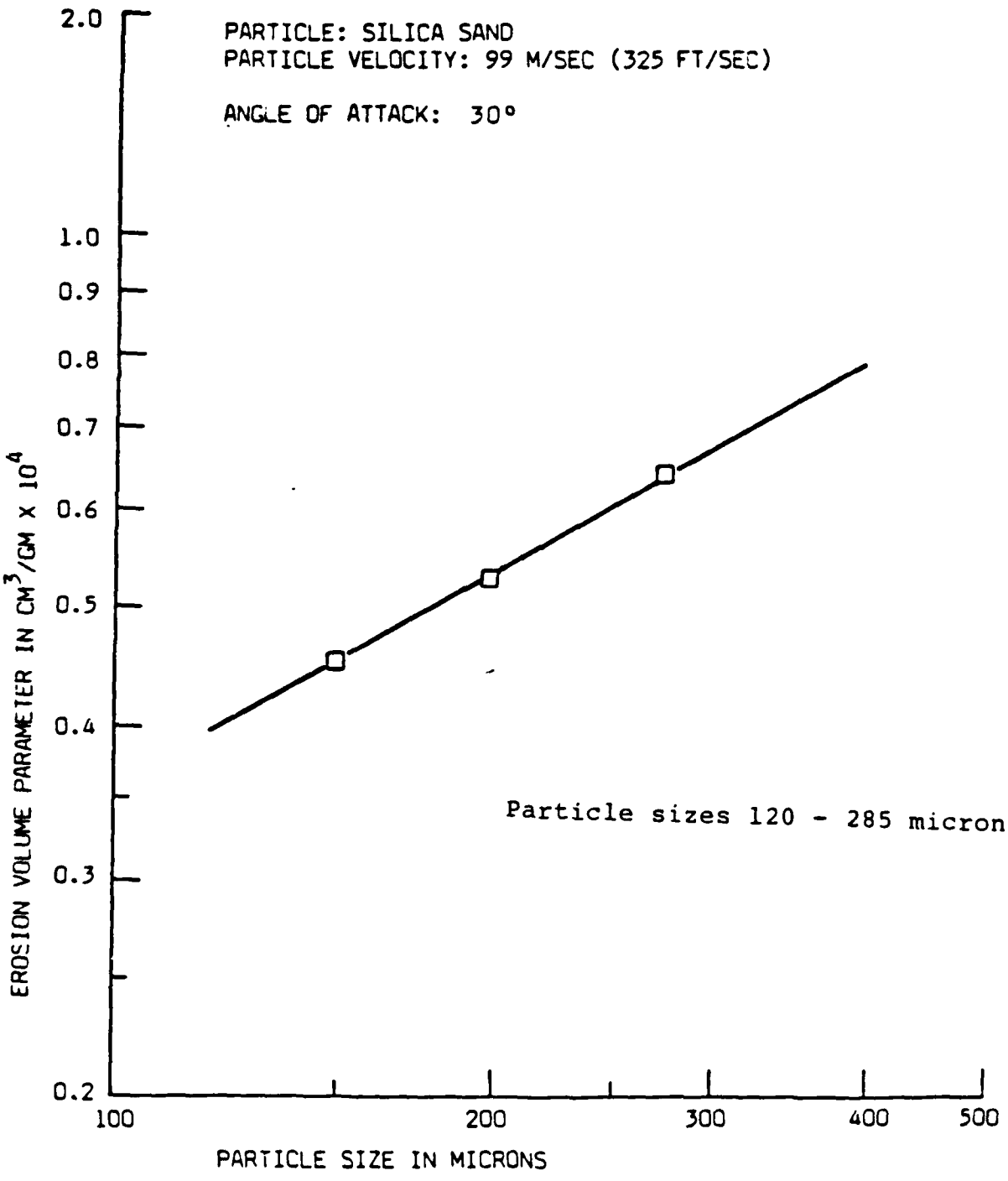

FIG. 15. EFFECT OF PARTICLE SIZE ON AM355 ALLOY AT ROOM TEMPERATURE

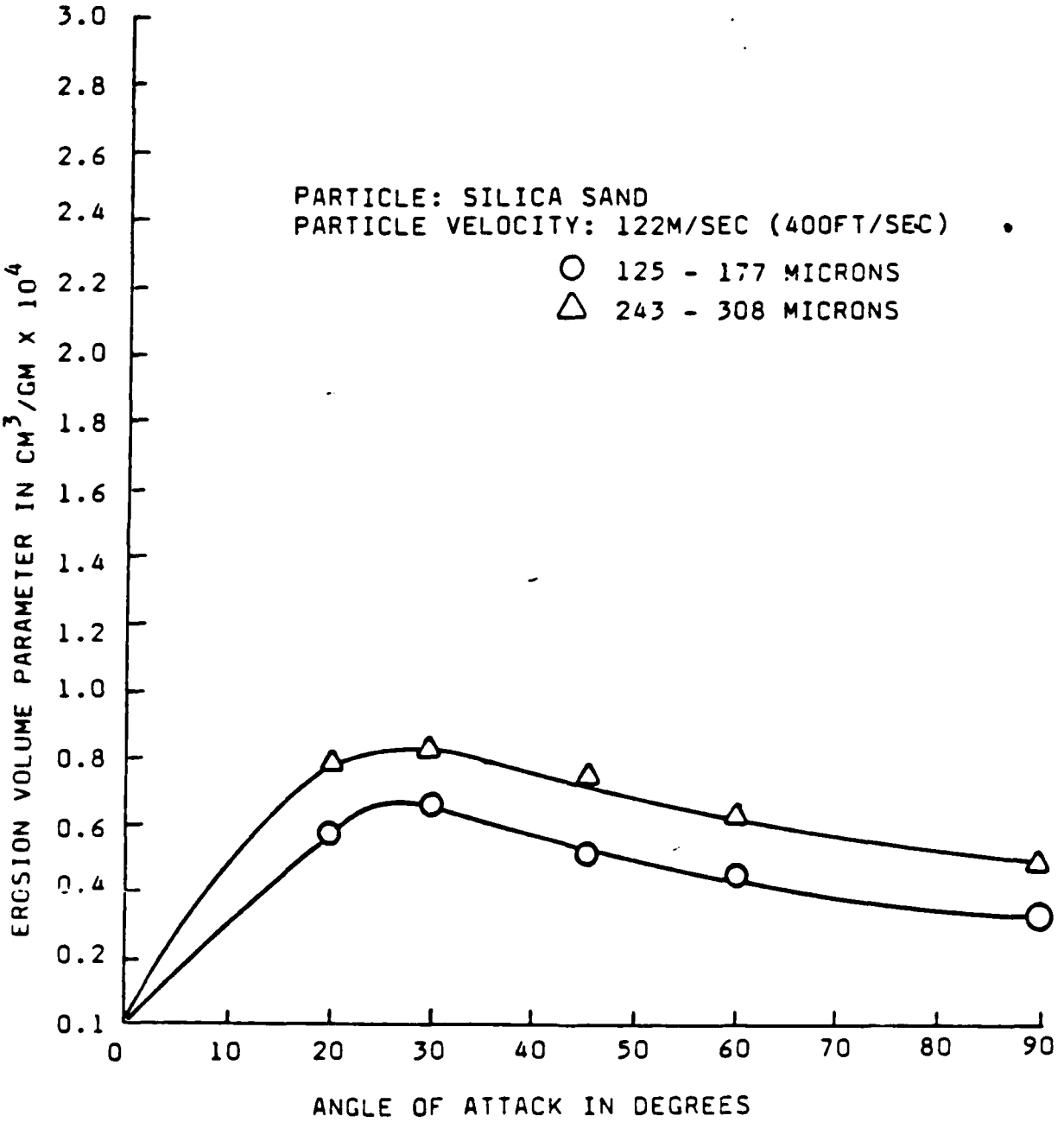

FIG. 16. EFFECT OF PARTICLE SIZE AND ANGLE OF ATTACK ON AM355 ALLOY AT 316°C (600°F)

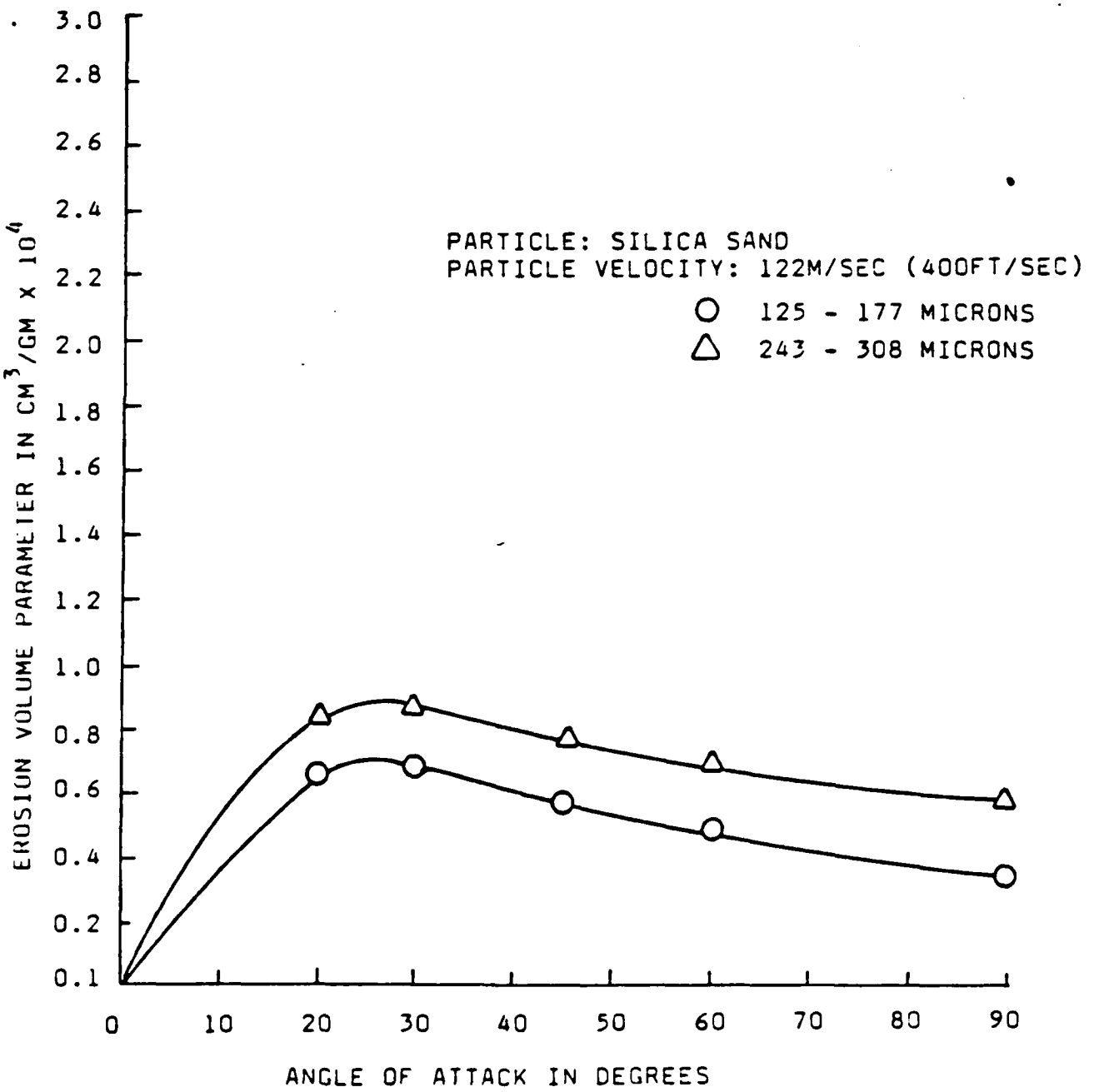

FIG. 17. EFFECT OF PARTICLE SIZE AND ANGLE OF ATTACK ON AM355 ALLOY AT 538°C (1000°F).

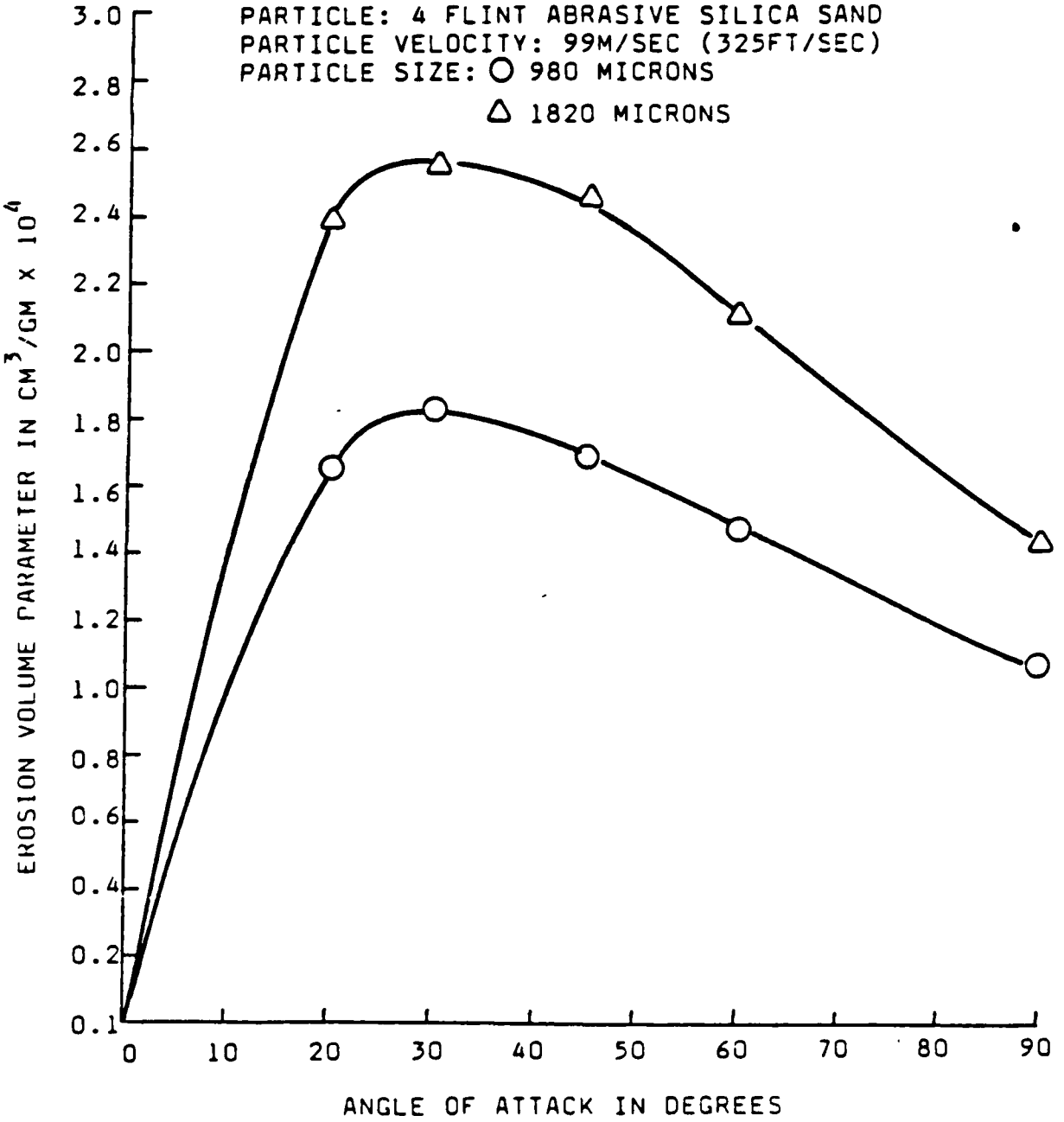

FIG. 18. EFFECT OF PARTICLE SIZE AND ANGLE OF ATTACK ON AM355 ALLOY AT ROOM TEMPERATURE

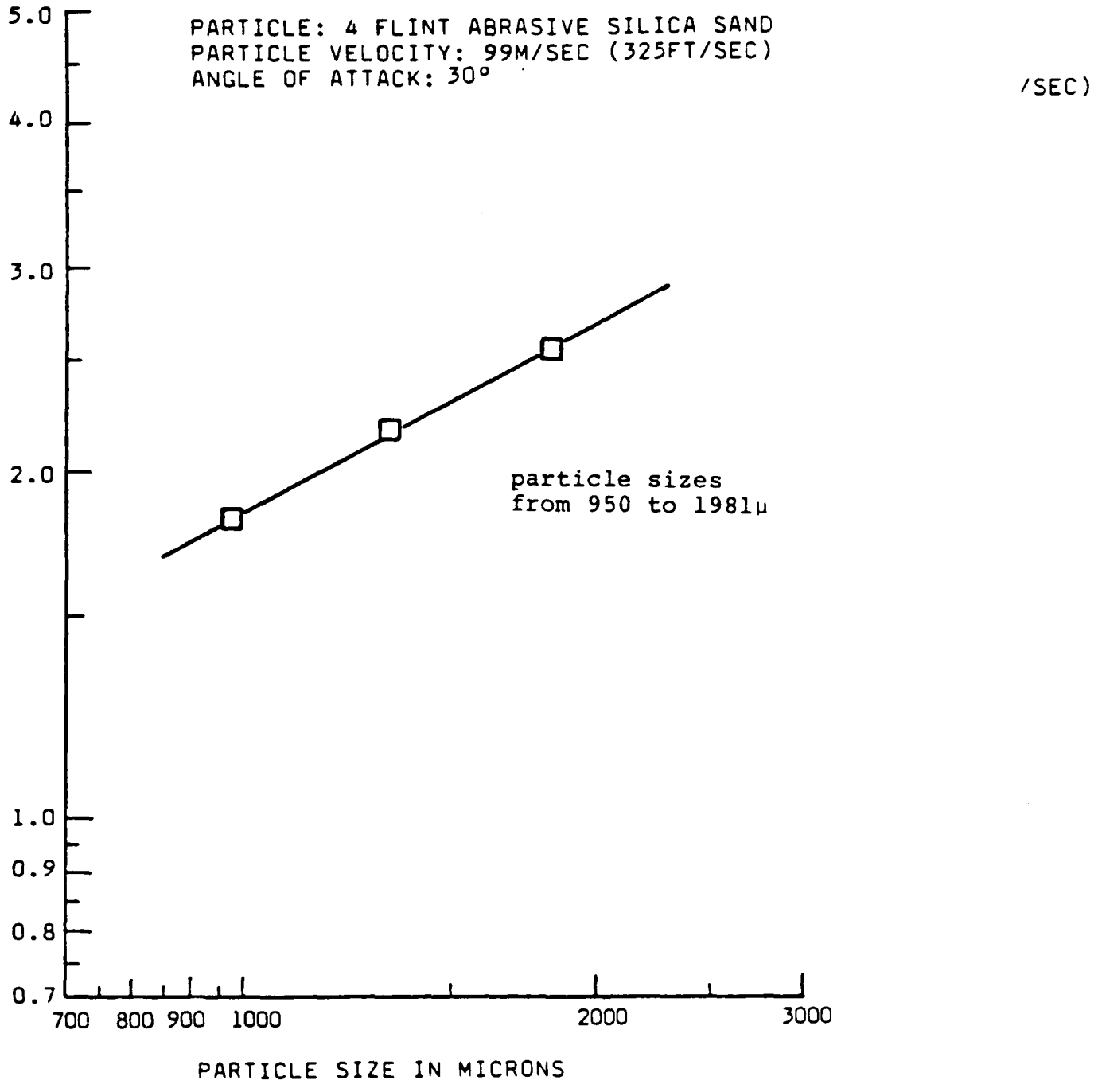

FIG. 19. EFFECT OF PARTICLE SIZE ON AM355 ALLOY AT ROOM TEMPERATURE

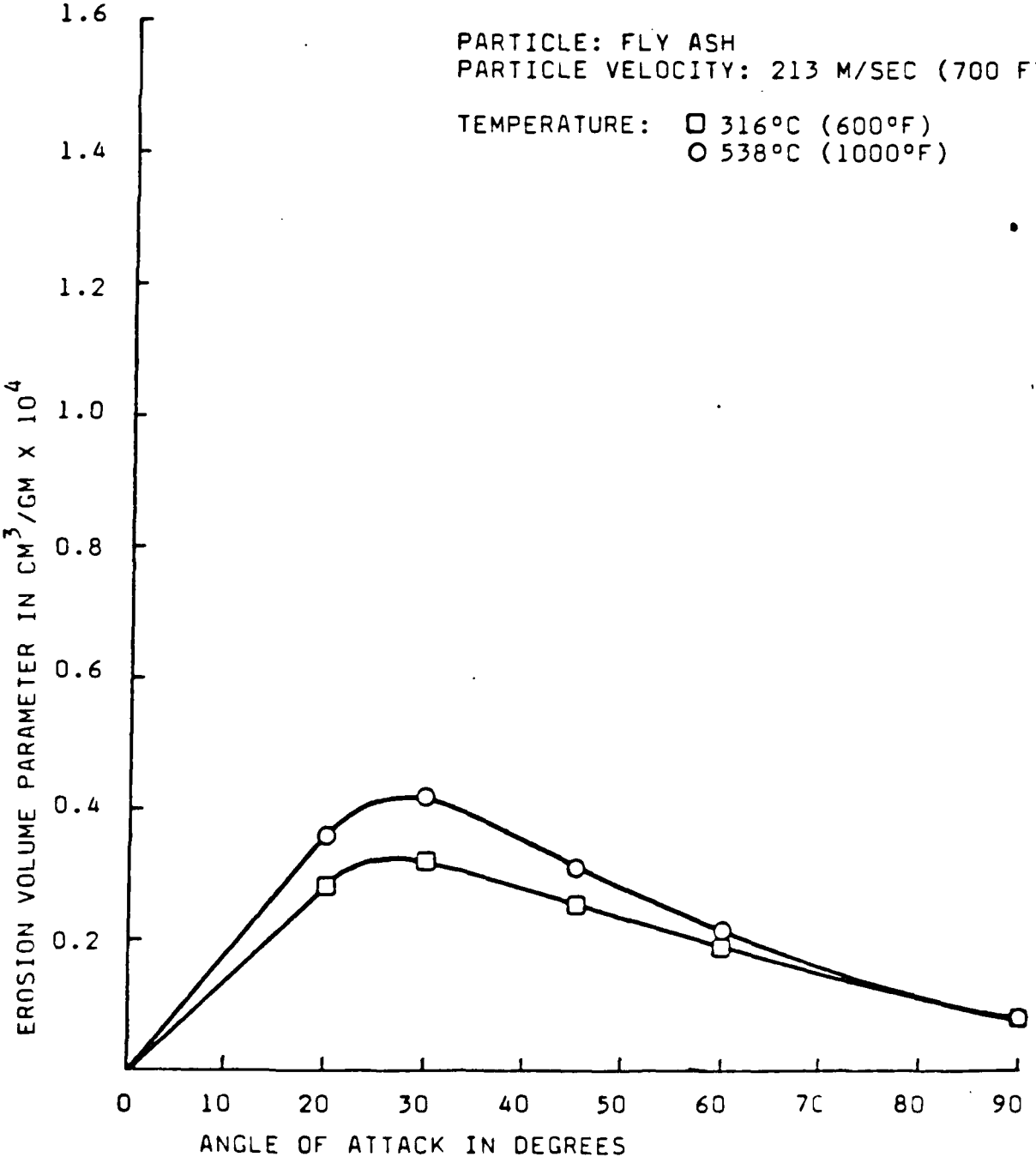

FIG. 20. EFFECT OF TEMPERATURE AND ANGLE OF ATTACK ON AM355 ALLOY

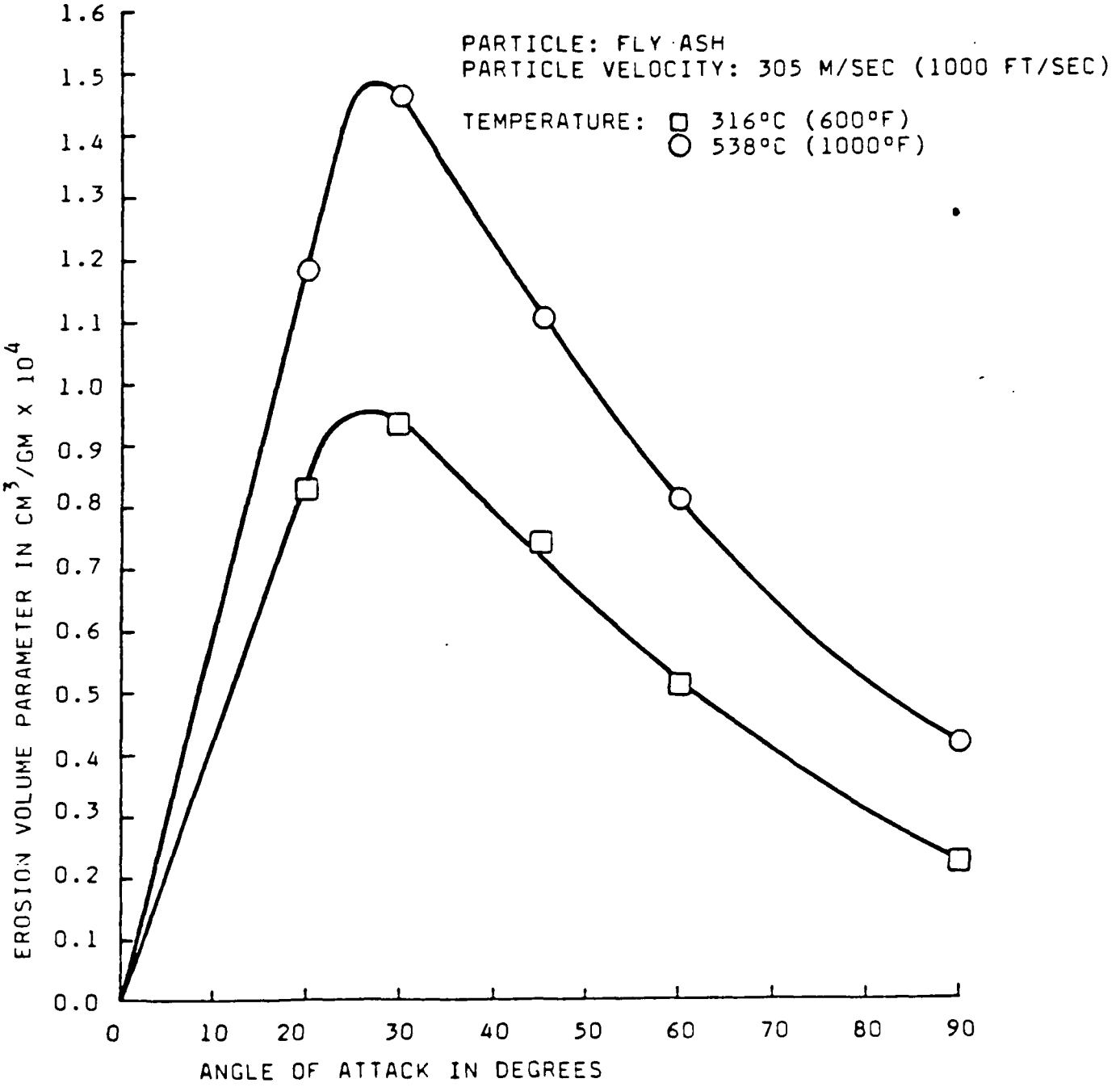

FIG. 21. EFFECT OF TEMPERATURE AND ANGLE OF ATTACK ON AM355 ALLOY

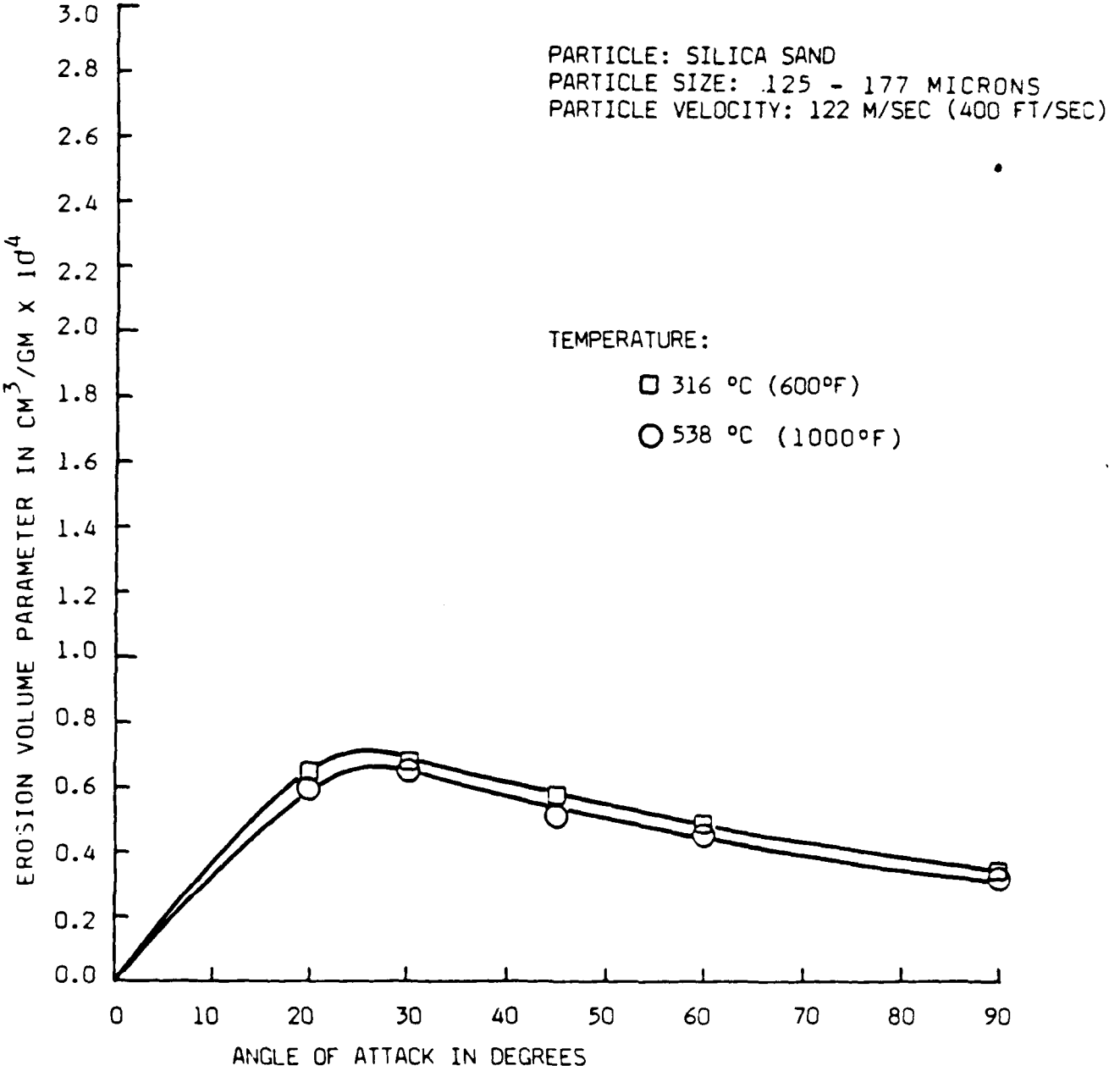

FIG. 22. EFFECT OF ANGLE OF ATTACK AND TEMPERATURE ON AM355 ALLOY

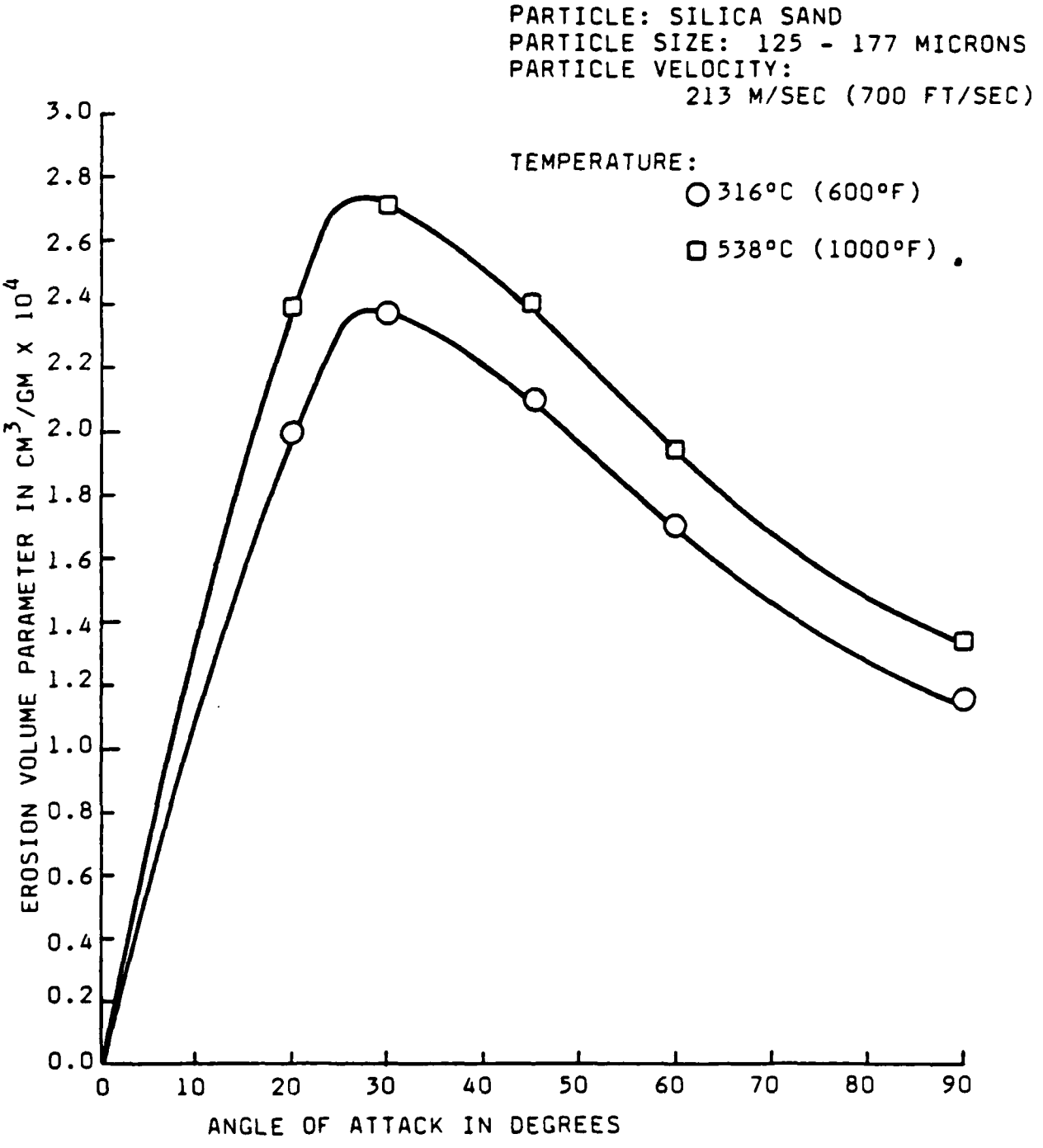

FIG. 23. EFFECT OF TEMPERATURE AND ANGLE OF ATTACK ON AM355 ALLOY

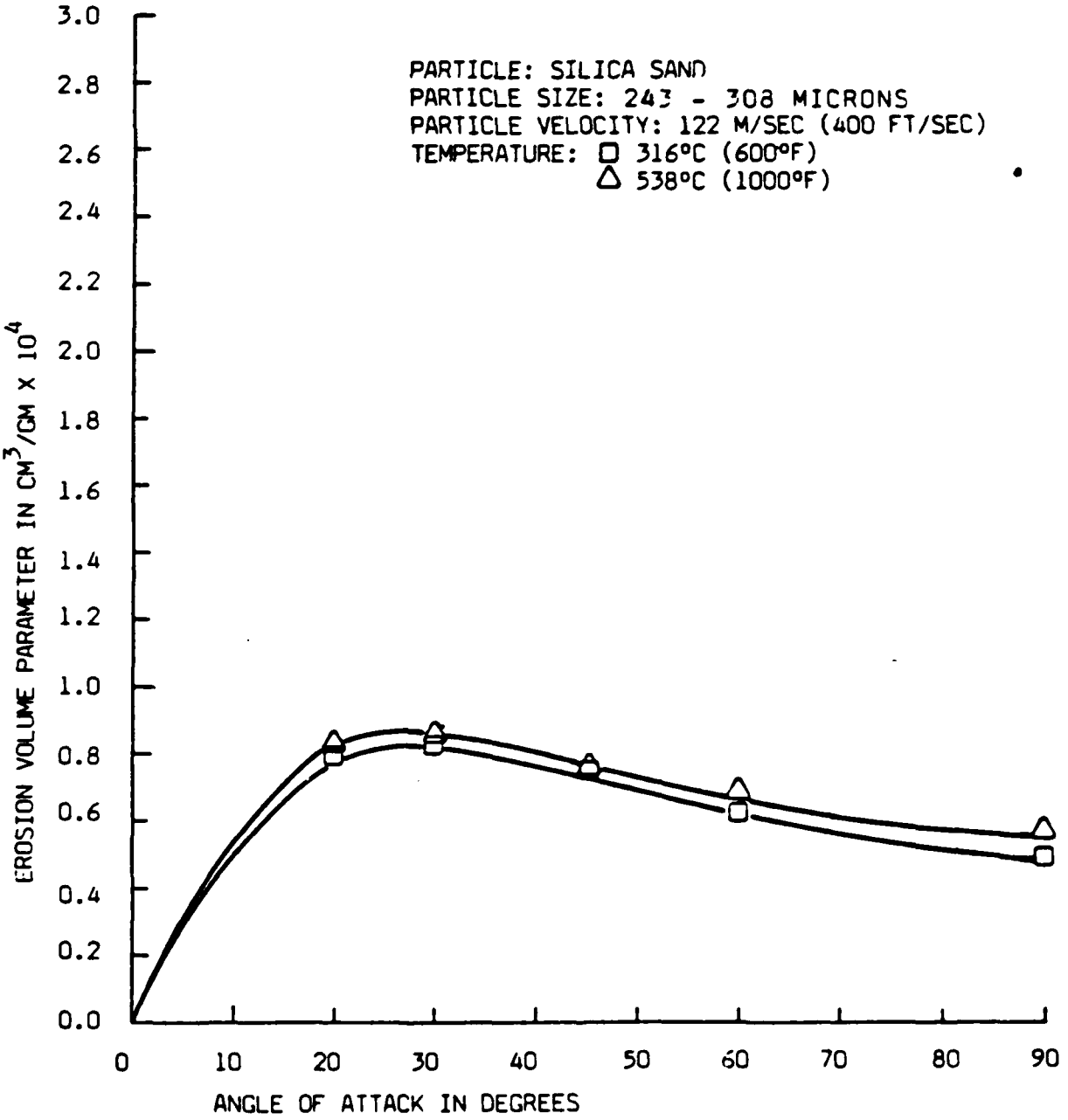

FIG. 24. EFFECT OF TEMPERATURE AND ANGLE OF ATTACK ON AM355 ALLOY

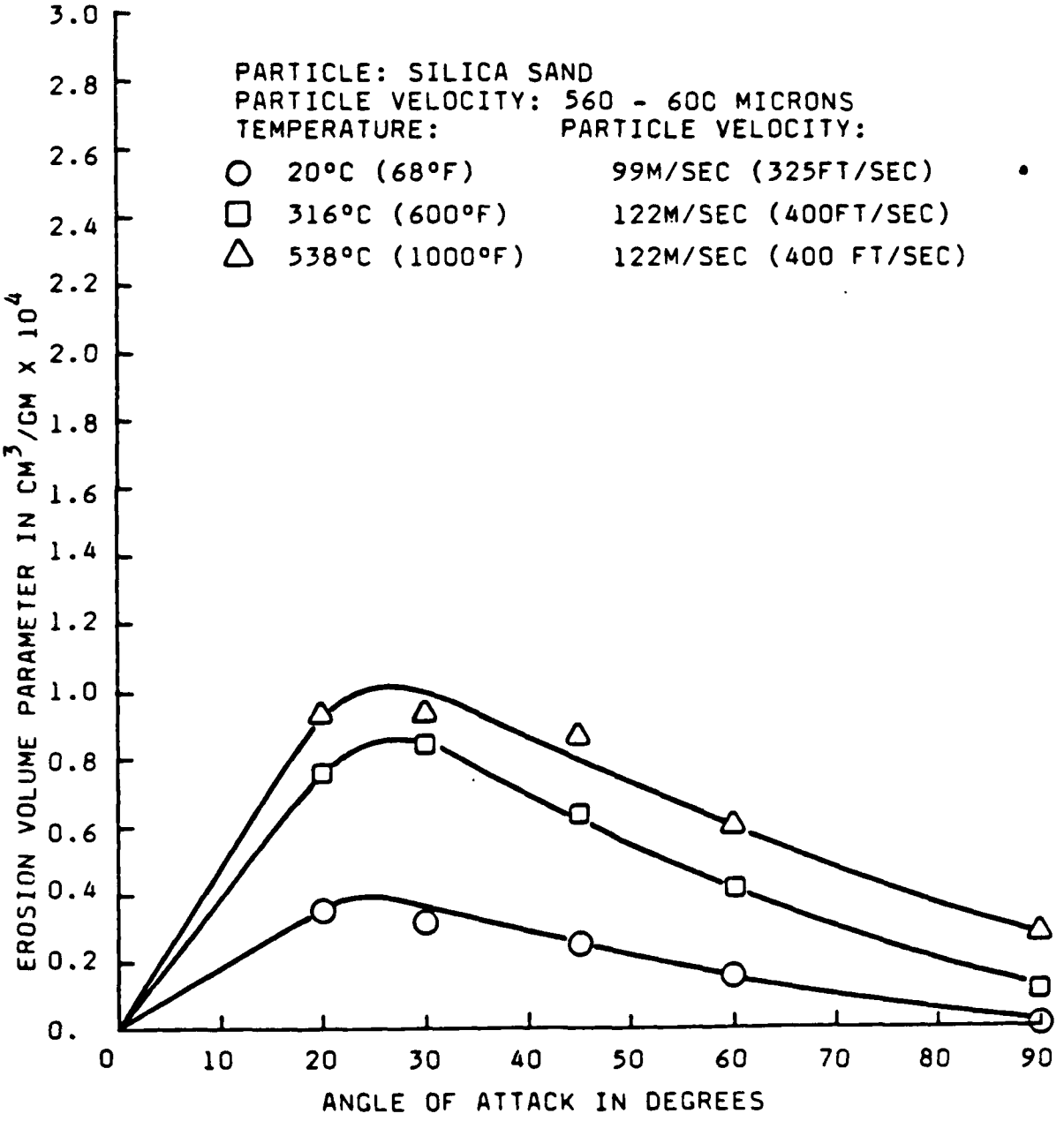

FIG. 25. EFFECT OF TEMPERATURE AND ANGLE OF ATTACK ON AM355 ALLOY

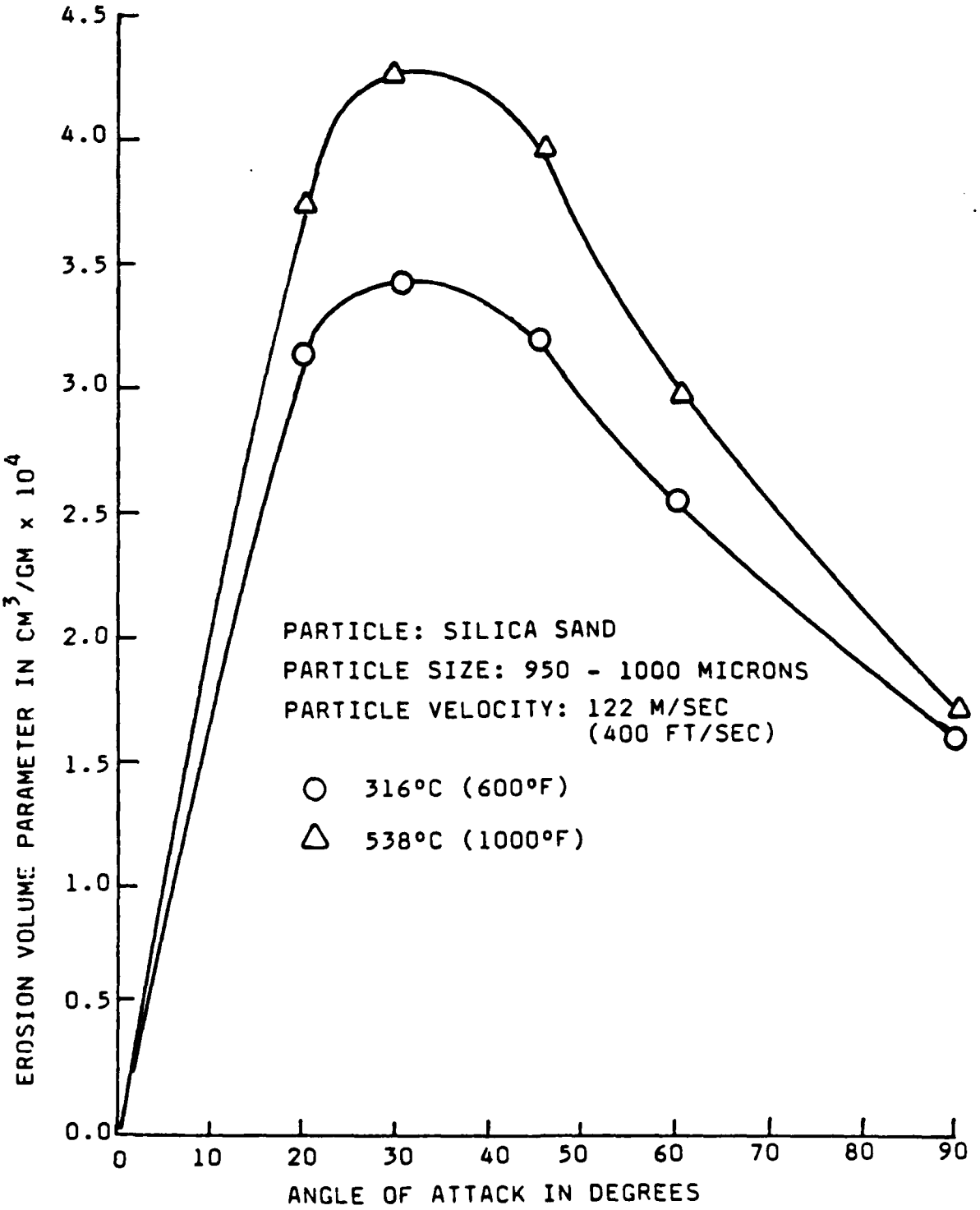

FIG. 26. EFFECT OF TEMPERATURE AND ANGLE OF ATTACK ON AM355 ALLOY

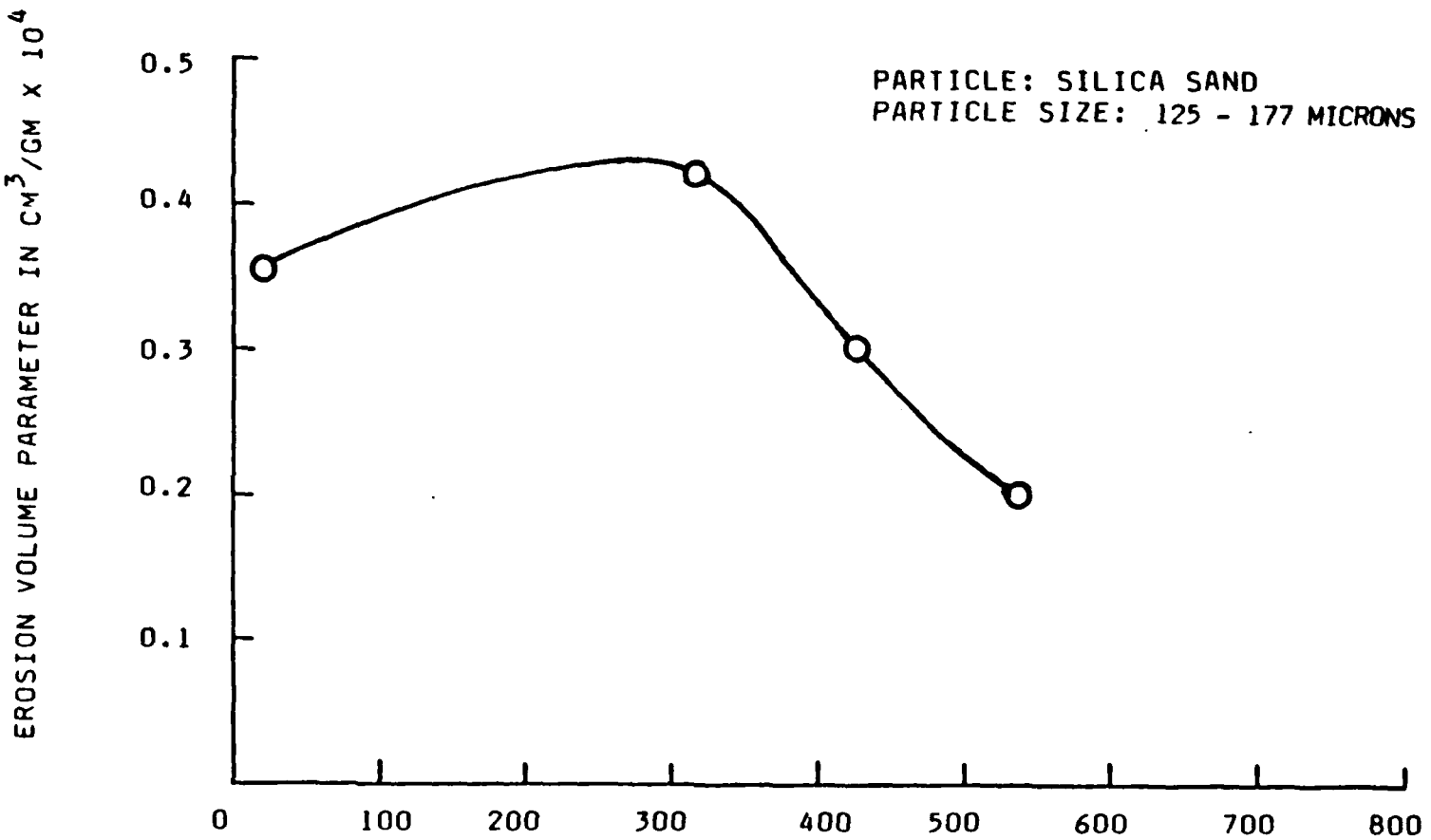

FIG. 27. EFFECT OF TEMPERATURE ON Al_2O_3 AT PARTICLE VELOCITY 137M/SEC (450 FT/SEC)

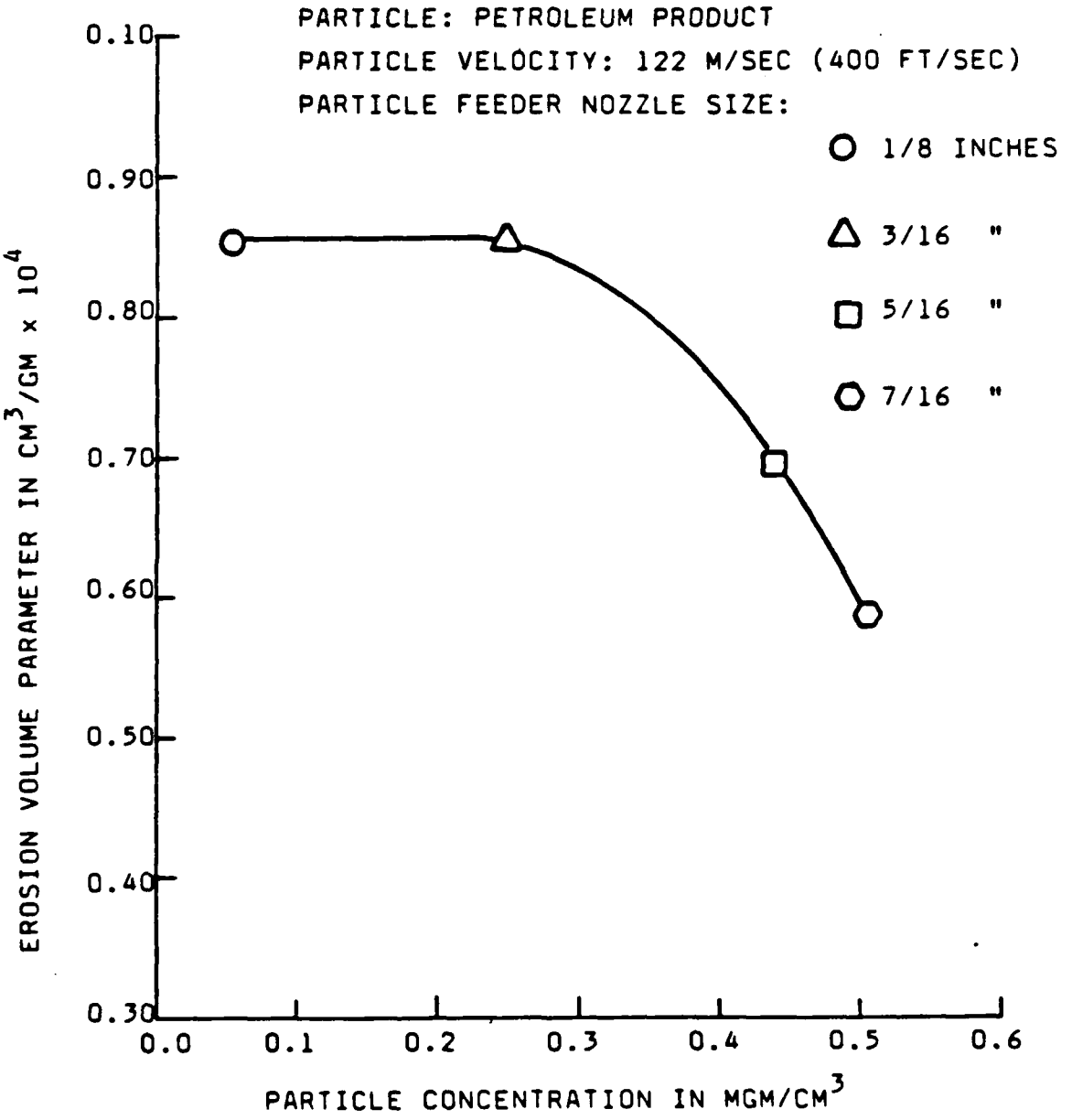

FIG. 28. EFFECT OF PARTICLE CONCENTRATION ON AM355 ALLOY AT ROOM TEMPERATURE AND MAXIMUM EROSIVE ANGLE OF ATTACK (30°).

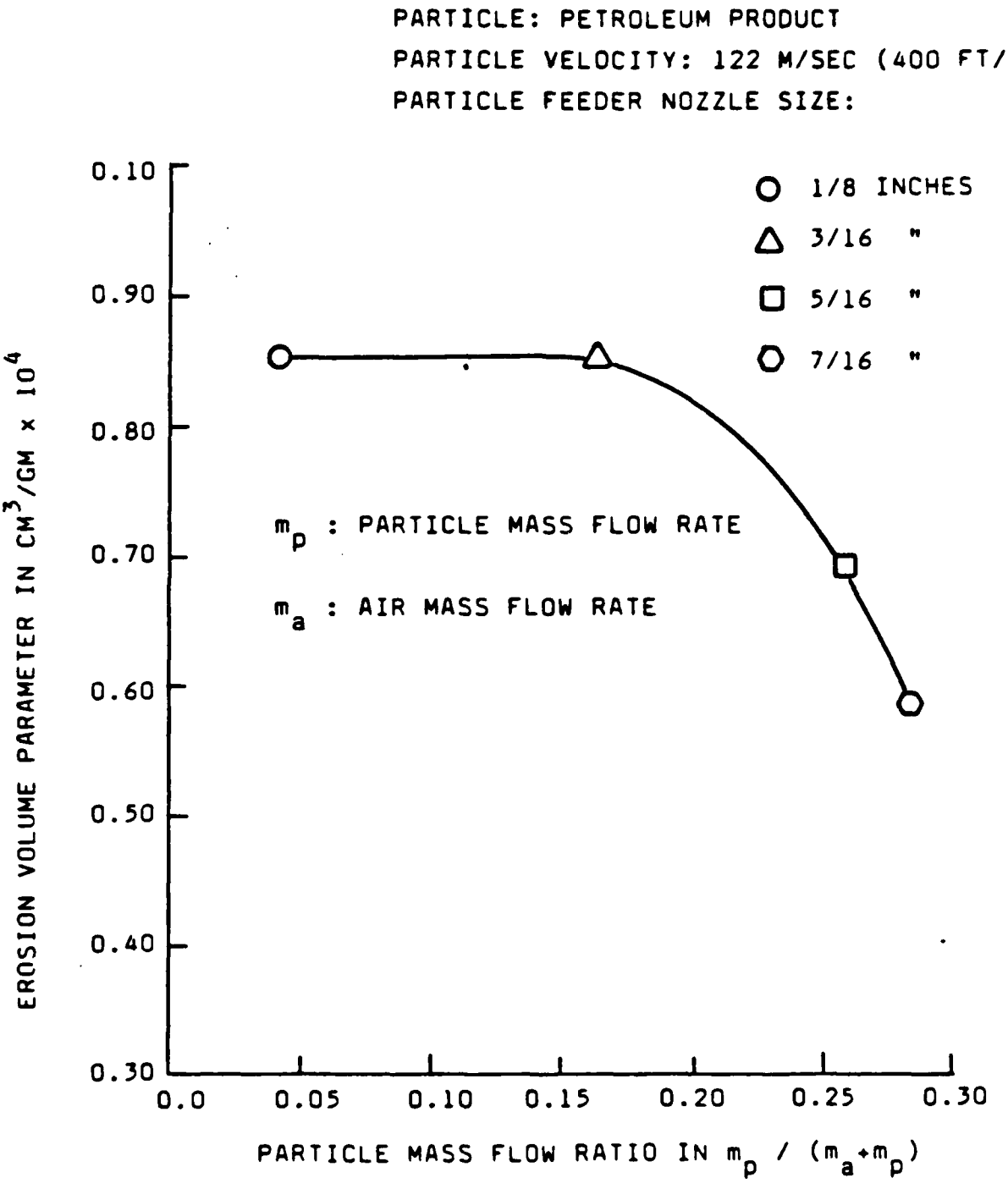

FIG. 29. EFFECT OF PARTICLE CONCENTRATION ON AM355 ALLOY AT ROOM TEMPERATURE AND MAXIMUM EROSIVE ANGLE OF ATTACK (30°).

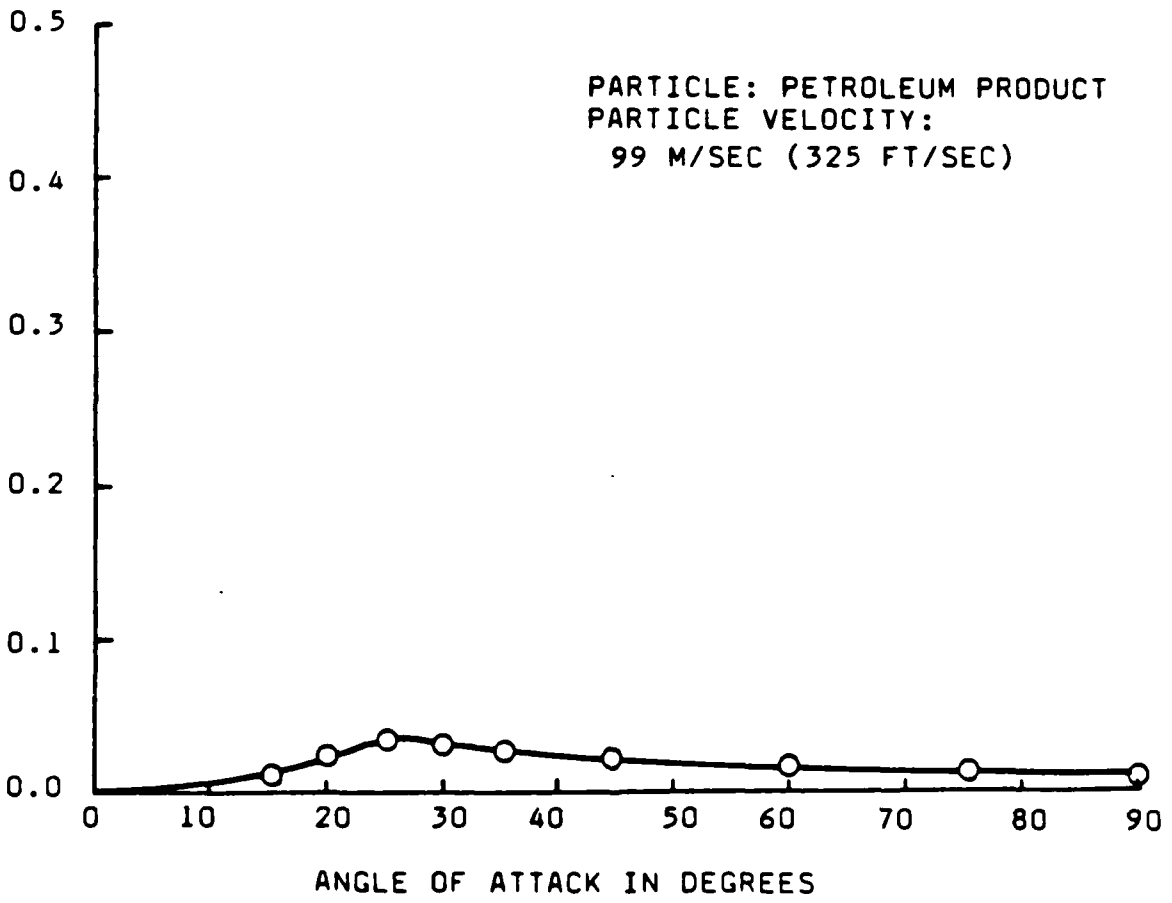

FIG. 30. EFFECT OF ANGLE OF ATTACK ON AM355 ALLOY AT ROOM TEMPERATURE

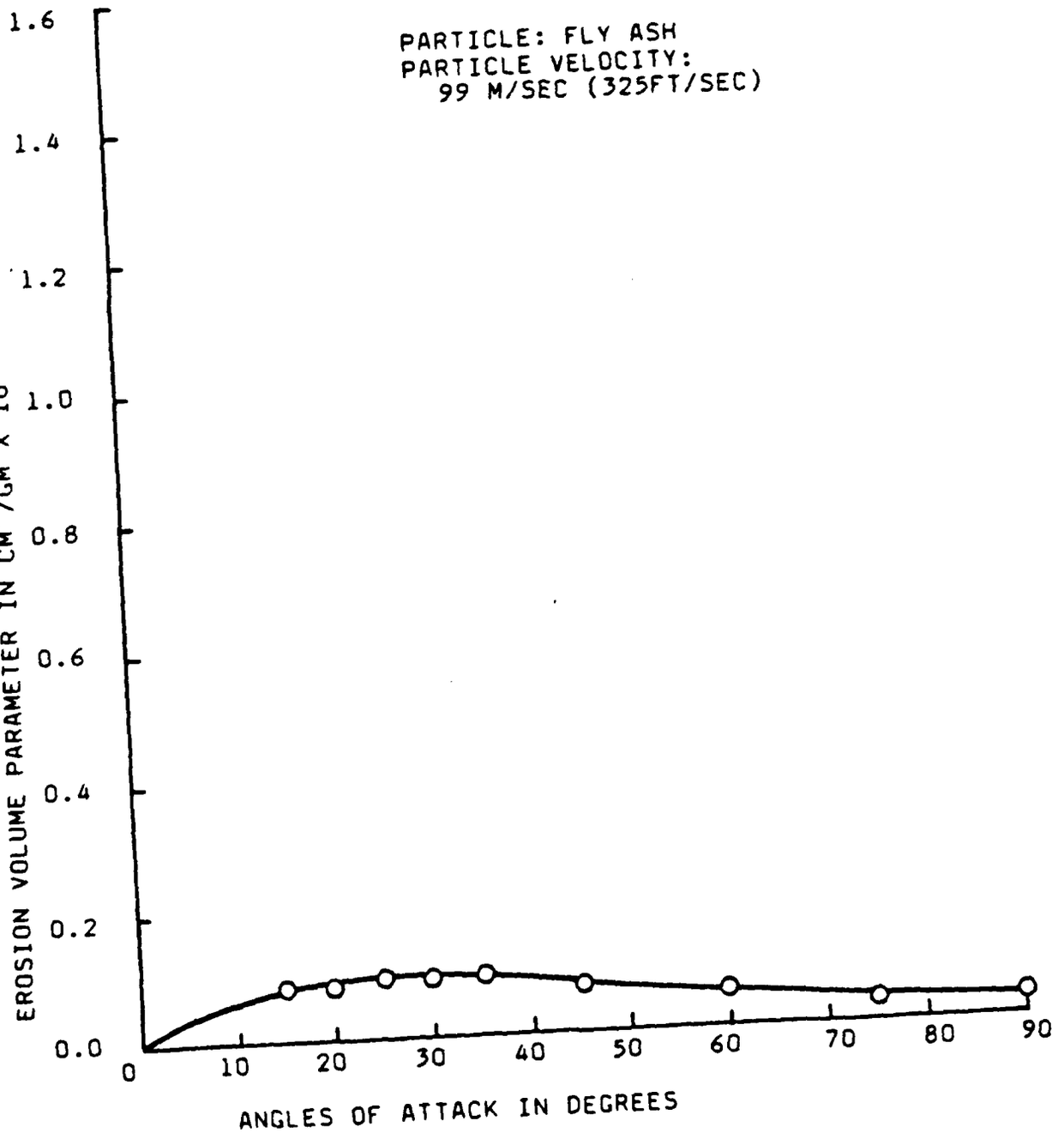

FIG. 31. EFFECT OF ANGLE OF ATTACK ON AM355 ALLOY AT ROOM TEMPERATURE

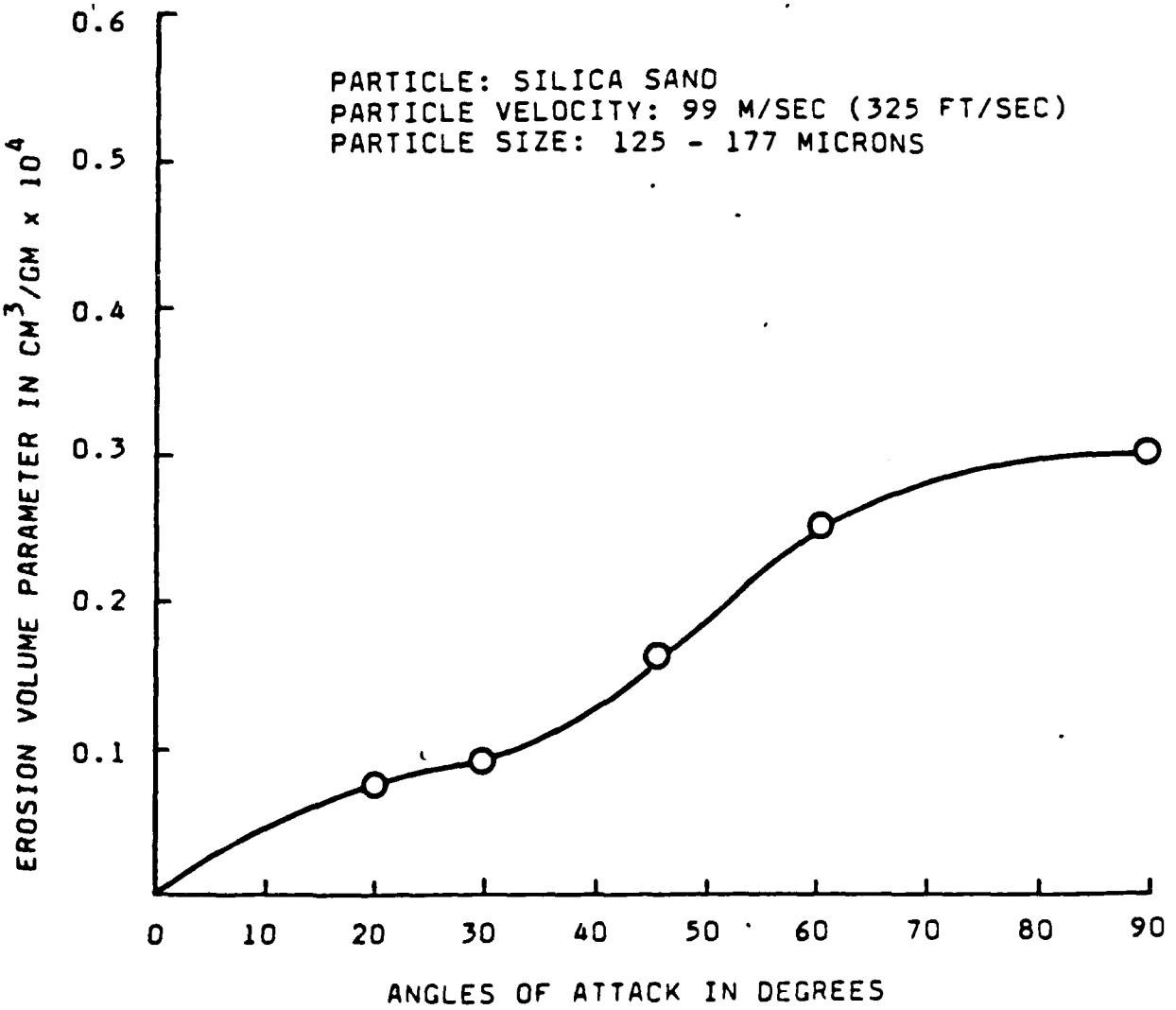

FIG. 32. EFFECT OF ANGLES OF ATTACK ON Al_2O_3 AT ROOM TEMPERATURE

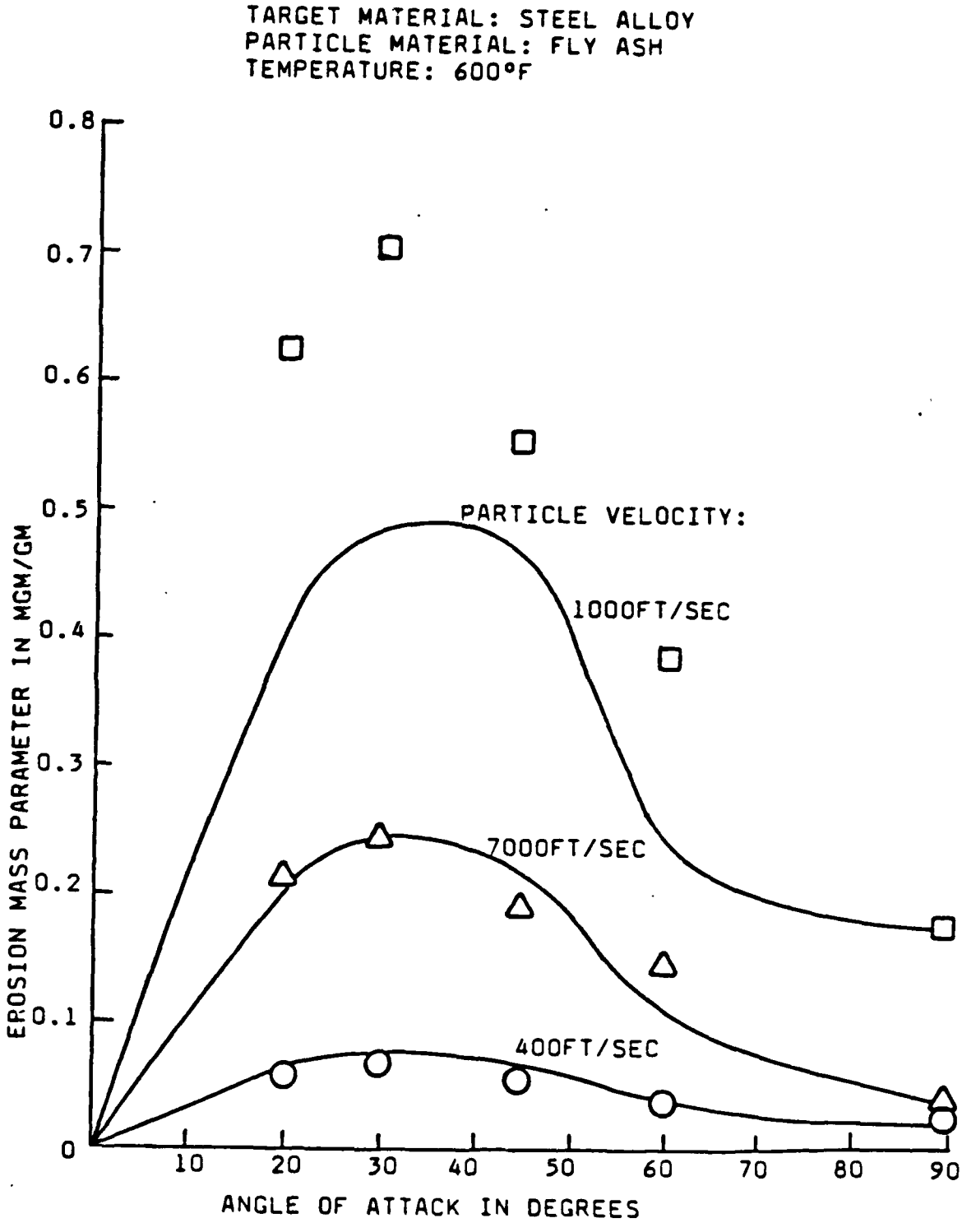

FIG. 33. EXPERIMENTAL AND PREDICTED EROSION RESULTS

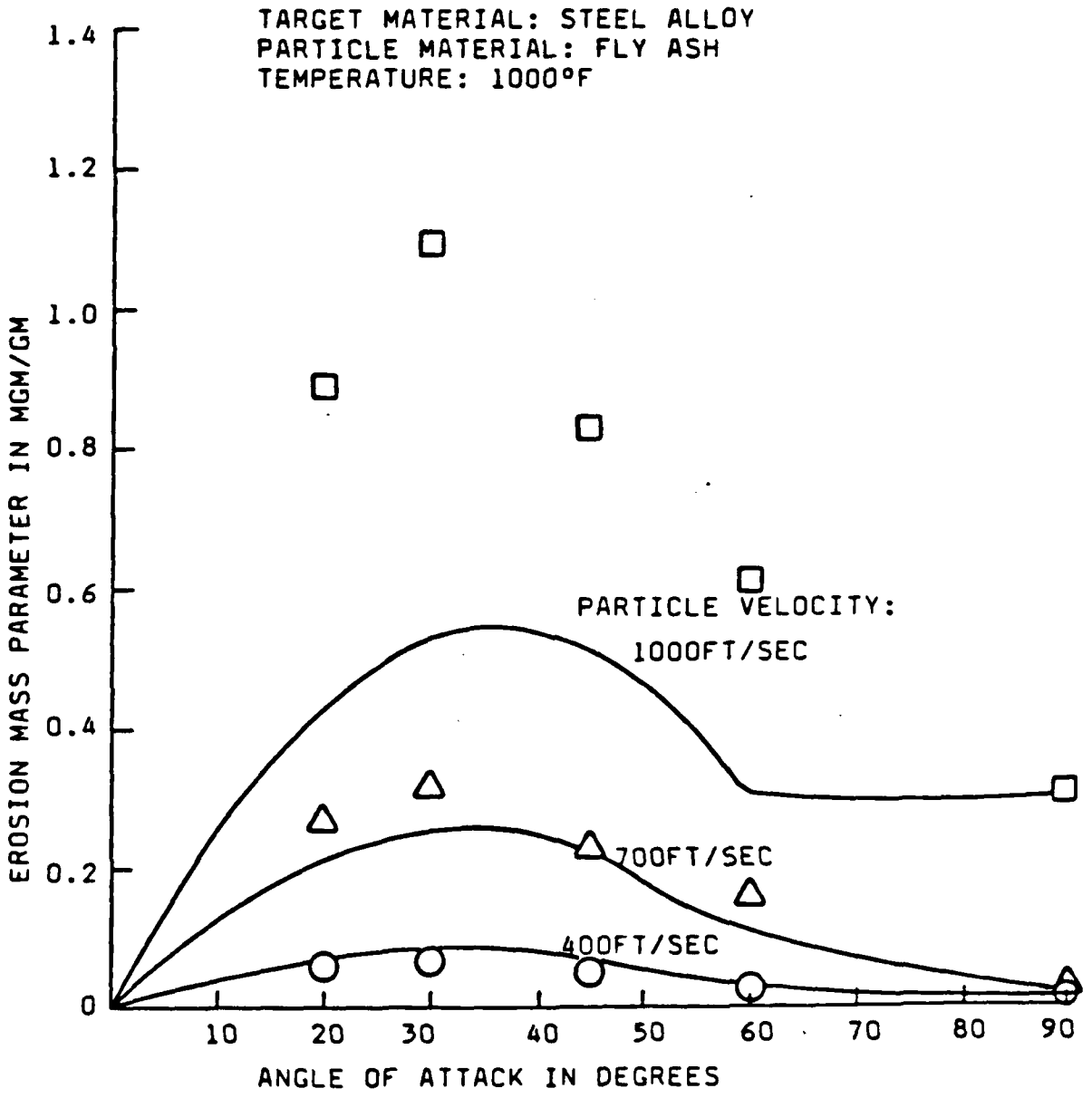

FIG. 34. EXPERIMENTAL AND PREDICTED EROSION RESULTS

TARGET MATERIAL: STEEL ALLOY
PARTICLE MATERIAL: SILICA SAND
(125 - 177 microns)
TEMEPERATURE: 600°F

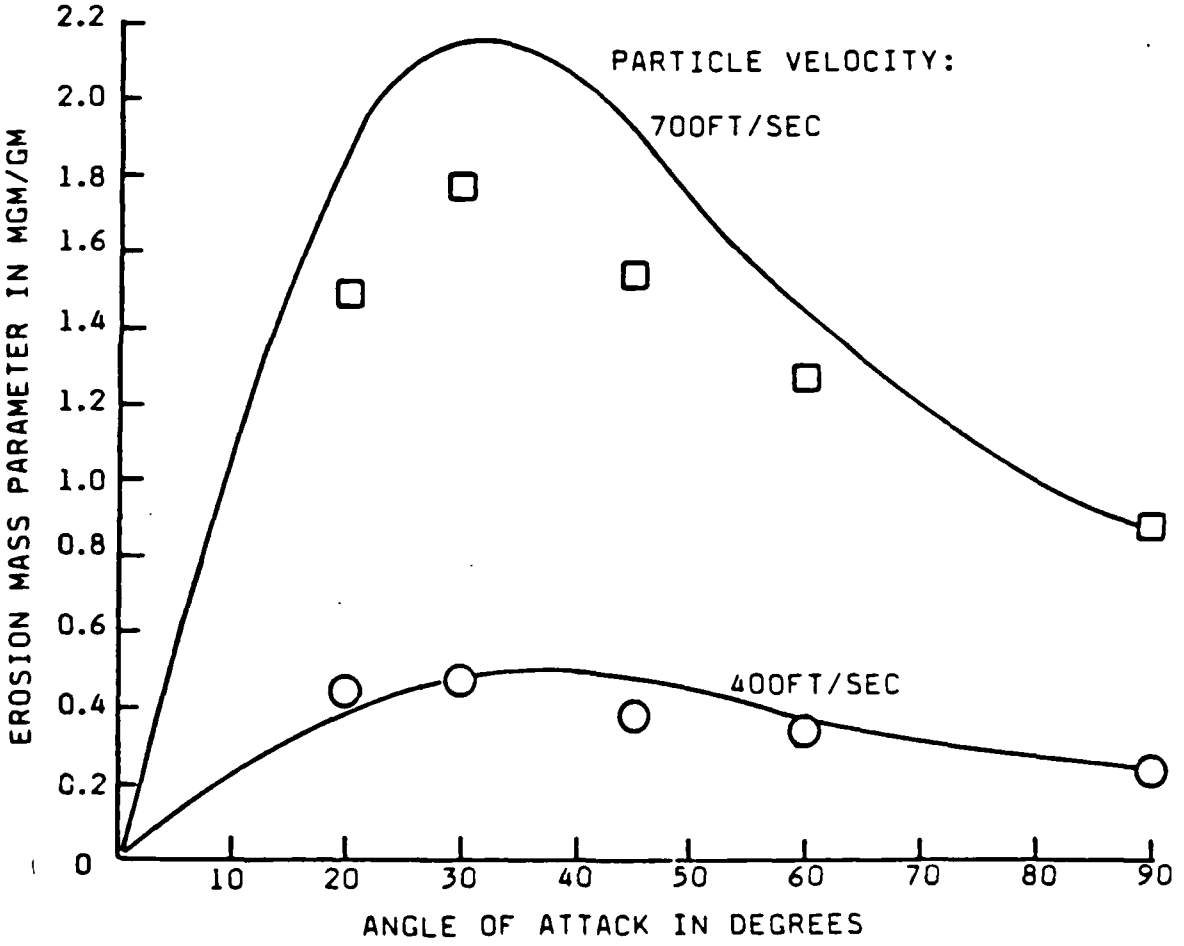

FIG. 35. EXPERIMENTAL AND PREDICTED EROSION RESULTS

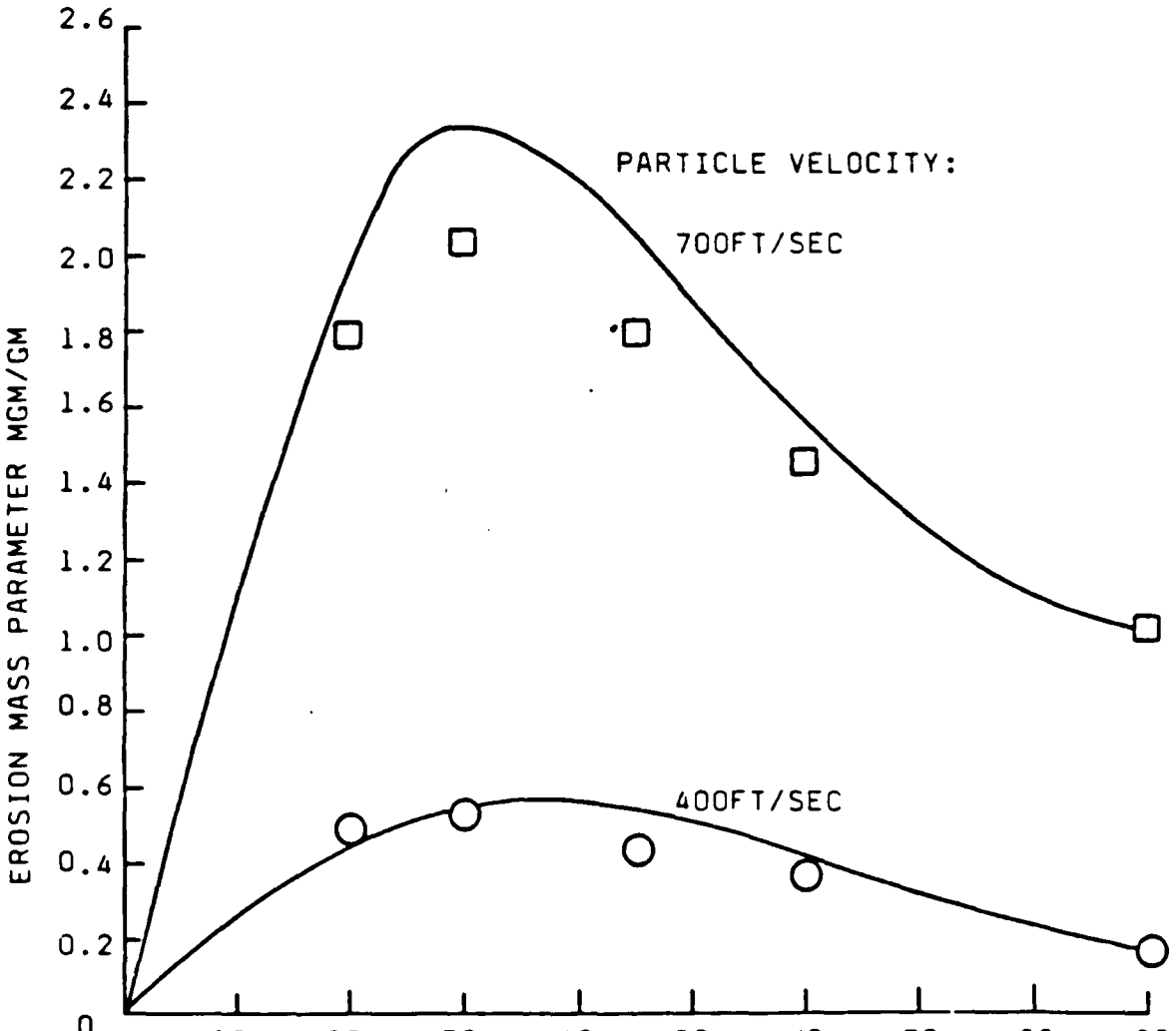

FIG. 36. EXPERIMENTAL AND PREDICTED EROSION RESULTS

40μ

magnified
500 X

FIG. 37. SCANNING MICROGRAPH FOR FLY ASH PARTICLES AVERAGE SIZE 15 MICRONS.

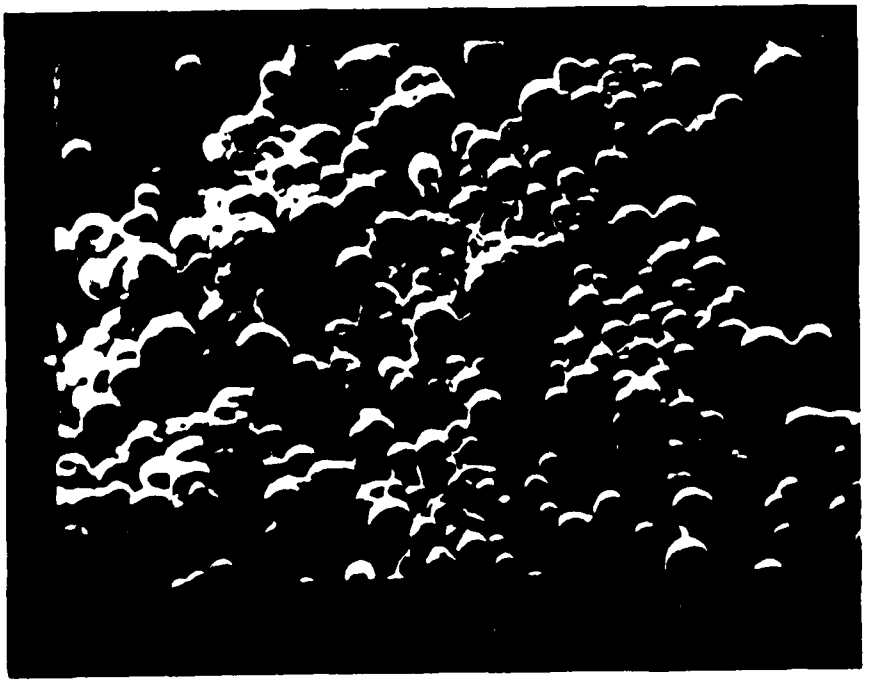

200μ

magnified
100 X

SCANNING MICROGRAPH FOR PETROLEUM PRODUCTS
PARTICLES AVERAGE SIZE 50 MICRONS.

200µ

magnified
100 X

|200µ|

150 Micron Sand Particles

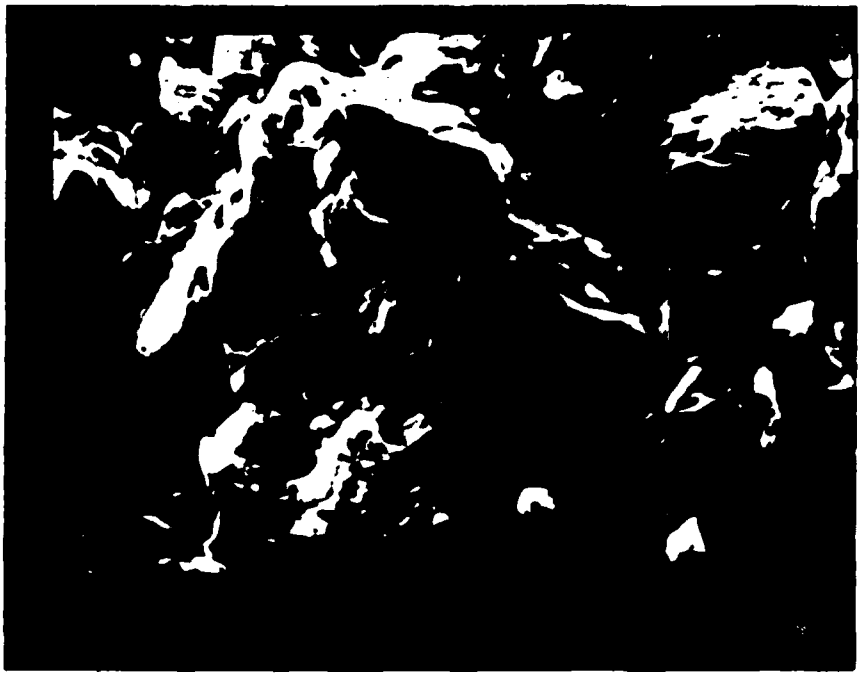

200µ

magnified
100 X

580 Micron Sand Particles

FIG. 39. SCANNING MICROGRAPHS OF TWO DIFFERENT SIZED SAND PARTICLES.

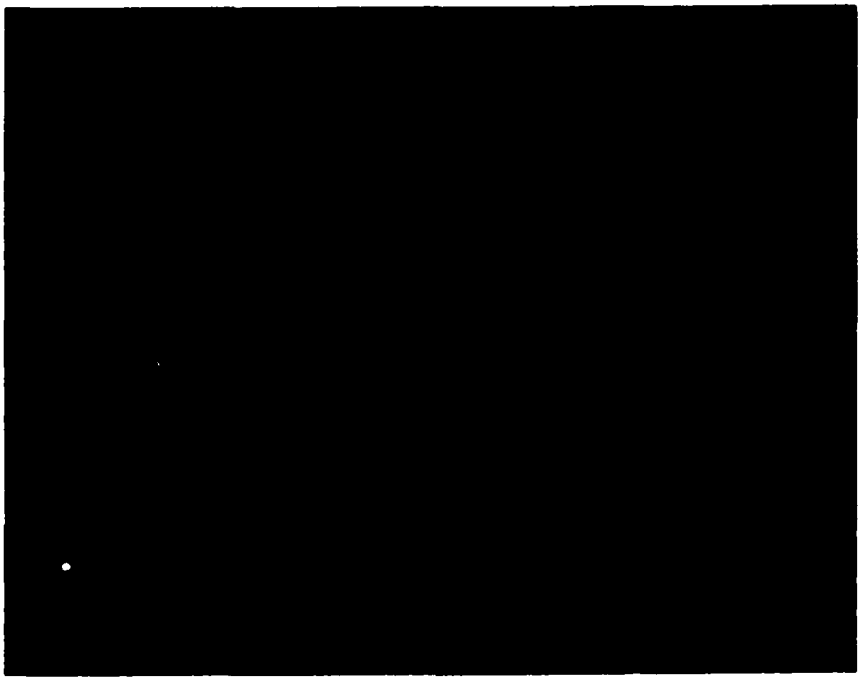

40μ

magnified
500 X

Steel Alloy (AM355)

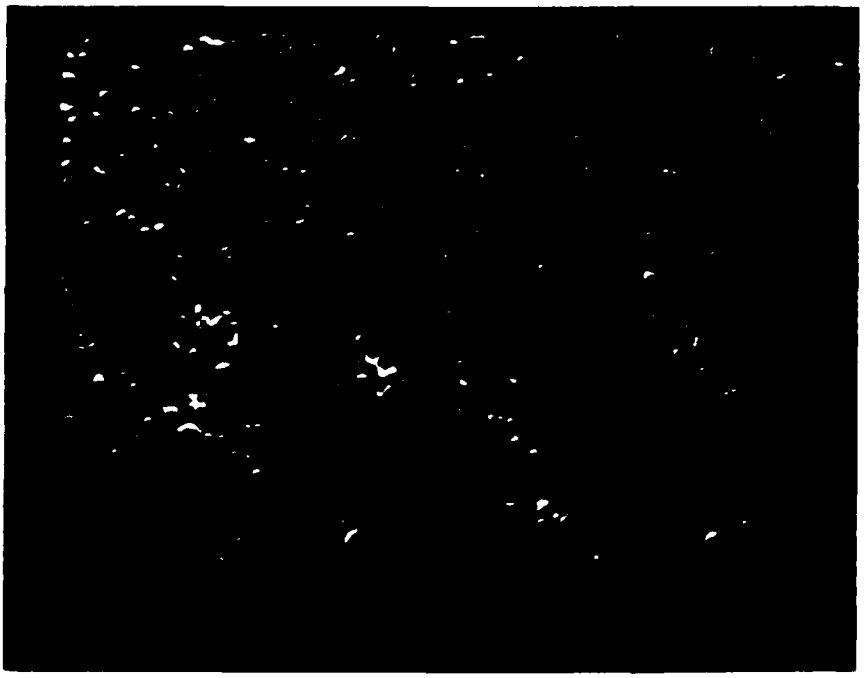

40..

magnified
500 X

CERAMIC (Al_2O_3)

FIG. 40. SCANNING MICROGRAPHS FOR TWO DIFFERENT UNTESTED SAMPLES.

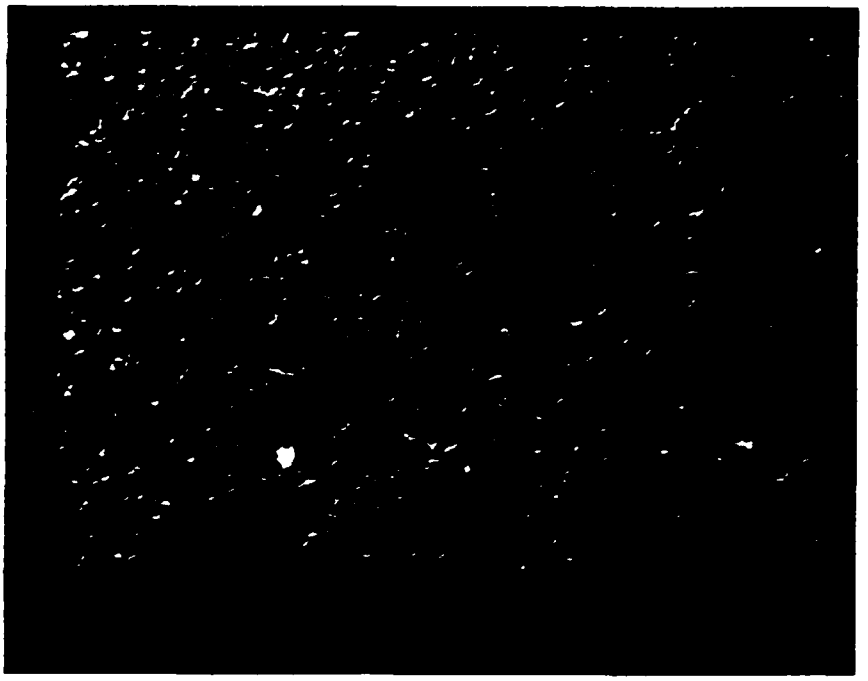

200μ

magnified 100 X

Velocity = 325ft/sec.

50 microns particles

Ceramic Al_2O_3, Room Temperature

200μ

magnified 100 X

Velocity = 325 ft/sec

50 microns particles

Steel AM355, Room temperature

FIG. 41. SCANNING MICROGRAPH OF Al_2O_3 AND AM355 ERODED SURFACES BY IMPACTS OF PETROLEUM PARTICLES.

40μ

magnified
500 X

velocity =
325 ft/sec.

α = 30°

FIG. 42a. SCANNING ELECTRON MICROGRAPH OF ERODED AM355 STEEL SURFACE AT ROOM TEMPERATURE (70°F)

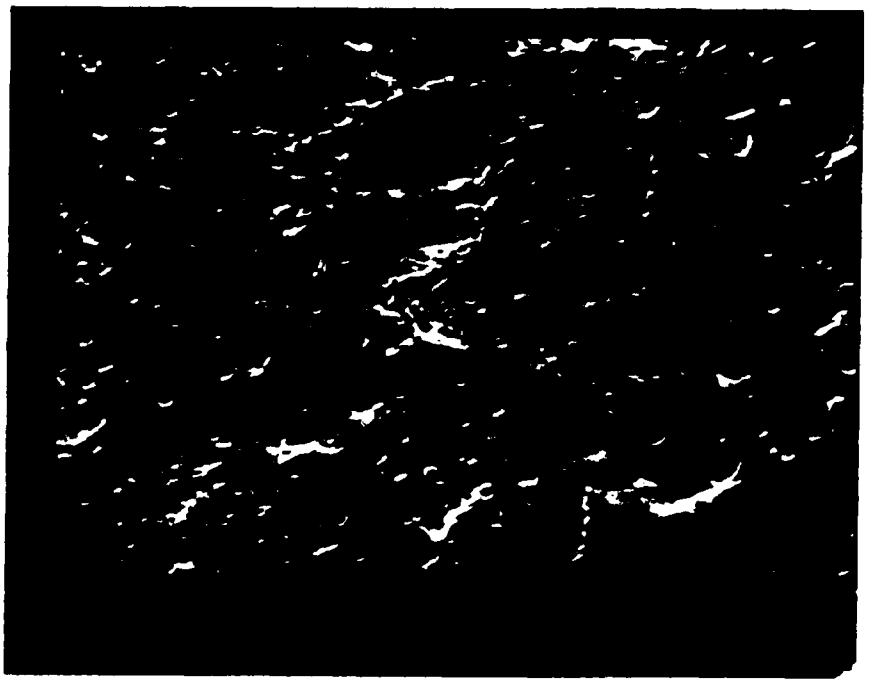

40μ

magnified
500 X

FIG. 42b. Velocity = 400 ft/sec., $\alpha = 30°$

40μ

magnified
500 X

42c. Velocity = 1000 ft/sec., $\alpha = 30°$

FIG. 42. SCANNING MICROGRAPH OF ERODED AM355 STEEL SURFACE AT 600°F BY FLY ASH PARTICLES.

100μ

magnified
200 X

42d Velocity = 700 ft/sec., α = 30°

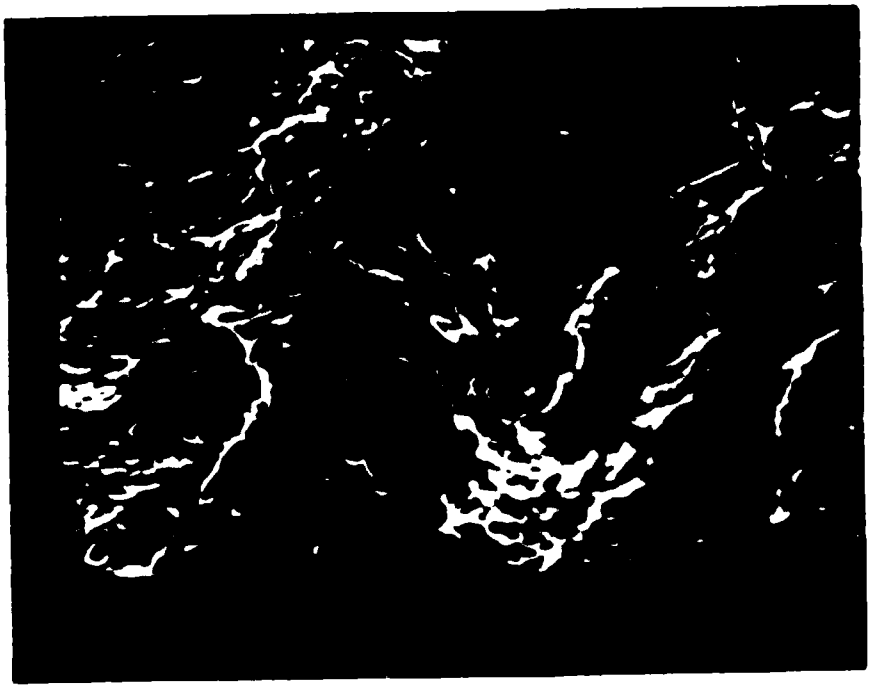

40

magnified
X

42e Velocity = 1000 ft/sec., α = 30°

FIG. 42. SCANNING ELECTRON MICROGRAPHS OF FRACTURE SURFACES AT [illegible] AND [illegible]

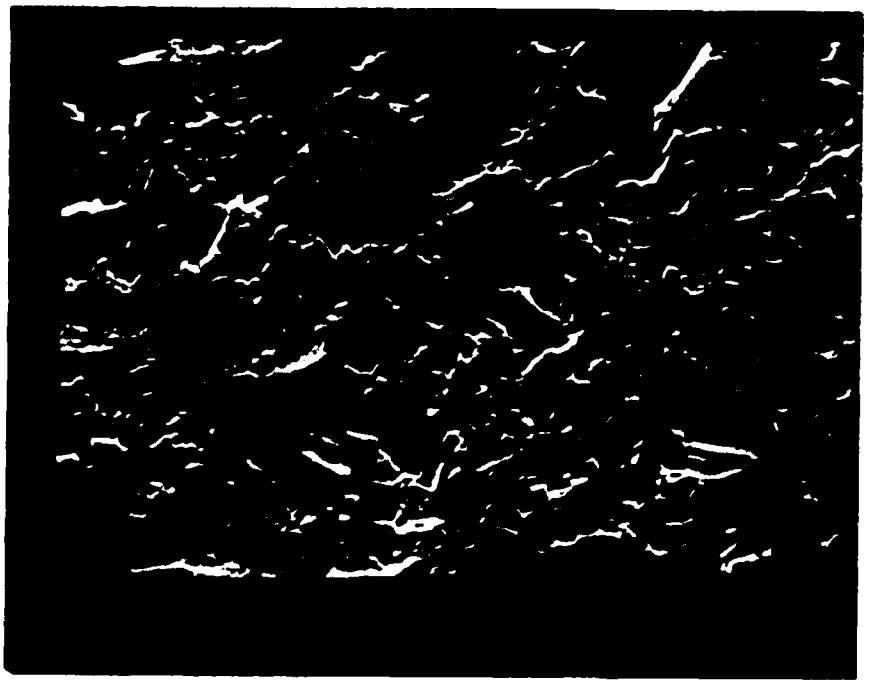

40μ

magnified
500 X

150 microns
sand particles
α = 30°

Velocity = 325 ft/sec.

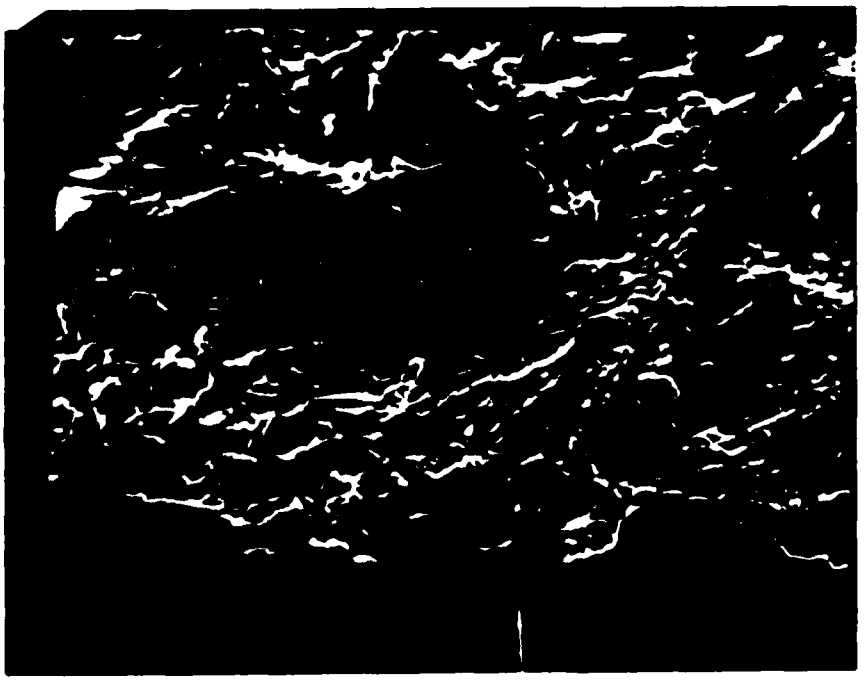

40μ

magnified
500 X

275 microns
sand particles
α = 30°

Velocity = 325 ft/sec

FIG. 43. SCANNING ELECTRON MICROGRAPH OF ERODED AM355 STEEL SURFACES AT ROOM TEMPERATURE (70°F)

40μ

magnified
500 X

150 microns
sand particles

Velocity = 400 ft/sec, α = 30°

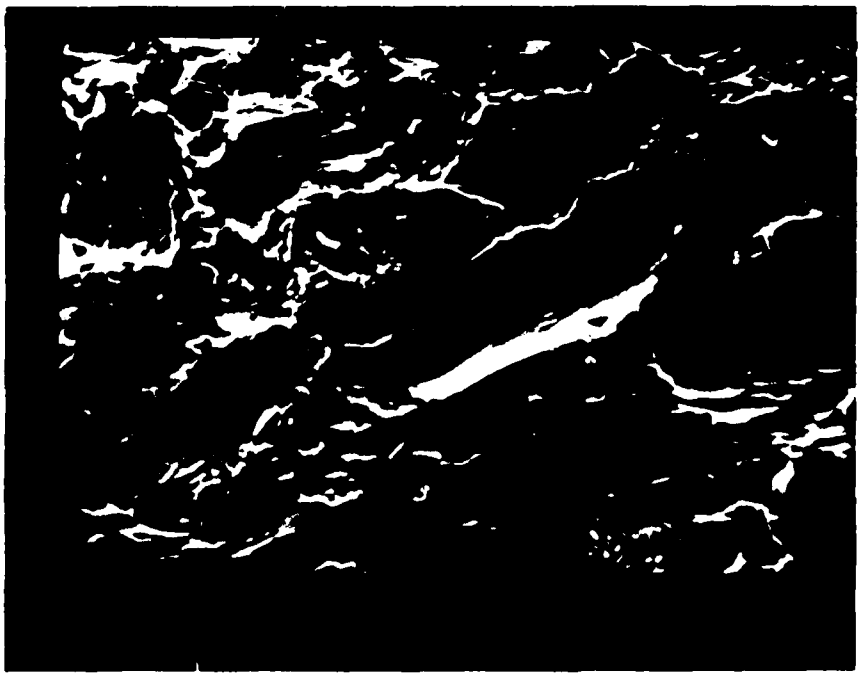

40μ

magnified
500 X

150 microns
sand particles

Velocity = 700 ft/sec., α = 30°

FIG. 44. SCANNING ELECTRON MICROGRAPH OF AM355 ERODED SURFACES AT 1000°F.

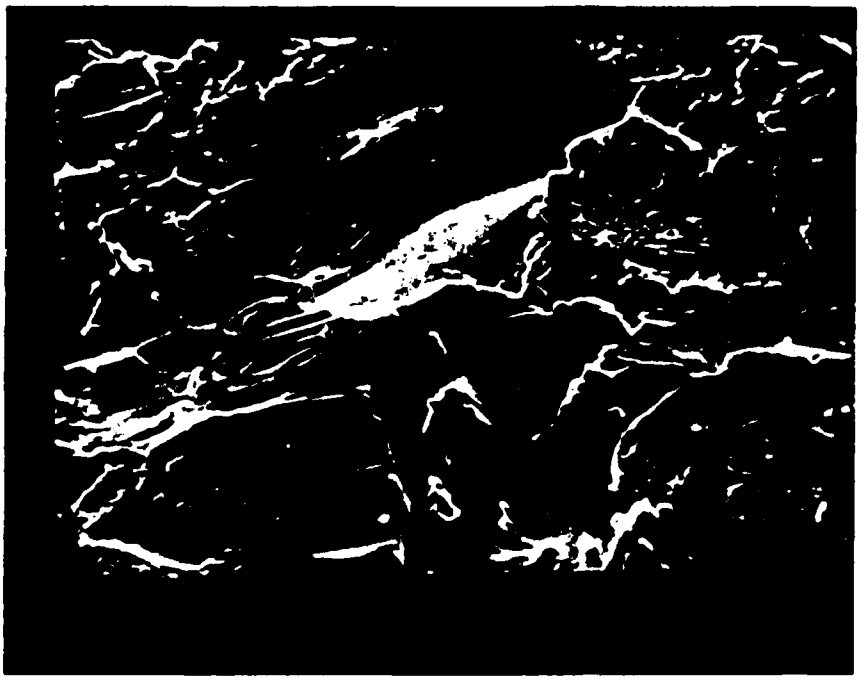

40μ

magnified
500 X

580 microns
sand particles

Velocity = 325 ft/sec., $\alpha = 30°$

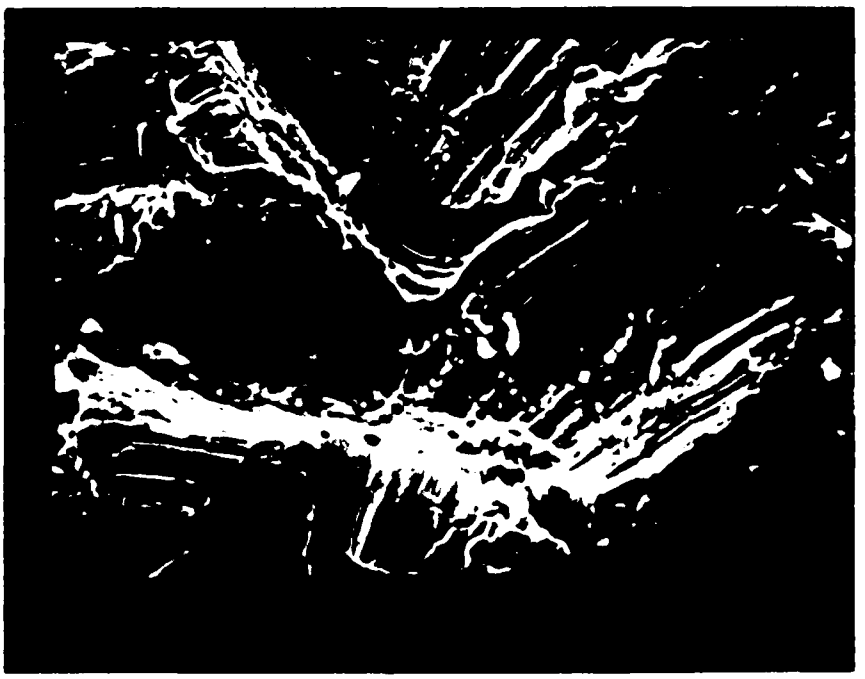

40μ

magnified
500 X

1981 microns
sand particles

Velocity = 325 ft/sec., $\alpha = 30°$

FIG. 45. SCANNING ELECTRON MICROGRAPHS OF ERODED AM[illegible]
STEEL SURFACES AT ROOM TEMPERATURE (70 F)

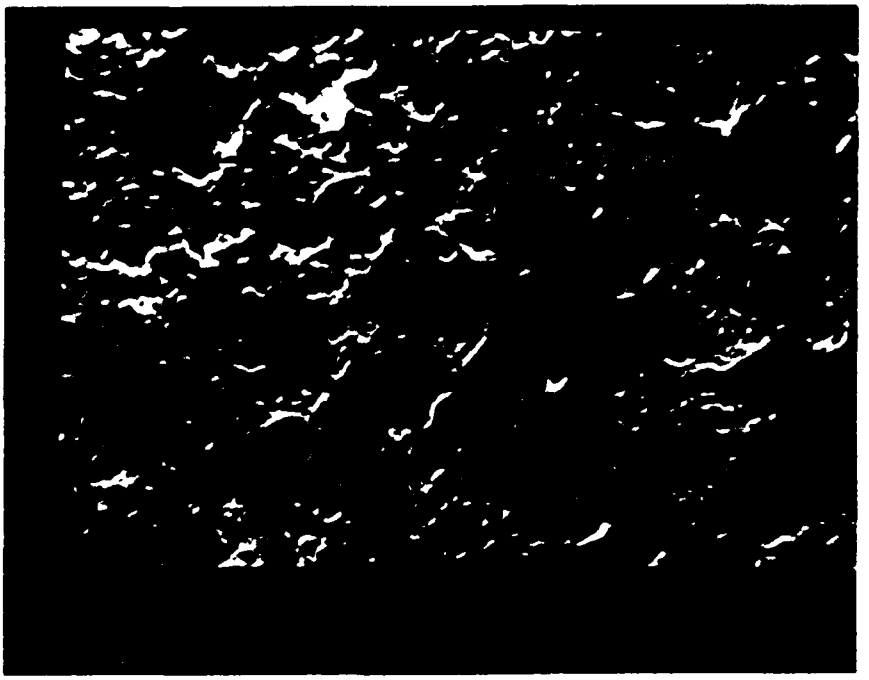

40μ

magnified
500 X

150 microns
sand particles

Velocity = 325 ft/sec., $\alpha = 90°$

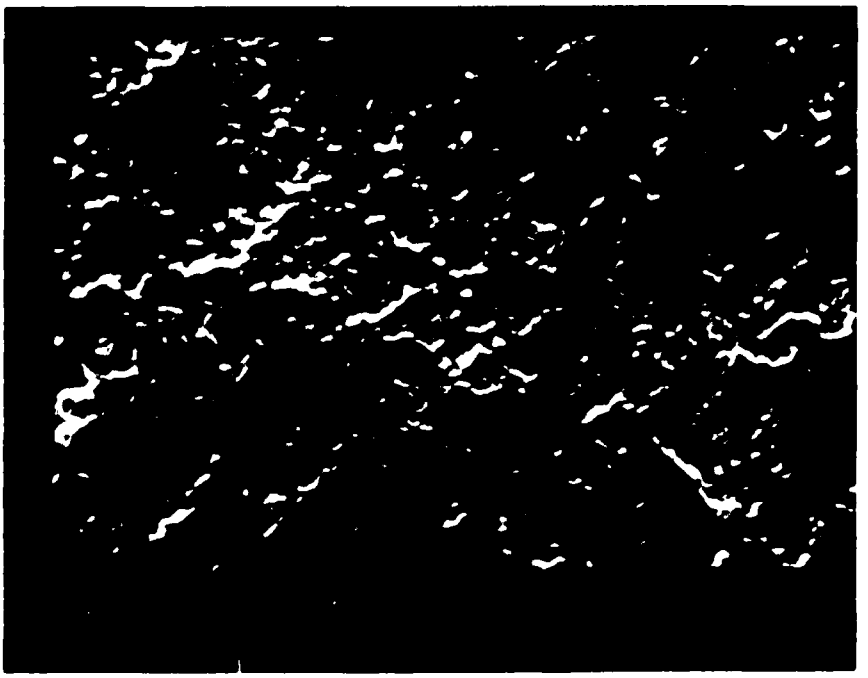

40μ

magnified
500 X

150 microns
sand particles

Velocity = 325 ft/sec., $\alpha = 90°$

FIG. 46. SCANNING ELECTRON MICROGRAPHS OF CERAMIC (Al_2O_3) SURFACES AT ROOM TEMPERATURE (70° F).

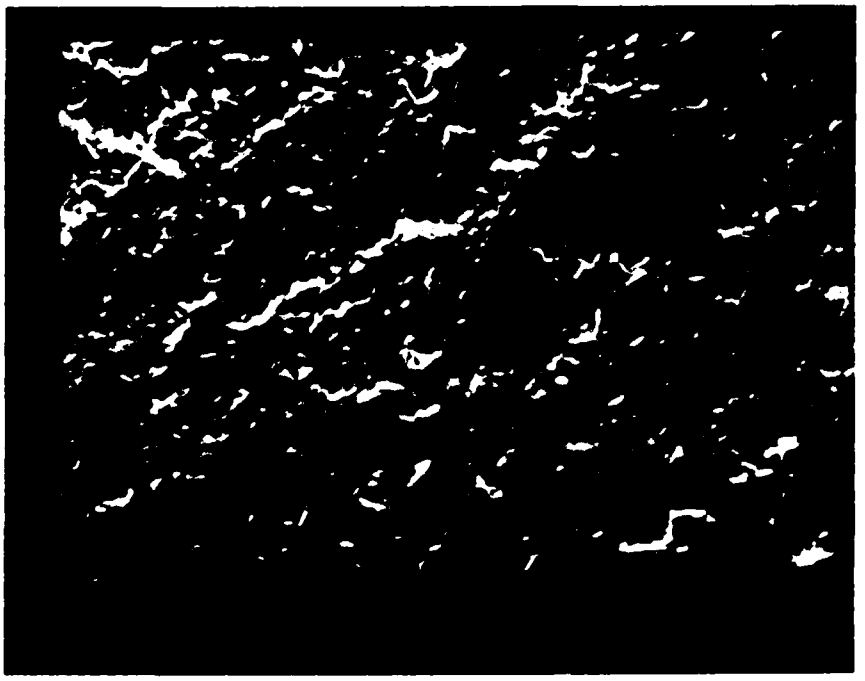

40μ

magnified
500 X

150 microns
sand particles

Velocity = 450 ft/sec., α = 90° and temperature = 600°F

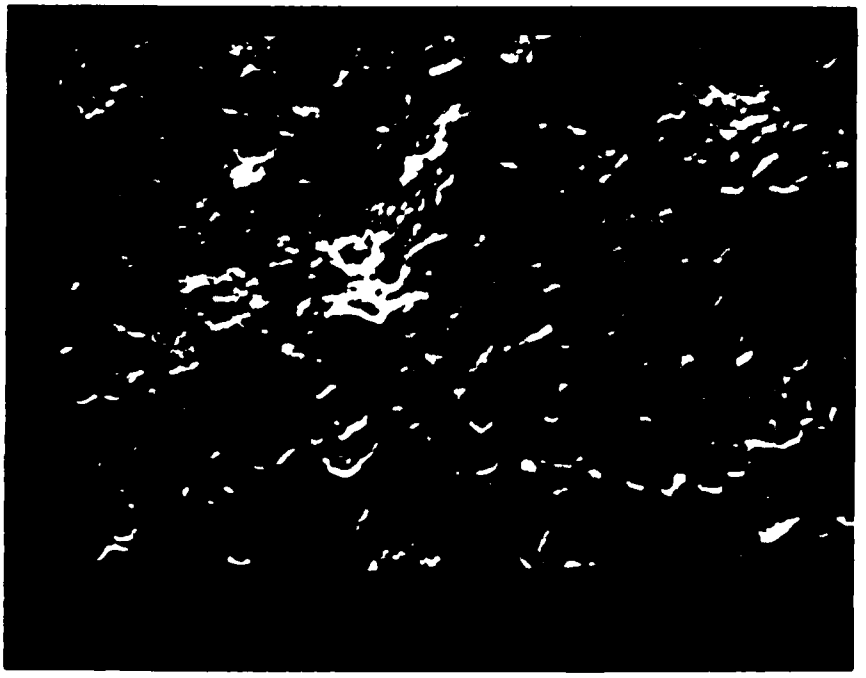

40μ

magnified
500 X

150 microns
sand particles

Velocity = 450 ft/sec., α = 90° and temperature = 1000°F

FIG. 47. SCANNING ELECTRON MICROGRAPHS OF ERODED CERAMIC (Al_2O_3) SURFACES AT 600 °F and 1000 °F.

END

5-87

DTIC